

Biological Plant Root Growth Detection from Spatial and Temporal Resolution Image Sequences

Submitted March 2011, in partial fulfillment of the conditions of the award of
the degree of Ph.D.

-- Chen Xiao Lin --
School of Computer Science
University of Nottingham
Malaysia Campus

Abstract

This thesis describes the development of a new approach to measuring the growth of plant roots. Work on changing the growth patterns of plants by the introduction of the right materials into their feed as well as the process of genetic manipulation is enhanced by being able to measure the growth of the plants roots in real time. Previous work in doing this has been subject to low reliability due in part to the nature of the problem. Plant root growth rates are of the order of $0.1 \mu\text{m}$ per second and thus have to be captured under the microscope. The plant surfaces show low contrast and have few predictable features so many methods prove to be inappropriate. Previous work in the measurement made use of the RootFlowRT software that uses a combination of a tensor based method and a correspondence method. However, the results from these methods have a high level of unreliability. The tensor method as applied shows a reliability of less than 10% and work carried out in this thesis shows that the correspondence method on its own cannot reliably predict the growth rates for large areas in any root.

The work has introduced the use of Scale Space Optical Flow method to replace the previous tensor method and this has been shown to have a reliability of greater than 30% in almost all cases. The results of this method are then used to refine the search space for the correspondence method and again increase the reliability of the measurements.

The validity of the final results using the current method are thus shown to be a great improvement on the previous method. For comparison:

Percentage of measurements in the correct direction and size

- RootFlowRT 70%
- Current method 95%

Maximum spread of invalid results

- RootFlowRT +/-200% in size and 100% in direction
- Current method +/-10% in size or direction

Acknowledgements

I would like to acknowledge the help and support of my parents and sister as well as my supervisor Dr Peter Blanchfield, without which I would not have completed this work.

Contents

| | |
|---|-------------|
| List of Figures | iv |
| List of Tables | viii |
| 1 Introduction | 1 |
| 1.2 Aims and Objectives | 5 |
| 1.3 Structure of the thesis | 6 |
| 2 Literature review | 9 |
| 2.1 Plant Root Growth and its Measurement | 9 |
| 2.1.1 Non Contact Optical methods | 11 |
| 2.1.2 RootFlowRT | 12 |
| 2.1.3 Measurements Using Confocal Microscopy | 15 |
| 2.2 Motion Estimation Background Review | 17 |
| 2.2.1 Differential methods | 20 |
| 2.2.2 Correspondence methods | 24 |
| 2.3 Summary | 26 |
| 3 Methodology | 27 |
| 3.1 Scale Space Optical Flow | 29 |
| 3.2 Correspondence methods | 34 |
| 3.2.1 Block matching basic approach | 35 |
| 3.2.2 Search Space and Multi resolution | 40 |
| 3.3 Implementation | 47 |

| | |
|--|------------|
| 4 Testing the Methods | 50 |
| 4.1 Measurements on the Test Image Sequences with the Scale | |
| Space Optical Flow Approach | 51 |
| 4.2 Measurements using the Multi Resolution Block matching | |
| Approach | 56 |
| 4.4 Combining the results | 58 |
| 5 Results and Analysis | 62 |
| 5.1 The Test Dataset | 64 |
| 5.2 Establishing Ground Truth | 67 |
| 5.2.1 Steps in using the semi manual method | 67 |
| 5.3 Measurements using RootflowRT | 73 |
| 5.4 Use of Optical Flow Data | 76 |
| 5.4.1 Tuning the Spatial Scale | 76 |
| 5.4.2 Using the Scale Space measure to limit the | |
| Correspondence Search Space | 79 |
| 5.5 Comparing Results | 80 |
| 5.6 Discussion of the result comparison | 91 |
| 5.7 Graphs of Growth on the Midline | 92 |
| 5.8 Value of the improvement in growth rate estimation | 97 |
| 5.9 Extension Experiments | 99 |
| 5.10 Summary | 107 |
| 6 Conclusions and Suggestions for Further Work | 109 |
| 6.1 Issues with RootFlowRT | 111 |

| | |
|---|------------|
| 6.2 Comparison of Results | 112 |
| 6.3 Future work | 113 |
| References | 115 |
| Appendix A: Practical issues in the implementation | 122 |
| A.1 Applying the Median Filter | 122 |
| A.2 Effect of changing Block-Size (BS) on the Motion Estimation | 127 |
| A.3 Motion Estimation Vector Field with respect to different size of Search-Space (SS) | 131 |
| A4 Effect of varying σ on the Scale Space Optical Flow Vector Field | 133 |
| A 5 Effect of varying the value of τ on Optical Flow Vector | 135 |
| A6 No Discontinuities in Vector Field | 136 |
| Appendix B Standard Test Image Sequences | 138 |

List of Figures

| | |
|--|----|
| Figure 2.1 Figure 2.1 The experimental arrangement for the interferometer (from Z. JIANG and W. STAUDE1 1989 [14]) | 10 |
| Figure 2.2 a typical root image | 14 |
| Figure 2.3 Network snake assignment algorithm | 17 |
| Figure 3.1 Block Matching within Search Space | 38 |
| Figure 3.2 Multi Resolution Susie Image | 41 |
| Figure 3.3 Searching the minimum value of SAD within the Search Space. | 44 |
| Figure 3.5 Example of multi-resolution pyramid image representation | 45 |
| Figure 4.1a) An original root image... | 51 |
| b) A section of that image, original, and transformed. | 51 |
| Figure 4.2 The same scene at different levels of scale. | 54 |
| Figure 4.3 Example vector plot from 1° per frame rotation for the test images using a) block matching and b) Scale Space Optical flow. | 58 |
| Figure 5.1 Identifying the location of the images used in the experiments. | 66 |
| Figure 5.2 An image from the first stack of the sample uaroux1. | 69 |
| Figure 5.3 a) Profile around chosen point from first image in sequence | 71 |
| Figure 5.3 b) Profile around chosen point from ninth image in sequence. The profile is similar to that in a) but the overall brightness is lower. | 71 |
| Figure 5.4 the first image in the first stack of the set labelled AJH1. Areas of high and low contrast are identified | 72 |
| Figure 5.5 A plot of the growth vectors for the method previously used. Vectors in red fit the backward forward matching criteria, blue do not. | 74 |
| Figure 5.6 Only the backward forward matches that agree using the previous method of measurement | 75 |

| | |
|--|-----|
| Figure 5.7 a comparison of the backwards forwards matching vectors for the method commonly in use with that proposed by this thesis. | 81 |
| Figure 5.8 A scatter plot of the data obtained resolved as growth along the midline | 83 |
| Figure 5.9 Image CGI1 Stack 1 Frames 1 and 9, showing small variation in light levels as observable by the naked eye. | 85 |
| Figure 5.10 Histograms of the mid root areas for the image sets shown in Figure 5.9. | 86 |
| Figure 5.11 The growth rate along the midline for two successive stacks from the sample CG1 | 93 |
| Figure 5.12 The growth rate along the midline for two successive stacks from the sample AJH1. | 94 |
| Figure 5.13 The magnitude of the growth rate along the midline for two successive stacks from the sample. | 95 |
| Figure 5.14 UAJI The magnitude of the growth rate along the midline for two successive stacks from the sample. | 96 |
| Figure 5.15 Result of median filtering of the midline growth data for the sample AJH1 – a set showing lower than usual growth rates. | 98 |
| Figure 5.16 Image for which the RootFlowRT software fails. | 105 |
| Figure A.1 5 Degree Rotation Image Sequence Motion Estimation Vector Field both images observed at BS=3, SS=1; Left Image with applied 5*5 Median Filter and Right Image without Median Filter | 123 |
| Figure A.2 15 Degree Rotation Image Sequence Motion Estimation Vector Field both images observed at BS=8, SS=2; Left Image with applied 5*5 Median Filter and Right Image without Median Filter | 124 |
| Figure A.3 30 Degree Rotation Image Sequence Motion Estimation Vector Field both images observed at BS=2, SS=2; Left Image with applied 5*5 Median Filter and Right Image without Median Filter | 124 |
| Figure A.4 5 Degree Rotation Image Sequence Optical Flow Vector Field both images observed at $\sigma=10$, $\tau=1$; Left Image with applied 5*5 Median Filter and Right Image without Median Filter | 125 |

- Figure A.5 15 Degree Rotation Image Sequence Optical Flow Vector Field both images observed at $\sigma=6$, $\tau=1$; Left Image with applied 5*5 Median Filter and Right Image without Median Filter 126
- Figure A.6 30 Degree Rotation Image Sequence Optical Flow Vector Field both images observed at $\sigma=3$, $\tau=1$; Left Image with applied 5*5 Median Filter and Right Image observed at without Median Filter 126
- Figure A.7 5 Degree Rotation Image Sequence Motion Estimation Vector Field Left Image observed at BS=3, SS=1 and Right Image observed at BS=1, SS=1 128
- Figure A.8 15 Degree Rotation Image Sequence Motion Estimation Vector Field Left Image observed at BS=8, SS=2 and Right Image observed at BS=2, SS=2 128
- Figure A.9 30 Degree Rotation Image Sequence Motion Estimation Vector Field Left Image observed at BS=2, SS=2 and Right Image observed at BS=1, SS=2 129
- Figure A.10 Suzie Image Sequence (see appendix B) Motion Estimation Vector Field Left Image observed at BS=8, SS=2 and Right Image observed at BS=1, SS=2 129
- Figure A.11 Claire Image Sequence (see Appendix B) Motion Estimation Vector Field Left Image observed at BS=6, SS=2 and Right Image observed at BS=1, SS=2 131
- Figure A.12 15 Degree Rotation Image Sequence Motion Estimation Vector Field Left Image observed at BS=8, SS=2 and Right Image observed at BS=8, SS=1 131
- Figure A.13 Bus Image Sequence (see appendix B) Motion Estimation Vector Field Left Image observed at BS=3, SS=3 and Right Image observed at BS=3, SS=2 132
- Figure A.14 5 Degree Rotation Image Sequence Optical Flow Vector Field Left Image observed at $\sigma=10$, $\tau=1$ and Right Image observed at $\sigma=2$, $\tau=1$ 134
- Figure A.15 15 Degree Rotation Image Sequence Optical Flow Vector Field Left Image observed at $\sigma=6$, $\tau=1$ and Right Image observed at $\sigma=2$, $\tau=1$ 134

Figure A.16 30 Degree Rotation Image Sequence Optical Flow Vector Field
Left Image observed at $\sigma=3$, $\tau=1$ and Right Image observed at $\sigma=2$, $\tau=1$ 135

Figure A.17 30 Degree Rotation Image Sequence Motion Estimation Vector
Field observed at $\sigma=8$, $\tau=1$ 136

Figure B.1 Two images from the Suzie sequence with the section of the
image highlighted that was used in the analysis shown in following 140

Figure B.2 Motion Estimation Vector Field for Suzie Image Sequence with
5*5 Median Filter and vary value for BS(Block Size), SS(Search
Space):Figure B3. Optical Flow Vector Field for the Suzie Image Sequence
with 5*5 Median Filter; $\tau=1$ and vary value for σ 141

Figure B.3. Optical Flow Vector Field for the Suzie Image Sequence with 5*5
Median Filter and vary value for σ and τ 142

Figure B.4. Optical Flow Vector Field for the Suzie Image Sequence with 5*5
Median Filter and vary value for σ and τ 143

Figure B.5 Two images from the Claire sequence with the section of the
image highlighted that was used in the analysis shown in following 144

Figure B.6 Motion Estimation Vector Field for Claire Image Sequence with
5*5 Median Filter and vary value for BS(Block Size), SS(Search Space):145

Figure B.7. Optical Flow Vector Field for Claire Image Sequence with 5*5
Median Filter; $\tau=1$ and vary value for σ : 146

Figure B.8 Two images from the Bus sequence with the section of the image
highlighted that was used in the analysis shown in following 147

Figure B.9 Motion Estimation Vector Field for Bus Image Sequence with 5*5
Median Filter and vary value for BS(Block Size), SS(Search Space): 148

Figure B.10 Optical Flow Vector Field for Bus Image Sequence with 5*5
Median Filter; $\tau=1$ and vary value for σ 149

List of Tables

Table 5.1 Typical results found in tuning the spatial scale parameter σ . The table shows the determined size of the search space indicated by the scale space optical flow measurement and the corresponding values obtained for U and V from the correspondence measurement. Image set used CG1 1 1. Manual value obtained U = -12, V = -5. Value of spatial scale leading to best match thus $\sigma = 1.85$. All measurements are in pixels per 100 seconds. 78

Table 5.2 Comparing the results for horizontal and vertical growth rates in μm per second for the method proposed in this thesis with that obtained by RootFlowRT (for the example shown in Figure 5.2) 81

Table 5.3 Comparison of Scale Space measured raw U and V vectors with raw U and V vectors for RootFlowRT and manual measurement. The values are average values for a given data set where the values are considered reliable. 88

Table 5.4 Comparison of midline growth rates parallel and perpendicular to the midline for the sample set of images. These images were chosen at random. The first images of each stack are shown in Figure 6.8. The location of each set is indicated on the relevant stack image in that figure. Note that in all cases the current work gives a much better error than the RootFlowRT which is the method currently employed by biologists 89

Table 5.5 Comparison of percentage of measurements which are "good" for the current method compared to the RootFlowRT. In both cases good is defined as the number of measurements for a given pixel where the growth rate is within one standard deviation of the value obtained in the 5 by 5 neighbourhood of the pixel. 90

Table 5.6 Comparison of error rate as a percentage of the midline growth rate as detected by RootFlowRT compared to the current method. 90

Table 5.7 Comparing the results from RootFlowRT and the current method for a wider range of targets. 100-104

Chapter 1 Introduction

In the world today the need for more efficient food production has been highlighted because of the ever increasing world population and the effects of climate change [1]. There is much debate about the correct response to the crisis that has arisen but it is clear that a response is needed. Plant biologists have taken the approaches of plant breeding programmes and genetic modification to try and match the huge need for improved food production efficiency. [2] The *"FAO has expressed deep concern over the lack of progress in reducing the number of hungry people in the world, which has remained persistently high."* [3] In order to test the changes the plant biologists have introduced, controlled experiments are necessary. Many of these will take place in the field, using field trials of new crops. Measurement of growth rates of plants over prolonged periods will be undertaken. However, this will also need to be supplemented by work in laboratory conditions where controls over climate can be introduced and measurements at a microscopic level can be made. In particular the need to measure plant root growth is of importance for understanding whether experiments to improve plants have worked. Examples of the importance of this work are many, for example the work of Svistoonoff et al [4] looks at how deficiencies in phosphates in the soil reduce the growth rate of roots. However, work on understanding this growth has enabled them to look at how to change plants to continue to grow well in such adverse conditions. Much work has been done on measuring root growth. For example

Chavarría-Krauser et al [5] have made advances in using image processing techniques to measure growth rate specifically to identify curvature in the growth. Particularly important work in the area has been undertaken by van der Weele et al [6] in a team led by Tobias Baskin of the Department of Biology, University of Massachusetts, Amherst, Massachusetts. This work established the most common method of measurement being used by plant biologists in measuring plant root growth; see for example [7][8][9][10]. The software developed and described in [6] is called RootFlowRT uses a combination of a tensor based method and a correspondence technique. However, initial work done with this method has shown that it has intrinsic problems. Of major importance in measuring root growth is the rate at which the change between new cell production and cell elongation takes place. For example for *Arabidopsis thaliana* – a brassica which has seen a lot of experimental work – the growth rate changes from approximately $5\mu\text{m}$ per minute in the region near the root tip (cell production region known as the quiescent centre) to between 10 and $15\mu\text{m}$ per minute in the elongation zone (further up the root) where the cells begin to expand. Initial experiments looking at the results obtained from the RootFlowRT software showed that it was commonly producing results that were incorrect. In particular the variance in the results obtained was often of the order of $5\mu\text{m}$ per minute – thus undermining any real confidence in the change that was taking place in the growth rate. Discussions with Prof Baskin revealed that he was also unhappy with the reliability and accuracy

of the method being used. It was thus an important motivator for this work to determine:

- What was causing the errors generated in the common current method?
- What approach to measuring the growth of plant roots is best suited to their specific characteristics?
- Whether a method could be developed that is more robust and accurate, thus potentially improving the work of the biologists?

The first stage of the current work was thus to look at how measurements of motion and other changes are commonly made using automatic means and determining what characteristics of the images being measured make those techniques suitable. Then it was possible to identify which methods gave the best potential for measuring the particular problem of plant root growth. After this a method of measurement was developed and tested using a number of sets of standard images and further a set of artificially generated images that contained the same characteristics as those of the plants. Finally the method was tested on plant samples and comparisons made to the RootFlowRT method. During this study answers for all the questions given above were found.

A number of techniques have been developed over the recent past and a number have become established as valuable tools in a theoretical sense for measuring motion in various different ways. However, many real problems

remain that need new approaches or adaptations of current approaches. In common spy fiction, moving images are analysed and improved as the fictional investigators probe CCTV footage for evidence of terrorist activity. The reality is of course far from that presented in these TV series and the process of analysing such footage is a real current problem that has yet to be answered. Many techniques can be useful in simple situations but none have the general impact needed to make them practically useful in the majority of real situations.

Medical data is often now stored in image forms. One possible use of tracking change in this area would be to look at how images produced from mammograms change as the breast tissue is subject to changing applied force. Current analysis techniques do not easily find tumours at their smallest and new techniques could allow the earlier diagnosis with the subsequently increased chance of early intervention leading to improved patient survival rates. Alternatively it is very difficult to differentiate between benign and malignant objects merely from the mammogram image and physically intrusive tests are often used to confirm diagnosis, even when the observed object is benign. Thus improved image analysis techniques would potentially reduce the rate of unnecessary physical intervention.

Of particular interest in the current work are recent developments have produced valuable results in analysing plant roots during their growth using

other optical means than the common bright field microscope used in [4] – [10] (see for example [11] and [12]). These experiments use confocal microscopes involving focused laser lighting and selective dyeing of the food sources of the plants. The result is a cross section of the plant as it grows, which gives specifically valuable information and for which different techniques have proved valuable. However, this method is very expensive and most plant measurements are still done with conventional bright field microscopes. Improving the measurements for this technique thus remains a vital requirement.

1.2 Aims and Objectives

The aim of this work is thus to investigate the following question. Is it possible to develop methods that are efficient in their implementation, effective (giving accurate results that extend the usefulness of the measurements) and improve on the reliability of the measurements? This question must be answered for low contrast high noise images as found in the root growth measurement. The objectives of the work were thus to:

- Investigate the methods being used to measure plant growth in general
- Determine the main characteristics of the images of plant roots used by biologists
- Determine a technique or combination of techniques that best match these characteristics

- Test those techniques in controlled conditions where the result is known. This would be done by
 - Generating test images of known changes
 - Using common image sets with known behaviour
- Test the techniques on sample images of roots which cover the full range of data met in real growth measurement situations
- Compare the performance with the system currently in use (RootFLowRT)

1.3 Structure of the thesis

Chapter 2 opens by looking in detail at ways in which measuring plant growth has been tackled. It then identifies the techniques described in the existing literature on the various methods of analyzing motion using images. Various different techniques have been proposed and this chapter identifies the value of these techniques for the problem at hand.

Chapter 3 looks in more detail at the techniques that have been found to fit the identified characteristics of the plant root images. The images of particular interest in the current work are those taken using standard bright field microscopes. Their major characteristics that make them particularly challenging to measure are

- The low level of contrast in the image
- The lack of any easily identifiable geometric features to base a feature tracker on.

- A surface with repeated but not regular surface structure that leads to possible miss matching in the image sequence
- The low growth rates of most of the samples

As a result two approaches have been identified as being of most value – a Scale Space Optical Flow method which can yield good levels of reliability on sub pixel motion estimation and a block based correspondence technique – which also uses the idea of scale to improve the efficiency of the measurement algorithm. In the experimental stage it was also found that it was important to have a good a-priori estimate of growth rate to aid the correspondence method in working well. This is provided by the output of the Scale Space Optical Flow method.

Chapter 4 looks at some of the experiments done to determine the effectiveness of the methods chosen. Some of the common issues faced in these methods are also highlighted in Appendix A. The data in the tests of Chapter 4 were generated test image sequences. A number of common motion sequences such as the “Suzie” image set are commonly used to test motion measurement. Some experimental output on a set of such image sequences is given in Appendix B.

Chapter 5 provides the experimental data for using the techniques used. This data was a set of real plant growth data provided by the School of Biological Sciences at the University of Nottingham. The effectiveness of the method proposed in this thesis is also compared to that of the current

method RootFlowRT and the main reason or the failure of that method is identified.

Chapter 6 summarizes the findings of the thesis and suggests some further work which is being implemented. The work for this thesis has been published and a copy of the paper is provided at the end of this thesis.

Chapter 2 Literature review

2.1 Plant Root Growth and its Measurement

Before the work of reported in [6] plant root growth was measured in a variety of ways. The earliest systematic ways are non-automated. The plant is germinated on a microscope slide in an aqueous agar solution and markers placed on the root. The measurements are made over long time periods so that significant growth can be seen. In the work of Wu, Ding and Zhu [13] for example the measurements took 7 days and were measured by ruler. Even under the microscope the resolution in such measurements is not good. None manual methods have been used, however. Jiang and Staude [14] have reported a method using interferometry. In their method a laser light is focused through the interferometer onto the plant tip. Plant growth will lead to sinusoidal variation in the light received at the output of the interferometer (see Figure 2.1). The size of the variations is dependant on the growth rate. Their reported resolution is down to growth rates down to 5 mm per day. However, the variation in this rate is plus or minus 10 mm per day. The main advantage of this process is that instead of the seven days reported in the manual measurement this process can produce results in a matter of minutes.

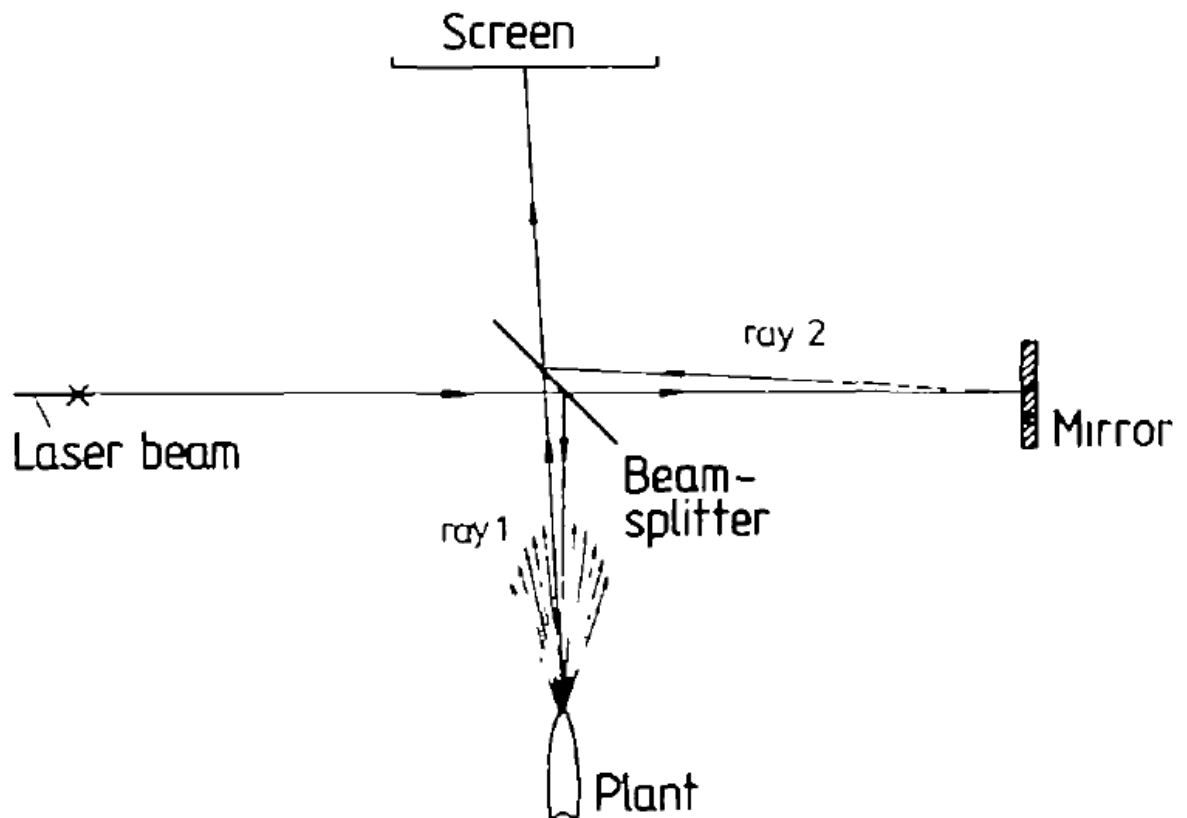


Figure 2.1 The experimental arrangement for the interferometer (from Z. JIANG and W. STAUDE1 1989 [14])

This approach was an alternative to that proposed by others who had used a mechanical technique made using a linear displacement transducer. This work was reported by Meur [15] and Penney et al [16]. The method is susceptible to the problem that it takes a long period (many days) to produce results but they do once again give a resolution down to 5 mm per day.

Typical mechanical techniques are exemplified by the work reported in [17]. In their experiment the growth rate of leaves was under investigation. The

process involved deliberately puncturing the leaves with needles and measuring the displacement of the holes produced using a ruler. The resolution of the measurement is thus low (plus or minus 0.5 mm) and measurements took between seven and fourteen days. It is significant to note here that as in the other work involving mechanical measurement the plant is interfered with and this will have an effect on its behaviour. However, this problem still persists with many non contact measurement methods.

2.1.1 Non Contact Optical methods

The common approach currently adopted by most Plant bio scientists and referred to as RootFlowRT by its designers as reported in [6] was built upon earlier work of a similar nature. The most significant work of that group is reported by Barron and Liptay in [18] based on the work of Horn and Schunck [20], or rather on the refinements by Lucas and Kanade [22] which itself was refined by Simoncelli et al [23]. It is useful to note that these methods have subsequently been refined further and it is this further refinement by Florack et al [24] and Niesen et al 1995 [25] as implemented by Niessen et al 1997 [26] that have been used in the current work (see chapter 4). The measurements by Baron and Liptay [18] claimed a resolution of 5 microns for images taken every two minutes over a period of 30 minutes. The experimental method set the scene for later work. This work measured growth rates down to 20 microns per second with an error rate of up to 10 microns per second. Subsequent improvements in available sensor resolution and the reduced cost of imaging systems would

imply that it would be possible to measure with a greater degree of reliability.

2.1.2 RootFlowRT

The work reported in [6] which is often referred to as RootFlowRT –the title given to it by its developers - was a combination of two techniques. The first is a measurement using a tensor method implementing the method of Barron and Liptay [18]. However, the approach proved of limited value and is reported by Jiang as giving only 5% reliability thus placing doubt on the work of Barron and Liptay. They chose instead to use a simple correspondence technique to base the major analysis on. This technique involves taking a sequence of images, generally one every ten seconds for a period of 90 seconds. Comparison is then made between blocks in one image and a subsequent image in order to find matches. The block matching method is potentially quite simple and effective. Their measurements were claimed to have high reliability (reportedly up to 85%) and give resolutions down to plus or minus one micron per second in growth rate measurement. The technique involves growing the roots in an agar solution much the same way as many of the previous techniques. The roots are then observed under a standard bright field microscope. The microscope slides are marked at different points in order to provide human identifiable registration points for later comparison between different parts of the root. The marking of the plants is thought to have some effect on the growth of the roots and the roots must be left for some time to readjust before measurements continue. One problem of the technique seems to be

that the roots are constrained to grow in a single plane (removing the natural out of plane spiral growth patterns normally experienced by plants) and are usually observed growing horizontally, rather than vertically, which would be the more natural direction for the roots to grow in. Observations are made along the root from the tip (which is referred to as the "quiescent centre" and is the point where most of the new cells are produced) to the area where the growth becomes more constant (and is associated solely with elongation of the cells). Measurements stop when side roots begin to be formed as other process start to dominate the growth at this point. The length of root that needs to be measured for the value of the experiments at the resolution used (about 4cm of root measured to a resolution of 1 micron) requires more than one stack of images to be taken. Registration of the stacks is achieved by the use of the external markers referred to earlier. An area of overlap of the order of millimetres is used between the slides to ensure that the full section of growth is measured. For each section (or stack) the images are captured of the background and then every ten seconds until 9 successive images have been taken. The stacks of images are taken by refocusing on the surface of the root. This has inherent problems as the field of view that is in good focus is limited and the level of reflectance varies over the surface. An example image is shown in Figure 2.2. The correspondence technique used will be described in full later in this chapter and the cause of major errors in this technique will be discussed later in the thesis (chapter 5). The technique has been popular and a high proportion of plant biologists in addition to its originators use

RootFlowRT to make their measurements to this day (see for example [33]). This method is also used in the University of Nottingham School of Biosciences. They report using a combination of RootFlowRT for fine analysis of growth variation and manual methods that last for periods of 5 days or more for their measurement. Private correspondence with one of the authors of [33] revealed that use of the RootFlowRT software was difficult. They showed some evidence of not understanding how the software worked and as a result had placed unnecessary restrictions on their own experiments. They believe their experience to be common for others using the software. [34]

2/07/2004 10:21:50

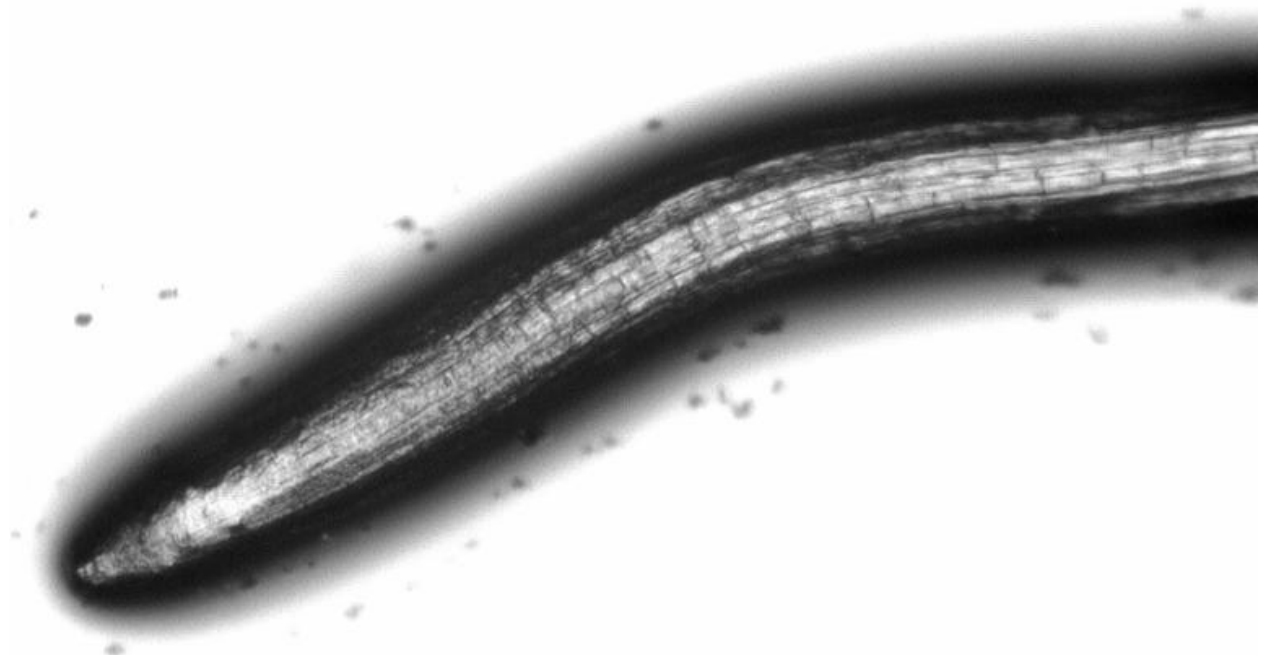


Figure 2.2 a typical root image used in the measurement of root growth. Notice that the tip area has a significantly different intensity level from the middle of the image and the middle section of the image is in better focus (and shows more detail as a result) than the extremes.

The RootFlowRT software was made available as open source and so it has been possible to use it for comparison purposes. The authors of [35] provided the current research with their results from using RootFlowRT as well as the image sequences they had used. Their experiments were repeated using RootFlowRT and the technique developed in this thesis. Significant differences were found in the initial measurements and so a set of experiments were carried out which have shown significant sources of error in the results produced by RootFlowRT. This is discussed further in chapter 6.

2.1.3 Measurements Using Confocal Microscopy

The basic concept behind confocal microscopy is to allow the microscope to focus on specific and limited focal planes, deliberately reducing the focal depth. The position of the focal plane can then be varied to obtain images at a number of different depths within the target. The method is explained in full in [37]. In plant biology the technique has obvious benefits. In particular for investigating the cellular structure of the roots the focal plane can be made to move through the root to obtain a cross-section of the root showing the outline of the cells.

Such techniques are more complex to operate and more difficult to set up than those using a simple bright field microscope. They are not, therefore, as widely used but provide an interesting new way to approach the

measurement of not just the root growth of plants but the cell growth directly. The process involves dying the foodstuff of the plants with fluorescent dyes which show up in the plant. This also allows the transport of the foodstuffs to be viewed. However, many of the dyes cause the plant to expire and are thus no use for measurements of growth. Work by Roberts et al [38] for example has succeeded in measuring growth of individual cells. They report that while the

"Lucas Kanade feature tracker ... was, as one would expect, accurate around resolvable structure. It was not able to track the smaller, repetitive cell structure in the root tip and was somewhat prone to identifying spurious features." [38]

They thus expand on this method using Bayesian methods and Markov random Field modelling. Of particular concern in their method is the fact that smoothing used to remove ambiguities from their results has lowered their accuracy.

Work by Sethuraman et al [39] has used the network snakes approach to measure and track the cell growth. They have concentrated on self initialization of the tracking snakes as this is necessary for the automation of the process.

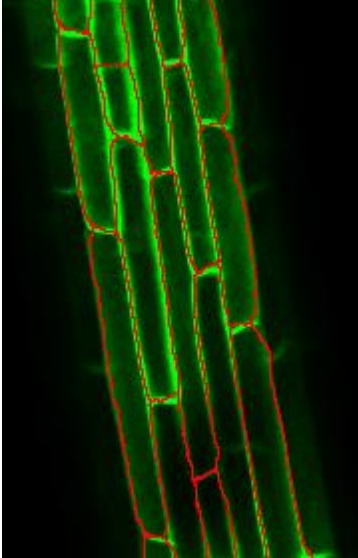


Figure 2.3 Showing the result of the network snake assignment algorithm (from Sethuraman et al [39])

While they report success in their technique they have not so far published results on the accuracy and resolution of their method.

2.2 Motion Estimation Background Review

While the work discussed in section 2.1.2 is an interesting extension of the process of measuring plant root growth it is an expensive and complex process and one which most plant biologists are currently not using. They are using the RootFlowRT software referred to before but as has also been stated this method has been demonstrated to be flawed both in its accuracy and reliability. It is thus useful to review how motion estimation has been carried out and identify the specific characteristics of bright field microscope images of plant roots that might introduce the problems encountered by users of RootFlowRT.

Many approaches to motion estimation have been adopted. These are usually adapted to the type of task they undertake. A lot of early work was done on tracking for the purposes of video compression. Work has also been undertaken for a wide variety of other purposes. The main techniques currently in use for measuring plant growth are differential measurement methods or block matching correspondence methods. The reason that these methods have been chosen is related largely to the nature of the images. The images have no reliable feature types for feature recognition. There are no edges or significant corners for example in the growth area so methods like those of Nistér et al [40] which make use of corner detection. Such methods have been particularly successful and can work at frame rates of normal video (25 frames per second). There are features of a low contrast and non geometric nature and while these can at times be detectable to the human eye they are not generally definable and so cannot be located automatically to aid tracking methods. Other successful methods of tracking require clustering of like local areas of images and identify features as the boundaries of these clusters. The method of Heikkila and Pietika [41] for example give very good tracking possibilities when working with images where the distribution of pixels in the target object are quite different from that of its neighbours. (For further examples of the background to these developments see [42][43][44][46][47][48][49][50] and [51]) While this would be significantly true for the root outline compared to its background the need in the case of root growth measurements is particularly to measure the difference of areas within the

root from one another. These differences are very small and so not only does a measurement method need to be accurate it also has to be reliable (have a low standard deviation). This will be discussed later as it is a particular problem with RootFlowRT.

Methods based on Kalman Filters and Markov models could be useful as they make use of statistical estimates of the distribution of flows in a given region. However, seeding of these will not be easy to automate. In the Kalman method for example a filter requires an initial estimate of the motion in order to provide the model which is used to modify the future measurements. The initial seeding of the filter would require some form of measurement such as derived from a tensor method or some form of correspondence method. However, as will be shown in the experimental chapters for the latter methods to work well the initial search space needs to be well defined. The former methods do not give sufficient reliability of the measurement to gain a good source for a Kalman filter model. For an example of a Kalman filter in use for estimating motion see [52] (Further work with tracking that uses such modeling and segmentation processes are found in [53][54][55][56][57][58][59][60][61] and [62]). The method of [52] for example uses a colour modeling method for identifying the features being tracked and in itself would be unsuitable as explained above. The grey scale distribution of any region of the root is very similar to any other region and so this also makes it impossible to identify any areas to use to automate the modeling and tracking process. A further example of use of

Kalman filters in object tracking can be found in [62] but again this relies on colour separation.

The methods that give most opportunity for measuring the root growth automatically are thus based around the differential methods and the block matching correspondence methods. It is thus useful to look at how these methods have developed. It is also valuable to note that it is a combination of these methods that have been used in RootFlowRT and yet this software has significant failings.

2.2.1 Differential methods

Differential methods have been tried for a long time and there have been a significant number of developments that have refined these methods. The first work in this area of real significance is that of Horn and Schunck [20] as mentioned earlier in this thesis. This method and most others make use of two general constraint equations. In words these two constraints can be described as the idea that all pixels will move with their nearest neighbours and the luminance constraint which is that pixels will have the same luminance in subsequent images. The two constraints lead to the basic equations for the method. These have been described elsewhere and in terms of the method used in this work will be given in detail below. The biggest problem found by Horn and Schunck was described by them as the "aperture problem". That is the direction of flow of a pixel cannot be guaranteed if the whole of the feature to which it belongs is not visible

within the image. In the original methods attempts were made to get around this by requiring that both the constraints be maintained simultaneously. The process was to find a minimal solution for the brightness constraint and then determine the error in the constraint that nearest neighbours should move together. This leads to a requirement that the result of the brightness constraint equation be re-satisfied. A sequence of iterations is then undertaken until the error in both sets of measurements is minimized. A lot of possible problems arise in this method. One simple practical one is that digital images are just that, digital. As a result they cannot be differentiated without some cost. The early work in the use of the differential methods made use of simple operators such as the Sobel operator. This by nature not frequency limited and so introduces the inevitability of producing aliasing. More recently the use of Wavelets and Gaussian differential functions has been tried. The advantage of these functions is that they can be chosen to have more limited bandwidth than the Sobel or other simple operators. Wavelets (such as the Debauchie 9, 7) have been used to great effect in the compression of video images. The resultant compressed images from this compression, which is used in the JPEG 2000 compression standard is a much less pixilated solution, so that even at high levels of compression the images appear to have few artifacts. In development of differential based optical flow measurements the Gaussian has been preferred as the basis for the differential operator. This has significant advantages for those working with them. Higher level differentials of the Gaussian function can be found by simple multiplication

and addition to lower level differentials. This makes the computation process both in terms of time taken and memory usage much more efficient. Its proponents (such as Niessen et al [26]) also propose it as a suitable system for vision applications because of the similarity of the Gaussian function to the processing done by the human front end vision system. This may or may not be a reason for using this but one real practical advantage is the flexibility of the Gaussian function being used as a scaling factor. The Gaussian in one dimension is given by the formula below

By changing the value of σ a degree of blurring will occur. This is similar to the effect of stepping backwards (or forwards). This has the value of reducing the effect of high frequency features and allowing more general measures to be taken. It will be shown later that this can be very valuable when looking at the particular case of the measurement of plant root growth. However at a high value of σ there will be a lower resolution and so a means is needed of finding a finer scale measurement as well. In the work in this thesis this has been done by combining the scale space differential method with a high resolution correspondence method. The details of this are given in the next chapter on methodology and the background literature on correspondence methods is given in the following section.

Following on from the work of Horn and Schunck a number of developments have been made to improve on the effectiveness of these methods. One of the major approaches was proposed by Lucas and Kanade [22] as stated earlier. This method is particularly of note because it uses the assumption that flow is basically constant in a given area. This can introduce problems when a significant variation in local flow is concerned and in many areas it breaks down. With the low contrast images in use in the current work this method has not given any more significantly reliable results than those of the Horn and Schunck approach. For that reason further developments were investigated. However a number of people have used this approach and Bruhn et al [64] made interesting use of combining the two techniques. Others whose approach are based on one or other of these two techniques are Brox et al [63] whose work concentrates on the theory of warping and De Carlo and Metaxis [65] who earlier made significant use of similar techniques in their work on face recognition. Interesting later developments were introduced first by Niessen et al [26] and also developed by Florack and van Assen [31]. These methods make use of higher order differentials in their analysis. The results have seen significant success in a number of areas. In particular the work of Florack was extended by ter har Romeny and others [28] and is brought together by in book form in *Front-End Vision and Multiscale Image Analysis* [29]. The work by Becciu et al [30] give a detailed discussion of how the work of Horn and Schunck has been developed through the subsequent work and that of Lucas and Kanade with the improvements found in Brox and Bruhn and

later developments by Florack and Niessen have produced the approach espoused by Romeny in his book [29]. In that book he also proposes that scale space approaches can be used to solve any image processing and vision problem. His basic premise depends on the concept (as stated earlier) that the human eye processes images using a set of neural connections that have similar effects to the use of a Gaussian filters. This approach is particularly valuable for reasons that are pointed out in the next chapter. By using a continuous function as the basis of your differential operator the whole image processing process can remain mathematically rigorous and at the same time a great reduction in aliasing takes place. Thus rather than the methods of Horn and Schunck used by Jiang and others in previous work [6] the use of the scale space based method of [29] was adopted in the current work.

2.2.2 Correspondence methods

The simplest approach to finding where one pixel has moved from one image to the next in a sequence would be to search for all pixels of the same intensity in the new image. This would obviously result in a number of matches. Also though the brightness constraint requires that the pixel would in theory have the same value, fluctuations in lighting and sensor noise will result in significant variations and it is unlikely to find good matches. Block matching methods as for example used by [71], [72], [73] and [74] have often proved valuable. Here a combination of local area pixels are chosen as a block and the corresponding block is searched for in the new image. While this will still be subject to possible errors it is

possible to choose minimisation approaches that will choose the best fit between two blocks.

These methods have in general been quite successful. They were used for example by Puri et al [74] for motion detection in video sequences and have since been successfully used in standard compression for video film. Various algorithms have been used to improve the efficiency of this matching for example in for example Chan et al [71] and Gao et al [72] who developed a multi level elimination approach.

One of the major issues in using the RootFlowRT software of van der Weele et al [6], which is in common use by plant biologists, is that there are large variations in the results it predicts. This is despite it using what they refer to as "forward backward matching" to aid the robustness of the method. In principle this approach should improve the reliability of the measure. In principle a correspondence is only accepted between two pixels in the forward match if the backward match (treating the images in the opposite order) returns to the same pixel or to its nearest neighbours. In the current work the reason for this discrepancy has been found and is removed when a multi scale approach is adopted. This is outlined in the methodology chapter following.

2.3 Summary

In this chapter the importance of automatic measurement of plant growth has been highlighted. Some of the methods previously used have been emphasized. Despite the development of complex approaches to measuring growth for example the use of confocal microscopy, the main method currently in use by biologists is still the use of bright field microscopy. The main software that has been used in this work (RootFlowRT) by biologists has been identified as faulty and thus new approaches that give more reliable results are necessary. The approaches that seem to offer best opportunity of success are a combination of the Scale Space Optical Flow method of ter Har Romeney [29] and some form of correspondence method. These approaches were thus investigated as explained in the following chapters.

Chapter 3. Methodology

In chapter 2 the background to this research was identified. The motivation for measuring plant root growth was established and the need to do this bright field microscope image sequences was established. The alternative approach taken using confocal microscopy was also alluded to but it was pointed out that this method is very expensive and much work is still being undertaken by biologists using conventional microscopy. It was pointed out that the current software commonly in use is RootFlowRT and that this software suffers from major limitations. The major task of the biologists is to measure the change in growth rates along the central stem of the root. The information gained is critical in understanding the growth mechanisms of the plants and whether the experiments in the cell biology are being successful. The variation along the stem can be by as little as $5\mu\text{m}$ per second. However analysis of the RootFlowRT method (discussed further in detail in Chapter 5) has shown that it generally can only give measurements of $\pm 5\mu\text{m s}^{-1}$ and so it is vital to find a method with higher accuracy and repeatability. RootFlowRT is based around two methods – a modification of the tensor method proposed by Horn and Schunck and a block matching correlation method. As was pointed out in Chapter 2 the method of Horn and Schunck [20] has been extended and improved by others such as Lucas and Kinade [22] and this work has subsequently led to the developments of somewhat more reliable approach covered by ter har Romeny in [29]. The early work on RootFlowRt had shown their measurements using the tensor method to be unreliable so that they base most of their judgements on their block matching correspondence method. In this work it was thus decided:

- To look at the scale space optical flow approach to measuring the growth
- To look at the reasons for the failure of the block matching method used by RottFlowRT
- To search for a method of improving the output to improve the reliability of the block matching method and thus

- To improve the reliability and accuracy of the root growth measurement

The scale space approach to optical flow measurement was thought to be of better potential for measuring the growth than the approach taken by RootFlowRT because it makes use of the more physically realistic approach to taking differentials. This choice of scaling control chosen was the Gaussian as this can be flexibly and efficiently implemented. Other wavelet based approaches are possible but the flexibility of the final implementation and the closeness of the Gaussian function to the physical processing used in the human front end vision system were taken as a good reason for their use. The approach taken in the correspondence method was based around a simpler scaling method using a simple mean filter. This method has inherent problems in introducing spurious structure at the low level but the results of experiments showed that this had no effect on the final fine detail measurements. Other approaches, such as the use of image clustering techniques were rejected due to the low contrast nature of the images and the lack of identifiable features for feature tracking approaches.

The work was then broken down into a number of stages:

- Develop and implement the software for the scale space optical flow
- Test the method using a set of standard test image sequences
- Develop the scale based block matching algorithm
- Test this method using the standard test image sequences
- Compare the results of the first steps
- Develop a set of artificial test images with characteristics similar to those of the root images for testing the accuracy and reliability of the two methods
- Measure and evaluate the methods developed
- Select a set of representative real root images
- Develop some ground truth measurements for the growth in these images

- Measure these images using the RootFlowRT software
- Measure these again with the scale space and block matching algorithms
- Evaluate the results

The next two sections highlight the important details of the methods. After this the approach to establishing some form of ground truth for the real root image sequences is highlighted. The next chapter looks at the evaluation of the methods using the standard image sequences and this is followed by a chapter investigating the use of the methods developed on root growth image sequences and compares these with the previous work.

3.1 Scale Space Optical Flow

As described in Chapter 2 and mentioned again above the earliest work on optical flow using differential methods was outlined by Horn and Schunck [20]. Others followed on from this work and include Lucas and Kinade [22] who made much of the constraint on local image flow, ensuring that the local image gradients should be the same. This method has limitations for images such as those in the plant growth experiments as local field flow can be subject to large amounts of noise. According to Becciu et al [30] the method of Lucas and Kinade was "impressively improved" by Brox et al [63] and later by Bruhn et al [64]. Barron [32] later introduced a three dimensional optical flow estimator which was later applied to MRI by Florack and van Assen [31] who introduced the idea of a multi scale implementation. This approach was also presented by Niessen et al [25]. Ter Haar Romeny has provided an elegant description of this in [29]. In the current work the approach of ter Haar Romeny has been adopted. This approach is significantly more reliable than previous approaches. The use

of the scale factor (σ for the Gaussian when used as the basis for the scaling) enables the method to be tuned to give best results for a given problem. The following is a description of this method as implemented in the current work.

Assumptions made in developing the solution using the Gaussian Differential Operator for Scalar Optical Flow are:

- The observed intensities are constant over time
- The velocity smoothness constraint
- No discontinuities in the optical flow vector field – except at the occlusion boundaries
- The differential of the local luminance stays constant

A dynamic image as a function of position and time can be expressed as follows:

$$L(x + dx, y + dy, t + dt) = L(x, y, t) + L_x dx + L_y dy + L_t dt \quad (3.1)$$

Where $L(x, y, t)$ refers to image luminance at point (x, y) at time t , and L_x , L_y and L_t denote the partial derivatives of L (local luminance) with respect to x , y , and t . The work was implemented first using Mathematica and in that software the function $D[L, x]$ gives a value of partial derivative L_x .

Due to the intensity changing steadily, point (x, y) is translated some distance (dx, dy) during the interval dt then:

$$L(x+dx, y+dy, t+dt) \approx L(x, y, t) \quad (3.2)$$

From equation 3.1 and 3.2:

$$-L_t = L_x * \left(\frac{dx}{dt}\right) + L_y * \left(\frac{dy}{dt}\right) \quad (3.3)$$

The goal is to compute the velocity:

$$c = \left(\frac{dx}{dt}, \frac{dy}{dt}\right) = (u, v) \quad (3.4)$$

With the extra different external information/conditions provided, a set of spatio-temporal optical flow constraint equations can be obtained.

Assuming the spatial scales with respect to x and y are σ_x and σ_y and the temporal scale τ , the luminance distribution for the image with Gaussian Differential Operator in the spatial and temporal domain is:

$$g(x, y, t) := \frac{1}{\sqrt{2\pi\sigma_x^2}} \frac{1}{\sqrt{2\pi\sigma_y^2}} \frac{1}{\sqrt{2\pi\tau^2}} e^{-\frac{x^2}{2\sigma_x^2} - \frac{y^2}{2\sigma_y^2} - \frac{t^2}{2\tau^2}} \quad (3.5)$$

The convolution F of the image sequence with the Gaussian Kernel can be expressed as:

$$F[x, y, t, \sigma, \tau] = L \otimes g = \int_{-\infty}^{\infty} \int_{-\infty}^{\infty} \int_{-\infty}^{\infty} L(x, y, t) g(x, y, t, \sigma, \tau) dx dy dt \quad (3.6)$$

To capture the rate of change along the vector field, Lie Derivatives [29] are introduced here. Due to the fact that luminance doesn't change in the derivations we get:

$$L_{\vec{v}} F[g] \equiv 0 \quad (3.7)$$

Where $L_{\vec{v}}$ denotes the Lie Derivative with respect to vector field. We can express this equation using the Gaussian Kernel:

$$L_{\vec{v}} F \otimes g \equiv F \otimes (L_{\vec{v}} g) \quad (3.8)$$

The first Optical Flow Constraint Equation for Scalar Image (under convolution) derivative is thus:

$$-\int_{-\infty}^{\infty} \int_{-\infty}^{\infty} \int_{-\infty}^{\infty} L(x-x', y-y', t-t') \text{Grad } g(x, y, t) \cdot \nabla(x, y, t) dx' dy' dt' = 0 \quad (3.9)$$

In the normal constraint where the partial derivative L_x and L_y are constant, we get:

$$-vL_x + uL_y = 0 \quad (3.10)$$

We can derive the other 6 Optical Flow Constraint Equations from the equations [3.9] and [3.10] with respect to x , y , and t .

The velocity change along the Optical Flow vector field, for example u the x -component can be derived from the integration of the velocity change with respect to x , y , t . same to v the y -component, where

$$\left(u = u + x * u_x + y * u_y + t * u_t, v = v + x * v_x + y * v_y + t * v_t \right) \quad (3.11)$$

The 8 variables $\{u, u_x, u_y, u_t, v, v_x, v_y, v_t\}$ can then be approximated from the 8 Optical Flow Constrains Equations:

$$\begin{pmatrix} L_x & L_y & \tau^2 L_{xt} & \tau^2 L_{yt} & \sigma x^2 L_{xx} & \sigma x^2 L_{xy} & \sigma y^2 L_{xy} & \sigma y^2 L_{yy} \\ -L_{xt} & -L_{yt} & -L_x - \tau^2 L_{xtt} & -L_y - \tau^2 L_{ytt} & -\sigma x^2 L_{xxt} & -\sigma x^2 L_{xyt} & -\sigma y^2 L_{xyt} & -\sigma y^2 L_{yyt} \\ -L_{xy} & -L_{yy} & -\tau^2 L_{xyt} & -\tau^2 L_{yyt} & -\sigma x^2 L_{xxy} & -\sigma x^2 L_{xyy} & -L_x - \sigma y^2 L_{xyy} & -L_y - \sigma y^2 L_{yyy} \\ -L_{xx} & -L_{xy} & -\tau^2 L_{xxt} & -\tau^2 L_{xyt} & -L_x - \sigma x^2 L_{xxx} & -\sigma x^2 L_{xxy} - L_y & -\sigma y^2 L_{xxy} & -\sigma y^2 L_{xyy} \\ L_y & -L_x & \tau^2 L_{yt} & -\tau^2 L_{xt} & \sigma x^2 L_{xy} & -\sigma x^2 L_{xx} & \sigma y^2 L_{yy} & -\sigma y^2 L_{xy} \\ -L_{yt} & L_{xt} & -L_y - \tau^2 L_{ytt} & L_x + \tau^2 L_{xtt} & -\sigma x^2 L_{xyt} & \sigma x^2 L_{xxt} & -\sigma y^2 L_{yyt} & \sigma y^2 L_{xyt} \\ -L_{yy} & L_{xy} & -\tau^2 L_{yyt} & \tau^2 L_{xyt} & -\sigma x^2 L_{xyy} & \sigma x^2 L_{xxy} & -L_y - \sigma y^2 L_{yyy} & L_x + \sigma y^2 L_{xyy} \\ -L_{xy} & L_{xx} & -\tau^2 L_{xyt} & \tau^2 L_{xxt} & -\sigma x^2 L_{xxy} - L_y & L_x + \sigma x^2 L_{xxx} & -\sigma y^2 L_{xyy} & \sigma y^2 L_{xxy} \end{pmatrix} \begin{pmatrix} u \\ v \\ u_t \\ v_t \\ u_x \\ v_x \\ u_y \\ v_y \end{pmatrix} = \begin{pmatrix} -L_t \\ L_{tt} \\ L_{yt} \\ L_{xt} \\ 0 \\ 0 \\ 0 \\ 0 \end{pmatrix}$$

(Romeny [29])

(3.12)

As stated earlier these equations were first implemented in Mathematica.

The solution that is looked for is values for u and v . These are obtained from the measurements give the value of $L(x, y)$ at any point in the image.

The derivatives L_{xy} , L_{tt} , and so on can be derived using any differential operator but in this case appropriately the Gaussian derivatives have been used. The Gaussian derivatives of any order can be calculated from as a sum of derivatives of lower order by the use of the Hermite functions [76]. This makes the process relatively simple to implement. Once the various derivatives have been computed the value of the left hand side of equation (3.12) can be computed. Thus by multiplying both sides by the inverse of this matrix and performing the matrix multiplication it is possible to evaluate u and v directly (as well as u_t , v_t etc.) As stated above the particular value of using Gaussian derivatives for this process is that σ_x , σ_y and τ can be used as scaling functions. Normally $\sigma_x = \sigma_y$ is chosen as the dimensions are equivalent. Any value of σ can be used and is effectively the same as getting closer to or further from the image. This has the advantage in the current work that a scale can be chosen such that the effect of rapid local variations is reduced without limiting the resolution of the values of u and v too much. In practice in the main experiments, using root growth images, sequences of only 9 images were used and a value of $\tau = 1$ or 2 was the only sensible value applicable. Experiments showed that the rate of growth was sufficiently constant for this value chosen not to make a significant difference to the results.

3.2 Correspondence methods

In many ways block matching correspondence methods are the simplest form of motion estimation technique. The basic assumption of the method is that pixels move with their nearest neighbours. While an individual pixel

would have many hundreds or even thousands of possible matches in a given image a group of nearest neighbour pixels would be far less likely to have very similar matches in an equivalent image in a sequence apart from surrounding the equivalent pixel. However for the images in the root growth problem the situation turns out to be not so simple. The major issues that are common to block matching correspondence measures are:

- How big a neighbourhood block is needed?
- What are the limits of the search space?

In principle the bigger the block the more likely a match is to be unique.

However, the computation time of the best match is strongly determined by the number of pixels in the block. Again the search space used (the area in which a new block is searched for) will strongly affect the time taken for a match to be chosen. However, if the block is too small or incorrectly placed the pixel being searched for may not be within the search space. A best match may well be found but it will not be the pixel that is being searched for. The basic approach of the method is given below.

3.2.1 Block matching basic approach

As explained above, it is assumed that a pixel moves together with its neighbour pixels in a block. In order to find the movement for one pixel, the whole block's movement is measured. The immediate first issue of concern is the correct size of block to use. One key factor for choosing block size is the size of the objects that need to be tracked. E.g. in a traffic tracking application, the movement of each object in the scene might be considered significant. In the case of plant root growth it is vital to see changes in

motion over fairly short distances so the size of the block needs to be as small as possible while not inhibiting the recognition process. Bigger blocks are less sensitive to noise and smaller blocks produce better contours. It is a challenge to find a way to balance the size with respect to the amount of motions expected in the sequence. In the case of plant roots a number of other issues are significant. The insides of the roots have no distinct features so no feature related block shapes and sizes are relevant. However the nature of the image indicates that small regions of the image have very similar gray scale values and profiles. Thus factors like the amount of noise in the images, the texture of the objects and background also are factors to determine the block size.

In work on plant root images, sequences are taken with time interval of 10 seconds and 9 images in a sequence. Plant roots grow at rates of the order of 5-8 μm per minute [36] which is a relatively a slow motion compared to many other cases, so the distance moved over the full sequence is of the order of 8 to 12 μm which is equivalent to between 3 and 10 pixels over the sequence. This has implications for the block size and the size of the potential search space. Many of the motions being measured will be of non integer pixel distance. This combined with the rapidly changing surface orientation of the roots imply limits to the possible accuracy of matching of small blocks. However, as has been said earlier large blocks would result in a considerable time overhead. Thus, a range of block sizes has been applied and tested in this work to prove its suitability for the investigation.

Test results of various block sizes have been given in the next chapter. The fact of a measurable spatial motion in a sufficient period of temporal sequence will allow the algorithm to return a matched block within the sequence.

In this method it is assumed that at least one matched position will occur for a block within the search space. Figure 3.1 illustrates the general approach. This figure represents two images from a sequence in which a match is being searched for. The original pixel, shown in black in the left image has moved to the position indicated by the black square in the right picture. The red rectangle (in this case a 5 by 5 block) represents the neighbourhood of the pixel being tracked and the larger rectangle in the right hand picture the search space in the new image. In the experiment both the block dimensions and search space were varied to determine the most suitable dimension for both. In the final software the search space is determined automatically from the output of the scale space optical flow measurement as will be explained later.

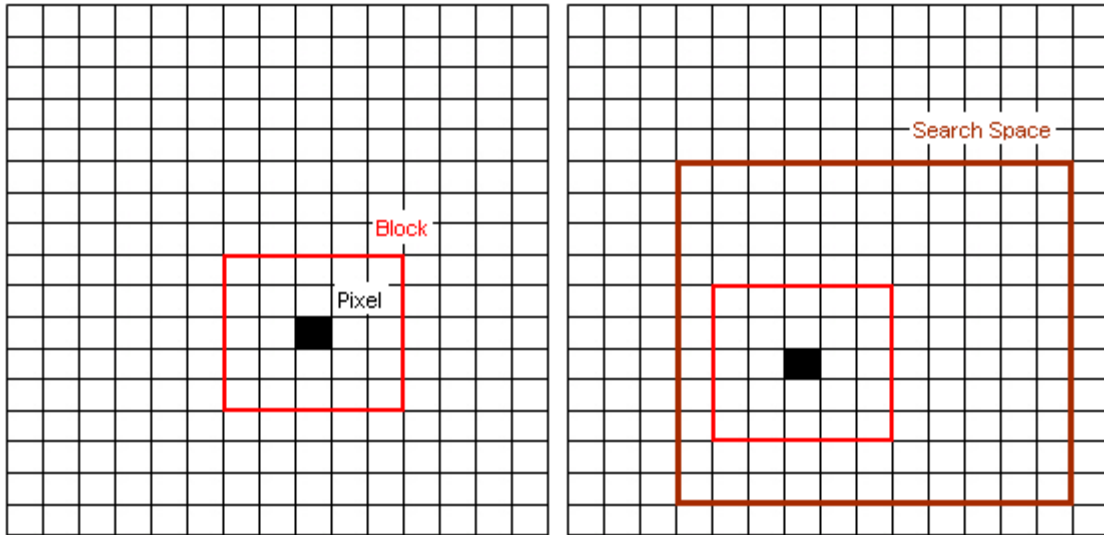


Figure 3.1 Block Matching within Search Space - Assume the Pixel highlighted in Black in the left image has moved together with its neighbour pixels in a block of 5x5. Due to the small amount of expected movement in between images (as explained previously) a limited search space can be predefined.

A match between blocks within the search space is derived as follows:

$$L_1(x+dx, y+dy) = L_2(x'+dx, y'+dy) \tag{3.13}$$

Where

- $L_1(x+dx, y+dy)$ Denotes the pixels in the first images and
- $L_2(x'+dx, y'+dy)$ denotes the matched pixel found in the second image.
- $|dx| \& |dy| \leq BlockSize$
- $|x'-x| \& |y'-y| \leq SearchSpace$

Initially there will be one-to-many matches so a means has to be found to determine the best match within the search space. Many ways of

determining a best match have been used. In the current work the absolute values of the difference between the original block and the matched block with the minimal value is chosen. In other words, pixel L_1 has matched pixel L_2 within the search space only if their local luminances have the closest value:

$$SAD = \sum_{\substack{|dx| \leq BS \\ |dy| \leq BS}} |L_1(x, y) - L_2(x+dx, y+dy)| \quad (3.14)$$

Therefore the motion vector field can be defined as:

$$\vec{v}(x, y) = \text{Arg}(\text{Min}(SAD(x', y')))$$

Where $\vec{v}(x, y) = (u_x, v_y)$ and u_x is the x motion at the current point and v_y is the y direction motion.

It is also possible to add the process of forward and backward matching correspondence to this process to improve the reliability of a measure. However, as will be shown in the results of the experiments on actual roots this should also take account of whether the constraint that neighbouring pixels all move together has been taken into consideration. Forward and backward matching is the process where a match between pixel (x_1, y_1) in the first image with pixel (x_2, y_2) in the second image is accepted if and only if the best match for pixel (x_2, y_2) in image two is with pixel (x_1, y_1) in the

first image. It may not be obvious at first why this might not be the case.

However, it should be remembered that in root growth:

- Image motion is not generally an exact integer number of pixels
- The surface texture varies rapidly
- Many surface features repeat regularly
- Some rotational motion occurs as the plant root grows

3.2.2 Search Space and Multi resolution

It remains a challenge to determine the size of the search space. In this work the search space has been adapted using Multi-resolution or multi scale technique, it not only helps to determine the size of search space but also saves computation time and improves speed and accuracy. In this way the vector field is first calculated for at a lower scale (coarser level) resolution then is refined for a higher-scale/finer resolution image.

Information from the coarser resolution image is used to limit the search space used for the finer resolution image. In the final implementation the values of search space were also modified on the basis of the results of the scale space optical flow measurements.



Figure 3.2 Example of multi-resolution pyramid image representation. Images are scaled by a linear factor of 8 (left hand image) and matching done at this level. The results are quickly obtained from this measurement and used to restrict the search space for the scale 4 image (the second image). This is repeated till the full scale image has been dealt with. The advantage is that general values can be quickly found at the low resolution stage leaving a much smaller search space in the high resolution thus leading to a more rapid overall calculation time.

A number of approaches have been proposed for efficiently and accurately producing the scaling used in the multi resolution method. The work of Bergen et al. [62] for example is based on a Laplacian pyramid and a coarse-to-fine Sum of squared difference (SSD). This method tends to cause major errors at coarse levels then it passes the values to finer level. Singh [75] first computes the SSD values with three adjacent band-pass filtered images then propagates the velocity using neighbourhood constraints. Ultimately these methods provide reasonably accurate results but the computation speed usually poor. It sometimes depends on how close the motion was to an integer number of pixels per frame. For all these methods it is difficult to measure sub-pixel motion, as the block size and search space must all be integers. In this work two approaches have been taken in scaling. The first uses a simple mean filter. A second approach is

to use a Gaussian filter of varying values of scale factor to produce the scaling. The time saving on using the mean filter makes this more acceptable and the accuracy found in the experiments was not improved by using the more complex filter. The mean filter was thus adopted for the measurements

The motion estimation algorithm proposed here is Block-Matching Motion Estimation with Adaptive Search Space and Median Filter.

The assumptions behind the block matching approach can be summarised as follows:

- Two sequential images are input to the system
- The observed intensities are constant between images
- Images are composed of moving blocks
- Maximum velocity – no point will move further than a certain distance thus allowing a limit to the size of the scan space
- One and only one block in the second image matches a given block in the first image
- Common motion – all points in a block move in the same way

Other than block size the parameter that has to be set is the search space – over what area will the search take place in the second image for a block from the first image? Assuming a set maximum velocity can limit the size of search space, which will save processing time.

If the process starts with an assumption that the direction of motion is unknown but the maximum speed is n pixels per image in any direction. The search space will then be fixed as $2n + 1$ in all directions. Thus if $n = 1$ the search space will be 5 by 5. The matching condition thus becomes:

$$L_1(x, y) \approx L_2(x' + dx, y' + dy) \quad (3.15)$$

Where $|x' - x| \leq n$ and $|y' - y| \leq n$.

It's unlikely that the block in the new image will have exactly the same luminance value as the equivalent block in the first image at all the times. In the current application to determine which block in image two that corresponds to a block in image one, the Sum of Absolute Difference (SAD) between the block in image 1 and all the blocks in image 2 is calculated within the search area. This is illustrated in Fig 3.4

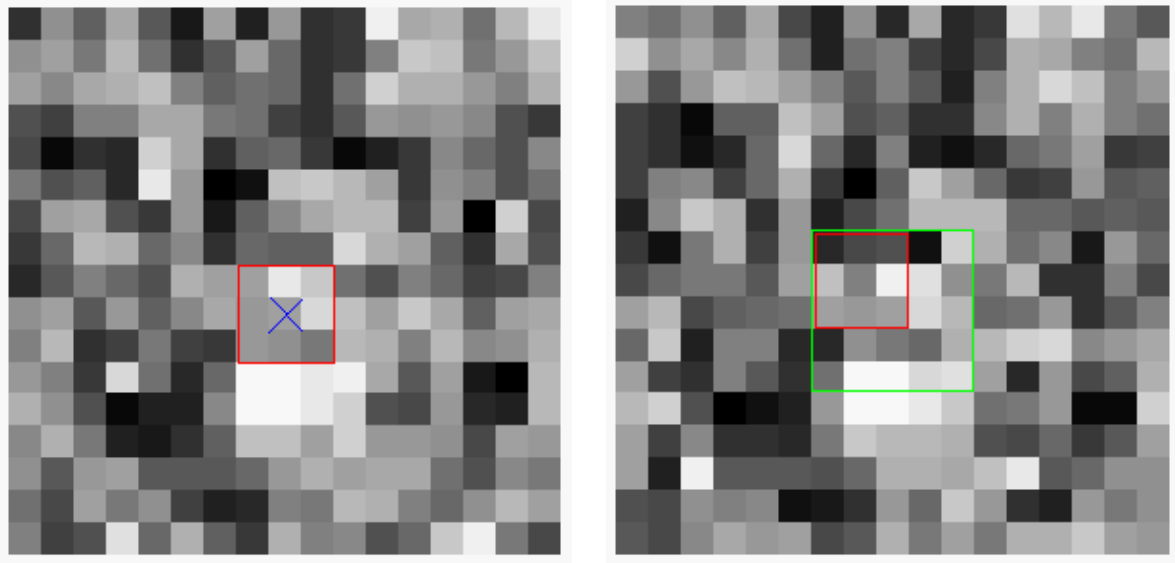


Figure 3.3 searching the minimum value of Sum the Absolute Differences for each block within the Search Space. (In order to measure the displacement for the centre pixel – marked with X in the left hand image, it is assumed that it moves together with its neighbours forming a block. Right hand image – the block is searched for within the Search Space in the 2nd image in the sequence. Normally it starts searching from the upper left corner and proceeds to the right and down until the bottom right corner of the search area, one row at a time)

To save memory usage and improve the searching speed the multi resolution approach is taken. In this approach the motion vectors are first calculated for a lower resolution image and the information from this used to modify the search area for a higher resolution image. While this introduces an extra step it significantly reduces the time taken to do the search at the higher resolution. This process proceeds as follows:

The original image 1 and image 2 are reduced in resolution (assume that the original images are all at resolution level 0) to a lower level in order to get a smaller image size for processing. At level 0 image1(x, y) is reduced

to for example level 1. The new pixel values in the level 1-image1 are calculated using:

$$Level_1 [image_1(x, y)] = Level_0 \left[image_1 \left(\frac{x+1}{2}, \frac{y+1}{2} \right) \right] \quad (3.16)$$

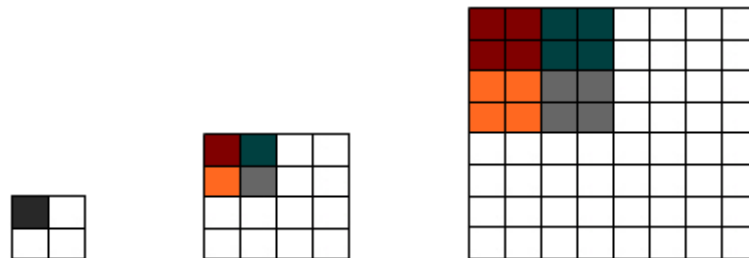


Figure 3.4 Example of multi-resolution pyramid image representation

Motion vectors at lower level resolution image will be calculated first. Instead of working on a given / fixed value of search space, now we adapt the motion vectors from lower level of resolution as a reference to determine the higher-level resolution image's search space. Figure 3.6 gives an example of this process.

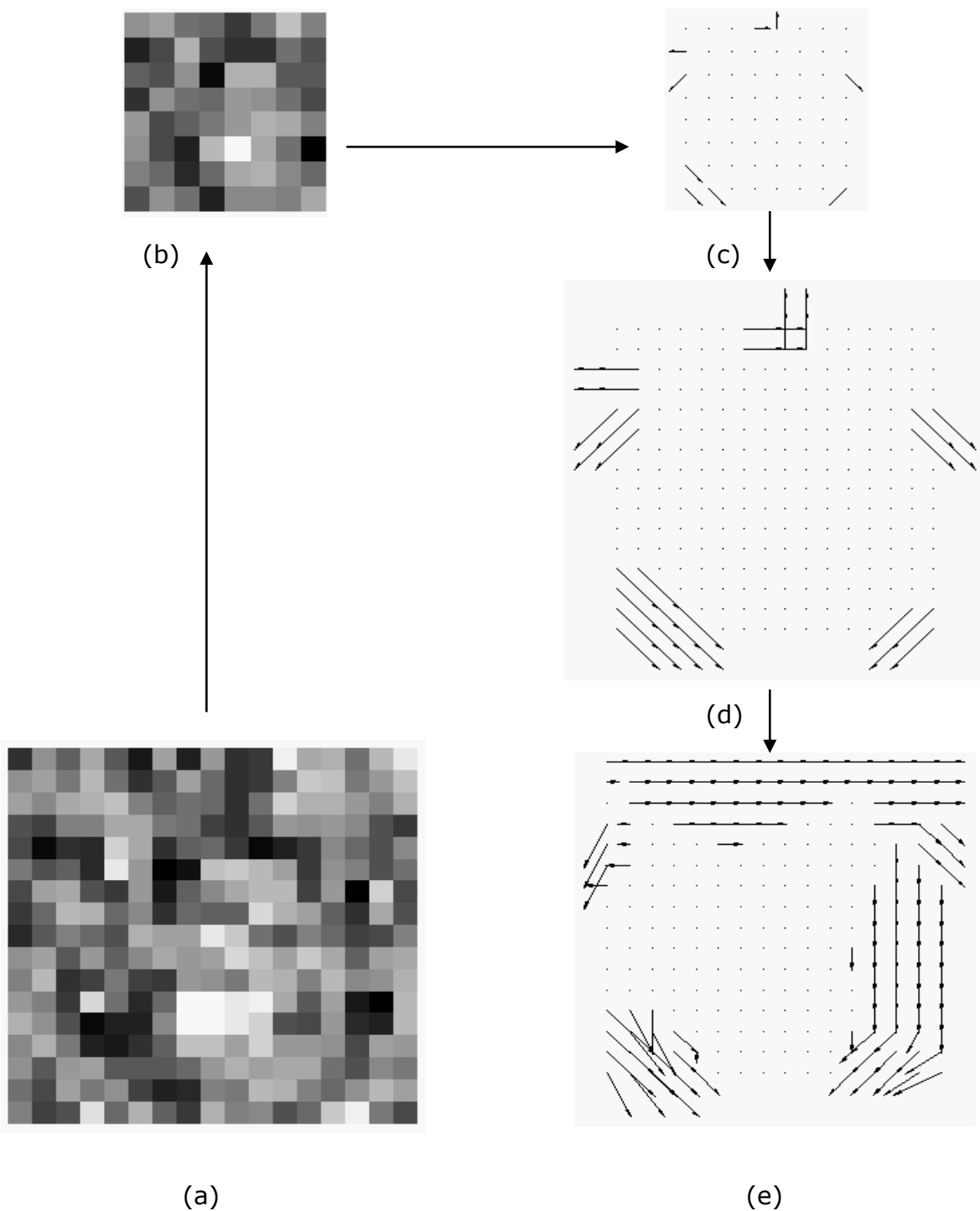


Figure 3.6 MotionEstimation with Adaptive SearchSpace (a) Original image with size 16*16 at Resolution Level 0. (b) Reduced resolution image (a) level 1 with size 8*8. (c) Motion/Vector field for image (b). (d) Adapt the vectors from level 1(8*8) to level 0 (16*16). (e) Motion/Vector field for image (a) with using information from (d) to adapt the search space. For the central area of the image where no motion has taken place a search space of 0 could be used when searching at resolution 1

To clean up the vectors and enhance the accuracy of the estimation, a median filter is used. This helps to remove the noise and promote common motion estimates for adjacent pixels in the image.

The resultant vectors will suffer from some degree of error. To establish which vectors in a given point are more reliable two steps are undertaken. The first is to check for forward backward correspondence of the matches as described previously. If forward matches from image one to image two do not agree with the match from image 2 to image one to within some limit (in these experiments plus or minus one pixel in x or y) then their weighting in the final decision is removed. Secondly for pixels for which the first criterion applies it is assumed that they will move with their nearest neighbours. Thus a median filter is used to improve the estimate throughout region.

3.3 Implementation

The measurement of plant root growth was identified in chapter 1 as important in helping biologists to determine whether their experiments to promote plant growth have been successful. In chapter 2 possible methods for measuring motion were introduced and the problems with the current method used by biologists implied:

- A more reliable approach was needed
- The optical flow and correspondence approaches were still the most likely candidates for seeking a solution

In this chapter scale based approaches to both optical flow measurement and correspondence methods were introduced. These are the methods that have been used in this work. The first step in the methodology has been to identify if the implementation used in this work is appropriate and will give

reliable results. The methods outlined above were implemented first using Mathematica. This is a good system for implementing experimental approaches to both these methods. In particular the scale space approach has been described well by ter Haar Romeny in [29] and implementation of many of the methods are given in that reference. In order to be tested in practical applications these were next re-implemented using C++. This was thought to be necessary for a number of reasons. The processes involved are quite complex but potential users, plant biologists, are more content to use relatively straight forward IT applications. Using C++ it was possible to create a relatively simple to use graphic user interface. Mathematica makes most of its computations symbolically. To undertake calculations on realistic image sizes the amount of memory needed to implement these processes in Mathematica was prohibitive. In addition the time needed for the calculations was also prohibitive. Calculations of the scale space optical flow for a sequence of 5 images of 60 by 60 pixels using Mathematica took up to ten minutes. On the same computer the same process using C++ took a matter of seconds. It was thus possible to analyse whole root segments in less time than one section of the root could be analysed using Mathematica. There are significant effects of implementing the Scale Space Optical Flow method on a 60 by 60 image as errors can be introduced at the edge of the image due to the way the process proceeds. It was possible to limit these effects more easily in the C++ implementation. However, for the purposes of developing the algorithm the restrictions imposed by use of Mathematica were accepted. This problem is dealt with in more detail in the

next chapter. The next stage of the process was to evaluate the methods on a set of standard images and a set of artificially generated images of known characteristics to establish the limits of resolution reliability and accuracy of the methods. These experiments are described in chapter 4. Once the correct parameters for the measurements had been chosen the system was again tried on a set of real root images chosen as representative of the range of roots encountered in practice. This analysis is presented in chapter 5.

Chapter 4 Testing the Methods

The first step in checking the methods proposed for the measurement of plant root growth was to test them on a set of generated test images of similar characteristics to those of the plant roots. The characteristics of the roots that make them particularly difficult to measure are:

- The low range of grey values
- The lack of recognisable features
- The repetition of similar features

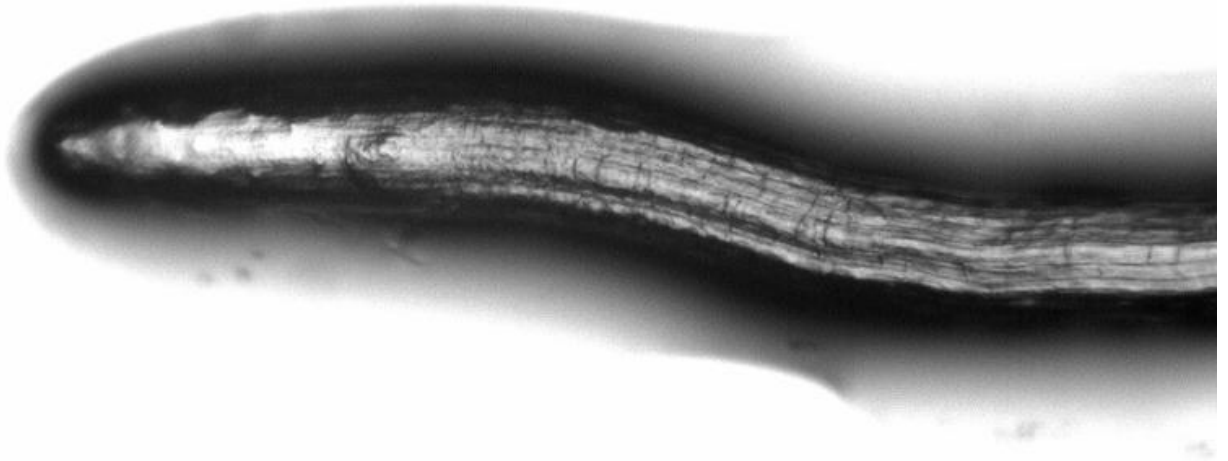
Test images selected were thus created by selecting a section of a typical root image. The images were generated from this by subjecting them to a number of transformations. These involved:

- Linear translations of the pixels horizontally – by differing numbers of pixels
 - 5 pixels per frame, 2 pixels per frame and one pixel per frame over five frames
- Linear translations vertically only by similar amounts
- Linear translations horizontally and vertically by similar amounts
- Rotations about the centre of the image
 - 1° per frame, 3° per frame and 6° per frame

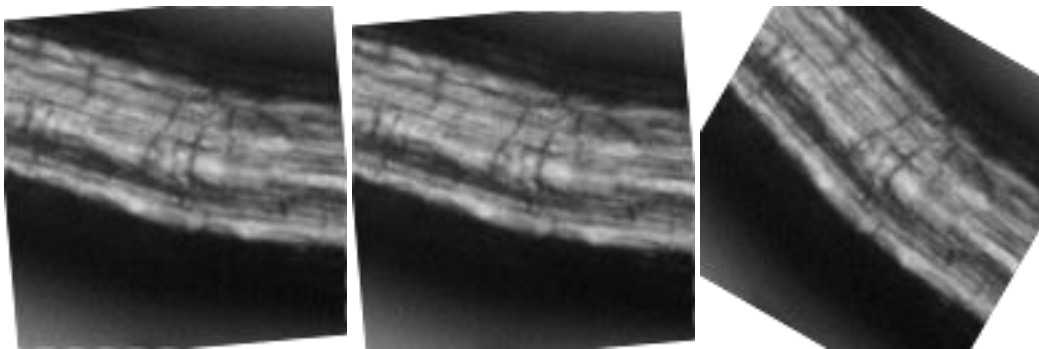
Examples of the test images are shown in Figure 4.1 below.

Figure 4.1a) The original image

3/09/2004 09:33:25



b) A section of that image, original, +2.5 vertically displaced and rotated 30°



These experiments were followed by a set of tests on standard images that have been measured by many systems before and with known motion rates. These other images sets contain characteristics that have meant other systems could use different methods. However, their characteristics being very different from those of the plant roots these comparisons are less valuable than those done on the artificially generated set which had characteristics more closely matched to those of the roots. For interest the vector plots for the standard image set are given in the appendix along with examples of the test images.

4.1 Measurements on the Test Image Sequences with the Scale Space Optical Flow Approach

The scale space approach allows the setting of spatial scale and temporal scale. The number of images needed in a sequence depends on the temporal scale used. This number is calculable from the scale based on the nature of the Gaussian distribution. The contribution of any pixel to the calculation can only be as great as the maximum intensity times the Gaussian at a given point. The effect of applying a Gaussian to an image is found by a convolution of the Gaussian $g(x,y,t;\sigma,\tau)$ with the image $f(x,y)$ given by

$$L(x,y,t;\sigma,\tau) = g(x,y,t;\sigma,\tau) \otimes f(x,y,t) \quad (4.1)$$

As $f(x,y,t)$ is a sampled signal the convolution will be replaced by the discrete version by discretizing $g(x,y,t;\sigma,\tau)$. The limits of $g(x,y,t;\sigma,\tau)$ must be set so that the convolution does not introduce any aliasing. To achieve this but have a suitable size of mask the mask will be truncated at the point where the product of the Gaussian function with the image cannot produce a significant contribution to the output image. In general a square mask in space will be used for the convolution and the nature of the Gaussian is that it reduces from a maximum at the centre to zero at the edge. Image luminance will be from 0 to 255 in most systems so that 255 times the largest edge element of the mask (the value on either major axis) must be less than 0.5. Thus from equation 4.1:

$$255 * L(x,0,0; \sigma,\tau) < 0.5 \rightarrow L(x,0,0; \sigma,\tau) < 0.002$$

As by the Gaussian function G in three dimensions is

$$g(x, y, t; \sigma, \tau) = \frac{1}{(2\pi)^{\frac{3}{2}} \sigma \tau} e^{-(x^2+y^2+t^2)/2\sigma} \quad (4.2)$$

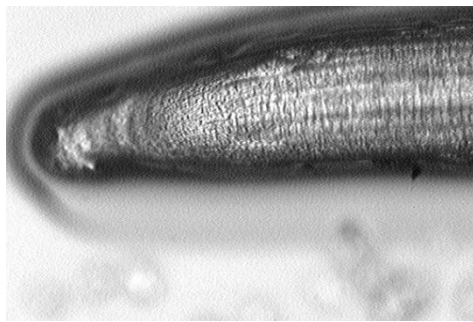
Therefore

$$\frac{1}{(2\pi)^{\frac{3}{2}} \sigma \tau} e^{-(x^2)/2\sigma} < 0.002$$

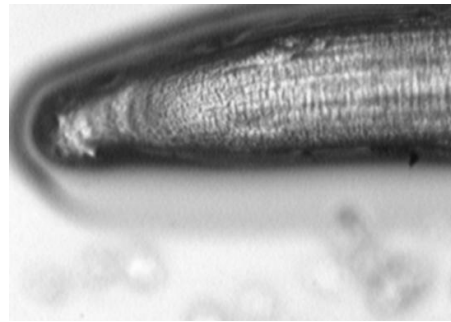
So solving this inequality for $\sigma = 1$, $\tau = 1$ for example gives $x \leq 2.79$. That is the mask must be at least plus or minus 2.79 pixels in x , y and t . A total of 5 images would thus be needed at minimum in a sequence to allow the calculation to be made at a temporal scale τ of 1.

For values of σ much less than one (apart from zero – or no scaling) the size of the mask becomes very small and the process is thus of limited value.

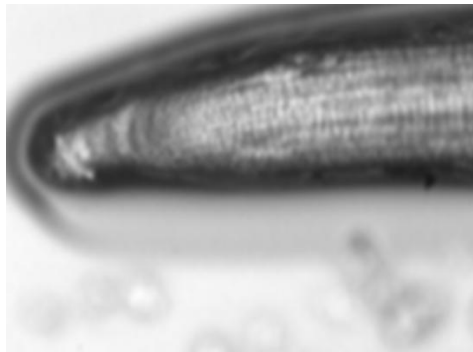
Examples of images at scales of $\sigma = 0$ (not blurred), 2, 8 and 16 are given in Figure 4.2 below:



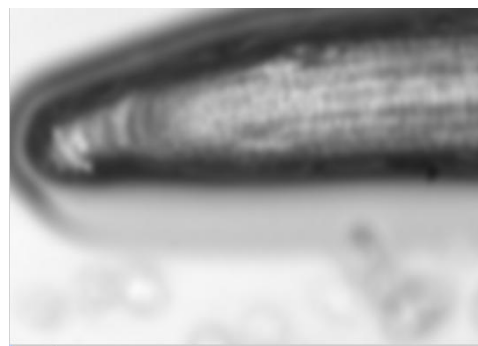
a) Scale 0



b) Scale 2



c) Scale 8



d) Scale 16

Figure 4.2 The same scene at different levels of scale. The blurring is very clear in the scale 16 picture but is still evident in the scale 2 picture.

Note that the effect of this blurring is that the resolution that can be attributed to this method will itself be limited. The actual resolution is difficult to estimate and so it was ultimately decided that in the final

implementation the Scale Space approach would only be used to limit the search space for the correspondence method.

An issue arises as to what should be done at the edge of the images when applying any of the calculation methods. Normally if it is necessary to look at the whole image it is necessary to make some compensation at the edge of an image. The pixels within the mask dimension of the edge will require pixels from "outside" of the image for the calculation to be completed.

Within the Mathematica implementation this was achieved by "mirroring" the pixels at the edges. That is when making calculations on the pixels $L(x, 0)$ on the top edge for example the pixels $L(x, 1), L(x, 2) \dots L(x, n)$ – where n is the dimension of the mask – were used instead of the pixels $L(x, -1), L(x, -2) \dots L(x, -n)$. Similar compensations were used on the other edges.

The result is that the region of the size of the mask will not give valid results. This can be a very significant issue for a 60 by 60 image. The solution to this problem in the C++ implementation was to use the actual pixels surrounding the image selection in the calculation. This is possible where the image selection is not near the edge of the image – which was always true for the midline measurements. The results of all the experiments gave good correspondence with bigger errors at the edges. Not including the edge pixels with a spatial scale $\sigma = 1$ the error ranges from +/- 0.5 pixels for motions of 1 pixel per frame to +/- 1 pixels for motions of 5 pixels per frame. The rotation measurements gave good measurements for larger rotations (+/- 0.1° for rotations of 6° per frame)

but at 1° per frame the errors were larger. The implication being that the method was more effective in measuring larger changes – more than 5 pixels per frame of rotation. This was somewhat surprising as the larger linear translations gave greater errors. However, the optical flow did outperform the correspondence algorithm for displacements near the centre of motion (see the next section for a comparison). In particular away from the edges the Scale Space Optical Flow measurement had always the correct direction of motion. These experiments were carried out for a 64 by 64 block of pixels around the centre of the image (the centre of rotation) and were done using the Mathematica implementation of the method. As was stated earlier the errors at the edge were due to using the mirroring of values to deal with edge overlaps. This problem was not present in the later C++ implementation.

4.2 Measurements using the Multi Resolution Block matching

Approach

The experiments were repeated with the same set of test images using the block matching approach. This approach is limited to plus or minus one pixel per frame between two frames but when a sequence of more frames (in the final experiments 9 frames are used) the results can be refined. The same set of test images were used for the initial testing. As the translations used were only whole pixel translations it is not surprising that by choosing the correct search space a set of perfect matches could be found. However, the rotations produced changes in orientation for the pixel blocks so the results for rotations were more valuable for testing the matching algorithm.

Errors in measurement were observed with the rotations. For small rotations (1° per frame) the pixel motions near the centre of rotation (up to 6 pixels from the rotation centre) are not detected. This should be compared to the Scale Space Optical Flow measurements where the flow is detected right down to the centre of rotation. This is illustrated in Figure 4.3 below. Notice in these figure errors occurring at the edges due to incomplete calculations being possible on the edge pixels are showing up as incorrectly orientated vectors. This effect is greater for the Scale Space Optical Flow as the mask size is larger for this approach.

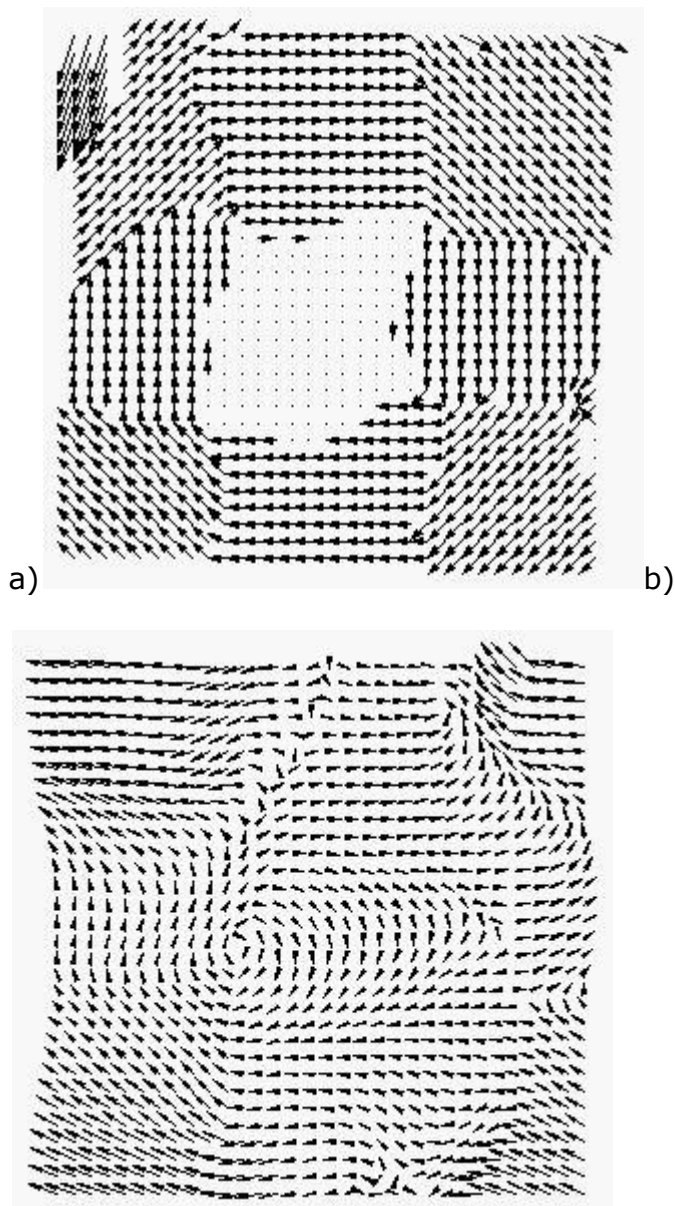


Figure 4.3 Example vector plot from 1° per frame rotation for the test images using a) block matching and b) Scale Space Optical flow. Note errors due to edge effects are greater for the optical flow. This is removed in the later experiments where the images are sub sections from full images and mirroring of edges is no longer needed.

4.4 Combining the results

There are obvious advantages and disadvantages of both techniques. The Scale Space Optical Flow approach is capable of detecting sub pixel changes with a high degree of reliability. However, to achieve this, the best value of

scale needs to be tuned to the individual problem. This is a time consuming process and also limits the maximum resolution that can be achieved. The block matching approach is very much quicker to implement but sub pixel measurement is not directly possible. A method was thus sought to combine the value of both of these processes. A series of experiments were carried out (see chapter 5) in which a typical sequence of real root growth images were analysed. The result of this was to determine a best value of scale parameter σ for measuring that image. This value was then used for a sequence of images and the results were always in agreement with a ground truth measure to within ± 1 pixels per frame the whole set of measurements. Using this fixed value of the spatial scale ($\sigma = 1.8$) for all the measurements would give a valid measure for all the measurements but only to a resolution of ± 1 pixel per frame. This would be equivalent to a growth rate measurement of $\pm 9 \mu\text{m}$ per second. As the changes to be measured were of the order of $5\mu\text{m}$ per second this resolution is then unacceptable. It should be noted, however that the measurement method currently in use by biologists – RootFlowRT – will be seen to have reliability of only $\pm 5\mu\text{m}$ per second in most cases.

It is observed that while the correspondence method can only measure reliably down to ± 1 pixel per frame if these frames are the beginning and end frames of a 9 frame sequence this will represent ± 0.125 pixels at the individual frame level or $0.9 \mu\text{m}$ per second, a considerable improvement on previous methods. Also if sufficient data can be taken in the neighbourhood

of a given pixel then a greater reliability can be assumed. The approach taken in this work is as follows:

Step 1: Using a spatial scale of 1.8 and a temporal scale of 1 the image sequence is analysed and a set of U_{ij} (horizontal) and V_{ij} (vertical) motion values is calculated for each pixel $L(i, j)$

Step 2: For the 5 by 5 neighbourhood of each pixel the mean U and V values (U_m and V_m) and the standard deviation in U_{ij} and V_{ij} values is calculated

Step 3: If the value of U and V at the pixel is more than 2 standard deviations away from U_m and V_m respectively the value at the point is ignored and the mean value used.

Step 4: From the U V values for the pixel $L(i, j)$, a search space is defined as ± 1 standard deviation as defined in step 2 for the given point.

Step 5: The correspondence match is made for all points in the image space between the first and ninth image in the sequence. A new set of U V values is calculated - the search space used at any point used is as defined in Step 4 above.

Step 6: The correspondence match is made for every point in image 9 in the sequence with image 1 in the sequence.

Step 7: The U and V values for any pixel where the matching from image 1 to 9 from step 5 does not correspond to the match from image 9 to image 1 in step six is eliminated.

Experiments were then undertaken on a set of real image sequences as described in the next chapter. In that chapter the results of this approach are compared to those of the previous method (RootFlowRT) as well as a set of pseudo ground truth measurements (manual measurements made with a significant level of care). The establishment of the ground truth and its own reliability is described in the next chapter.

5 Results and Analysis

This thesis has proposed that the current method in common use by most plant biologists who measure plant root growth using conventional bright field microscopes is faulty. In particular it has been observed that the measurements have a larger range of error (unreliability) than the changes in growth that are to be observed. It thus proposes a new approach to that measurement. This approach involves using the Scale Space Optical Flow measurement as a first measure of plant root growth and then refining this measure by a further correspondence method that uses the results of the scale space measurement to help restrict the search space and thus remove a tendency to choose bad matches. The scale space approach can only give an approximation to the growth rate. This is intrinsic to the scaling process which while it improves the reliability of the method greatly does limit its potential resolution. However, this initial value can be allowed to limit the search space for the subsequent correspondence method. This has the effect of enhancing the values produced by the correspondence method, leading to greater accuracy and greater robustness of the results. To demonstrate that the method proposed in this thesis is both more accurate and more robust than the previous method it was first necessary to establish a set of ground truth data for comparison. To do this a computer assisted manual measurement method was developed. It has to be remembered that this ground truth method is itself limited in its accuracy by how well the user is at using it and by the fact that at best a user can be accurate to plus or minus one pixel in measurement. By repeating the

measurement a number of times the reliability of the manual measurement can be refined. However, for some images the surface texture and resolution of the image mean that a good automatic method, which relies on accurate estimation of pixel match values, can predict the result better. Thus when comparing the ground truth to the automated measurement it is important not only to look at the absolute measurement achieved but also at the reliability represented as the spread in these results. This will show up in the results described below. In most cases the manual measurement has been less reliable than the method proposed in this thesis. In these cases it must be noted that the manual method, while being claimed as ground truth is in fact less accurate than the measured value using this method. In no case is that so with the method previously in wide use. The manual method is also time consuming and tedious to use for a whole plant root. Applied as a regular method of measurement it would undoubtedly be subject to even greater error as user fatigue would play a role in making a large number of measurements.

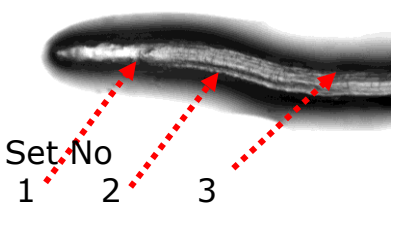
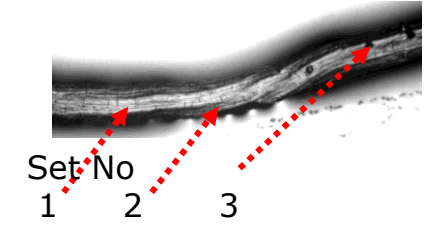
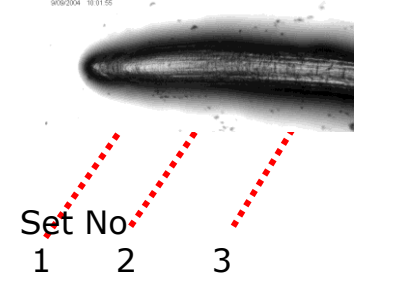
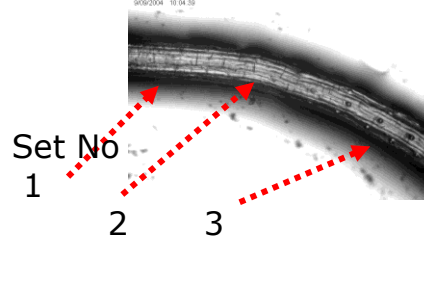
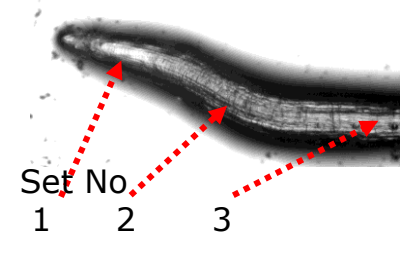
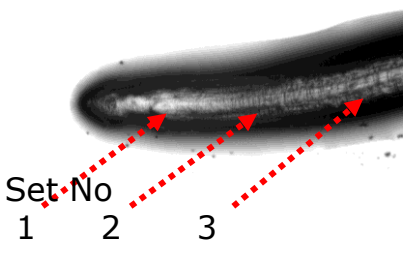
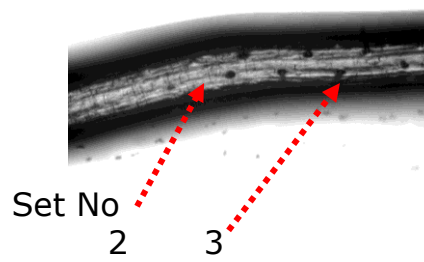
In experiments, plant biologists wish to know the root growth rate along the mid line of the root from the tip up the length of the root. This would involve many hundreds of measurements each of which takes a considerable time and thus this manual method while reliable – within its error limits - is not a credible alternative itself to a fully automated method. It also gives a limited resolution. Human users cannot detect the change

between two images to better than plus or minus one pixel and repeating this reliably for a large number of measurements is not realistic.

5.1 The Test Dataset

In order to demonstrate the validity of the proposed method it was first necessary to establish a means of providing a ground truth for the measurement of the plant root growth for a large number of samples and to compare this with the current method – RootFlowRT - and the proposed method from this thesis. To enable this, a set of example images were chosen from a large sample provided by the School of Biosciences at the University of Nottingham. The test group of images was chosen to be representative of real sets of data, both in terms of extremes of growth rate and texture of the roots. Examples were chosen that had different rates of growth, some with particularly low growth rates some with particularly high growth rates and some with more common growth rates. Examples were also chosen which were of different root types so that robustness to texture type was also measured. In total 20 sets of data were analysed from two image stacks from five samples. These were again sub sampled at 3 places covering the majority of the mid region of the root, which is the area of interest used by biologists to establish the effectiveness of the biological experiments. The image sets used in this initial test are shown in Figure 5.1 in which the location of sections measured is indicated. Subsequent experiments were performed on a set of 37 image stacks provided by the plant biologists. These are reported in section 5.9 later in this chapter.

The process was to measure the growth over a range of points using the semi manual method to establish the ground truth. Next measurements were made in the same way as used in the RootFlowRT method in common use by biologists at the moment with the search limits fixed as done in their software. Next the set of images were analysed using the scale space optic flow and the output of this data was used to set the search space for the measurements using the region correspondence method outlined in Chapter 3. The results were then separately compared to the ground truth measurement. Various ways are provided in this chapter for comparing the proposed method with that previously in use.

| Image | Stack 1 | Stack 2 |
|---|--|---|
| AJH1 |  |  |
| CGI 1 |  |  |
| AJOPA1 |  | |
| <p data-bbox="304 1339 724 1453">Figure 5.1 Identifying the location of the images used in the experiments.</p> |  |  |

5.2 Establishing Ground Truth

In order to make realistic measurement comparisons between the methods developed in the current work and RootFlowRT it was first necessary to establish ground truth data. This was established using a semi manual method that is outlined below.

A software system was developed to aid in this process. All software was first developed using Mathematica and subsequently implemented in C++ using Visual Studio as a stand alone software system as this was felt to be potentially easier for users with lower computing expertise.

5.2.1 Steps in using the semi manual method

The steps in using this software system in the semi-manual process were as follows:

1. Images for a sequence were loaded and viewed one at a time by the naked eye.
2. Areas of interest were identified by clicking on the image and an area surrounding the point at which the click was made was displayed at a higher resolution (using a simple linear "stretch blit" approach).

3. Features of interest were identified by eye as being likely to be resolvable in subsequent images. For example a particularly distinct intersection between two cells.
4. Next a second image from the sequence was selected and the area of the image at the point selected for the first image displayed in higher resolution.
5. The same feature was identified in the new high resolution image.
6. The user next clicked on an identified pixel in the first image and then on what they estimated to be the equivalent point on the second image.
7. Next the system calculated and displayed a three-d display of the profile of point intensities around the two points from the two images.
8. The user compared these profiles to determine the closeness of match.
9. When the user was satisfied they had selected the correct points the computer recorded the motion vectors for the chosen point as the difference between horizontal and vertical pixel location.

The process above was then repeated a number of times to check that the correct point had been chosen. However, this can only be done to a resolution of plus or minus one pixel with certainty. An example of the process is shown below.

Step 1 An image from a sequence is selected. The image shown in Fig 5.2 is from an image sequence labelled uaroux1 and is the first stack of images in that set.

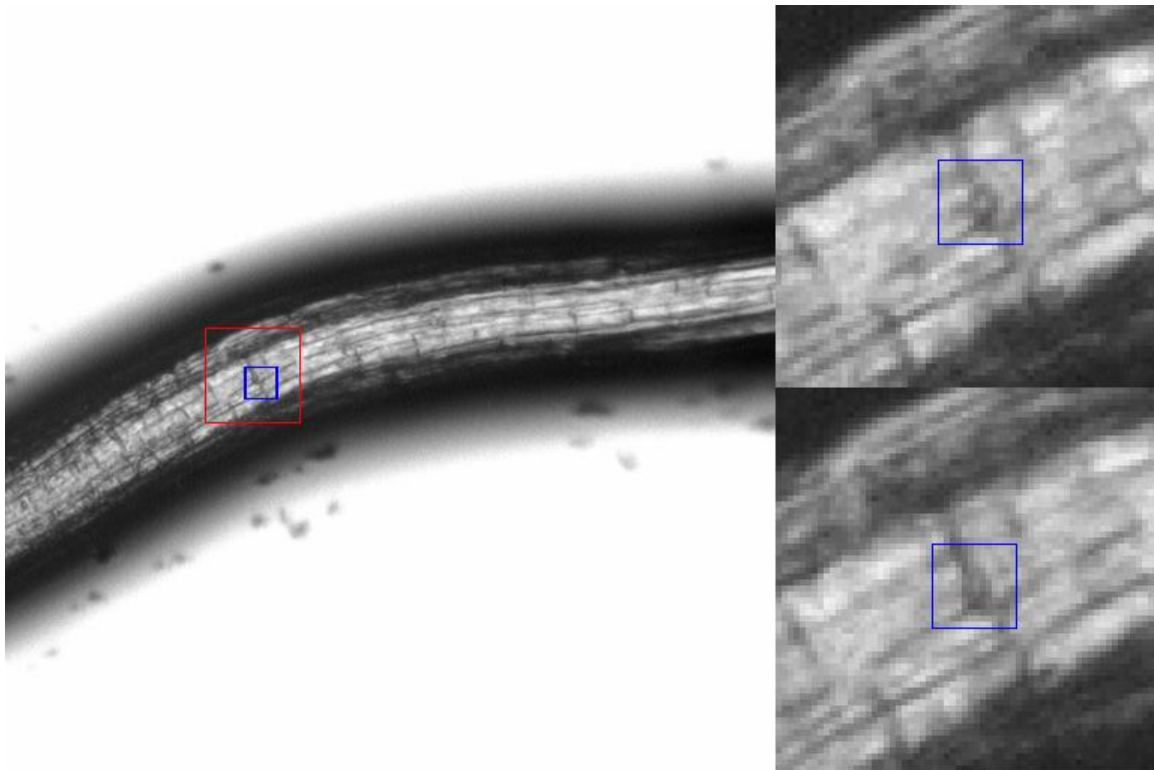


Figure 5.2 An image from the first stack of the sample uaroux1. In the main picture an area has been selected (outlined in red). The upper picture on the right shows this area as selected from the first image in the stack. The lower image shows the area from the same point in the ninth image in the same stack. In these pictures two areas are also outlined around a distinctive shape from both images (outlined by blue rectangle). The profile of pixels around this area is then presented to the user see Figure 5.3

Step 2. An area of the image is selected for study (outlined in red in Figure 5.2). The area selected is displayed to the user in higher resolution (shown in the top right of Figure 5.2).

Step 3. An area of specific interest is selected. In the case of the example in Figure 5.2 it is a join between 4 cells judged to be significantly distinct from others to have a reasonable chance of identifying it in a subsequent image using the human eye. This is outlined in blue in this image. The selection is made around the point at which the mouse is clicked.

Step 4. A second image from the stack is selected to be viewed. (In the current example this was the ninth image in the sequence.) The area of the image at the same point as in the previous step is selected and displayed to the user (shown in the lower right hand side of Figure 5.2).

Step 5. The same feature as selected in step 3 is identified in the second image area (outlined in blue in the lower right hand area of Figure 5.2).

Step 6. The user clicks on what they think are equivalent points in the two selected areas.

Step 7. The profile for these areas – as shown in Figure 5.3a) and b) – are displayed to the user

Step 8. The user inspects these profiles.

Step 9. When the user believes the points chosen are equivalent they select the instruction to the system to calculate and record the manual estimate of the plant growth at the selected point.

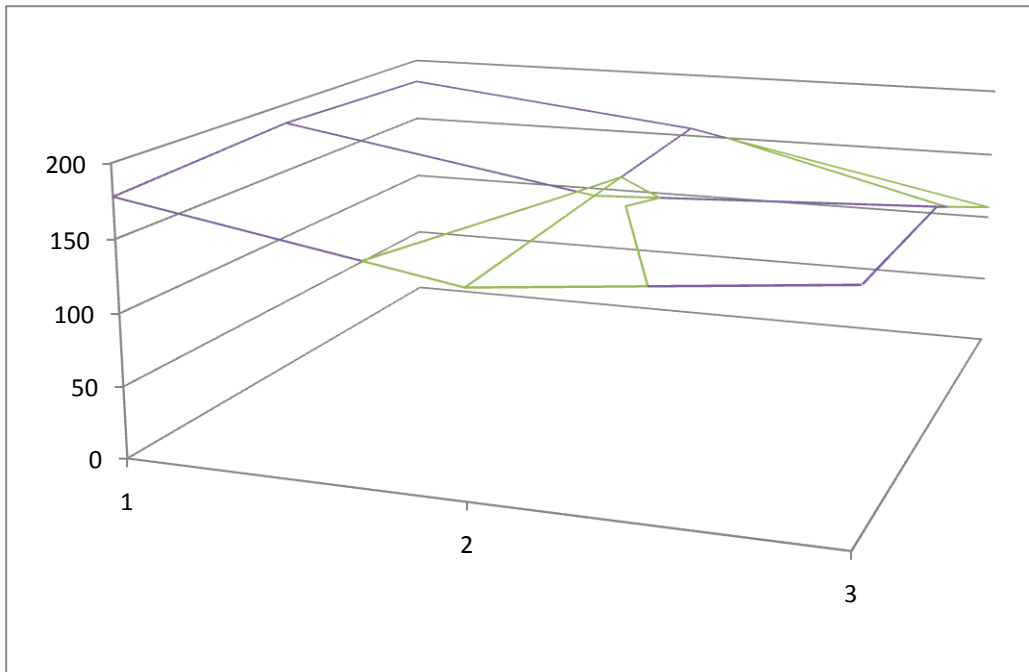


Figure 5.3 a) profile around chosen point from first image in sequence

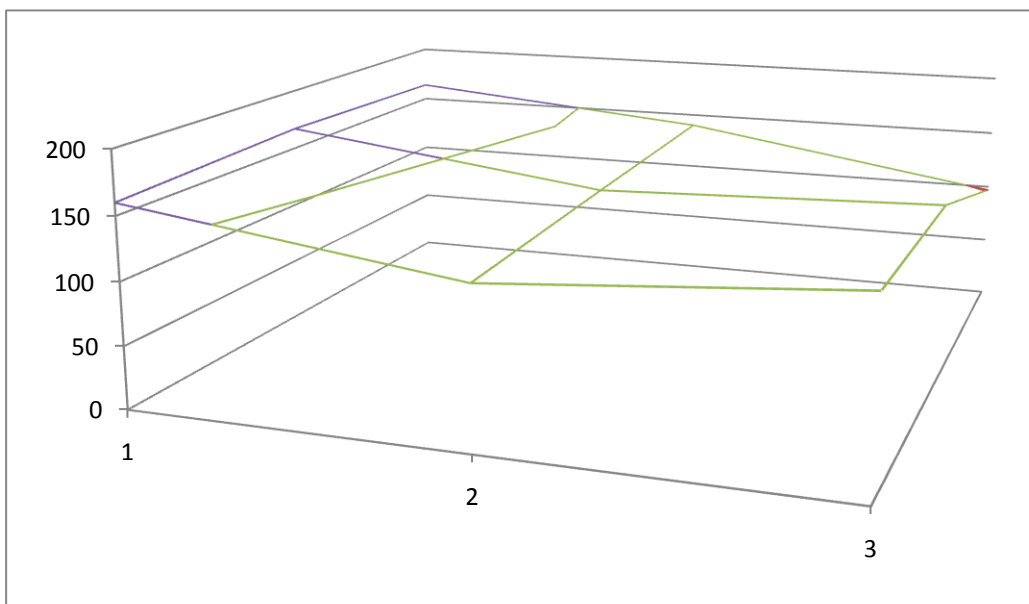


Figure 5.3 b) profile around chosen point from ninth image in sequence. The profile is similar to that in a) but the overall brightness is lower.

Ten measurements were taken in any one region and the reliability of the measurements given by the standard deviation for the given set of measurements. For most of the images tested it was possible to find such a correspondence with a reliability of better than plus or minus one pixel anywhere in the area of interest. However, for some image sets this was only possible at certain points in the area of interest. This is particularly so for areas where there is low contrast for regions of the image. A typical example is given in Figure 5.4 below.

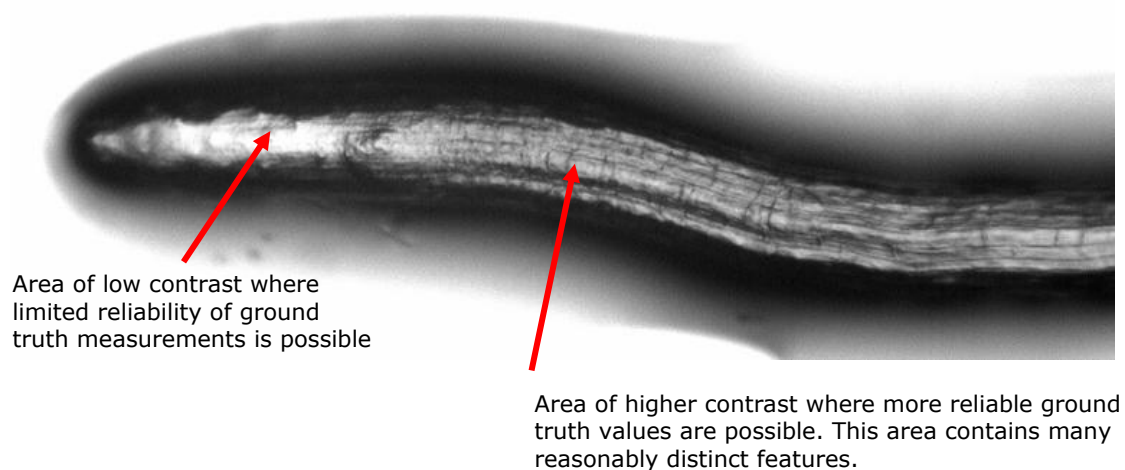


Figure 5.4 the first image in the first stack of the set labelled AJH1. Areas of high and low contrast are identified

From Figure 5.4 it is clear that in the high contrast areas there are many reasonably distinct features to the naked eye. However, it is not possible to use these features in an automated matching method as they are irregular and repeating. Also a number of features on any one plant can appear equivalent and this appears to be a contributing factor in the limitations of the method currently in use by many biologists. Note this semi manual

method is only accurate to plus or minus one pixel. The measurement taken in the example shown in Figure 5.2 led to a measurement of 10 ± 1 pixels in the x direction. This was equivalent to a movement of $0.11 \pm 0.01 \mu\text{m}$ per second or $6.7 \pm 0.6 \mu\text{m}$ per minute. This is a typical growth rate for the middle of the elongation range for the plants being studied.

5.3 Measurements using RootFlowRT

As stated in previous chapters it was the observed inaccuracies of the commonly used method that directed the current work to establish the new method. In order to establish the value of the new method it is instructive to compare results using it with those from the previous method. Thus the same sets of measurements were made using RootFlowRT and the method proposed in this thesis. Initial evidence of what is going wrong with the previous method can be seen by looking at plots of estimated growth vectors from this method. An example of this is given in Figure 5.5. Here the vectors from RootFlowRT are plotted for the region shown in Figure 5.2 and highlighted by the red rectangle in that image. The vectors found from this method are shown in Figure 5.5 in two colours, red for vectors which satisfy the backward forward matching criteria and blue for those that do not.

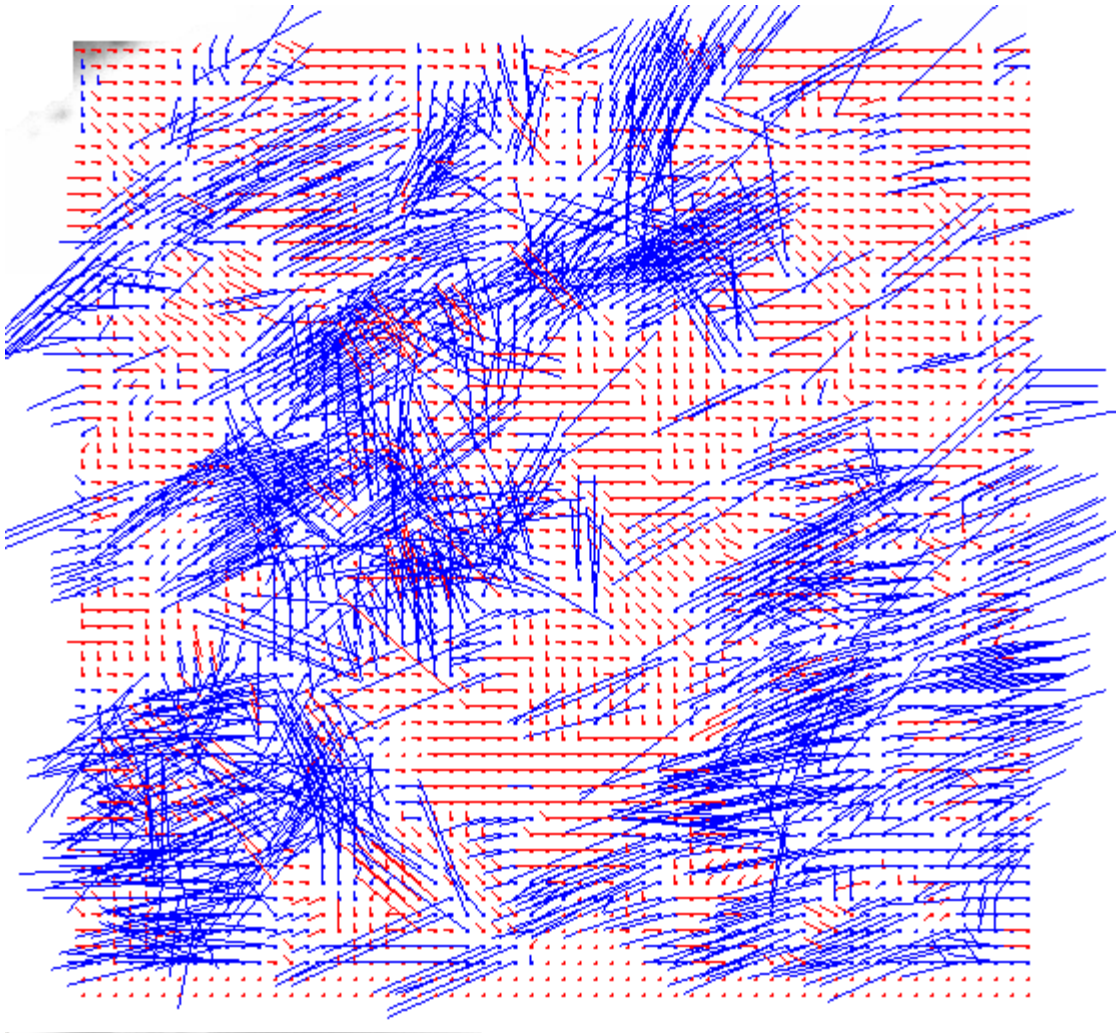


Figure 5.5 A plot of the growth vectors for the method previously used. Vectors in red fit the backward forward matching criteria, blue do not.

From this diagram it can be seen that a high proportion of the vectors are of the wrong size and pointing in the wrong direction. The actual size of plant growth that would be estimated from such vectors would be incorrect and these values are discussed further later. RootFlowRT tries to improve this by accepting only vectors for which backward and forward matching gives good agreement. For this typical example these are as shown in Figure 5.6

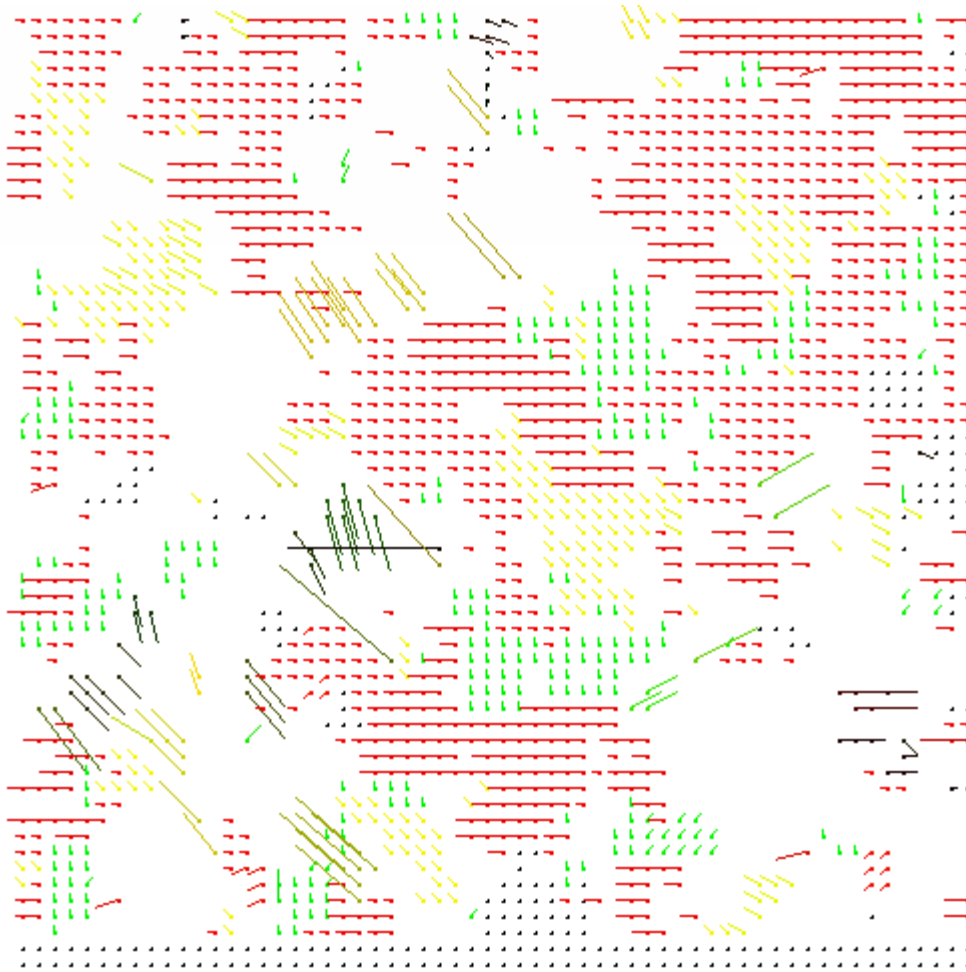


Figure 5.6 Only the backward forward matches that agree using the previous method of measurement

As can be seen from Figure 5.6, even when only the matches that agree in terms of forward and backward matching are used there is still a high variability of vectors. A significant number of vectors are the wrong size and point in the wrong direction. The ground truth measure of $0.11 \mu\text{m}$ per second in the x direction is equivalent to the horizontal red lines in Figure 6.5. The vectors provided by RootFlowRT vary between $+2 \mu\text{m}$ per second and $-0.5 \mu\text{m}$ per second in the X direction and $+1 \mu\text{m}$ per second and $-0.5 \mu\text{m}$ per second in the y direction (where the ground truth measure would

indicate $0.00 \pm 0.01 \mu\text{m per second}$). Less than 50% of the measurements are actually recording the correct value and so the mean value (as returned by RootFlowRT) varies significantly across the region. In particular the variance for the measure is $\pm 0.2 \mu\text{m per second}$ which is greater than the real change over the full root measurement.

5.4 Use of Optical Flow Data

The set of images used in the previous parts of the experiment were also analysed using the optical flow method outlined in Chapter 3. To apply this method accurately it is at first necessary to choose the most appropriate value of the spatial scale. This is equivalent to adjusting the viewing position for the image set until the motion of larger scale features dominates the measurement rather than apparent but unrealistic motion at the pixel level. In principle this “tuning” process should be undertaken before every measurement. However, such a process would be complex and time consuming and so unlikely to be acceptable to potential users. As an alternative it was decided to tune the scale to match a number of different image sets then use the value which gave best response from each of these sets.

5.4.1 Tuning the Spatial Scale

This process involves using the ground truth data values to evaluate the result of a given measurement. The probability of a measure being correct is determined from the magnitude and direction of the derived vectors at a

given point as compared to the ground truth measure at the nearest equivalent point. The variance of output values is then computed at all points and the scale that gives the best set of matches to the ground truth values is chosen. A best set of values (for the image set CG1 1 1) is given in Table 5.1 below. Initially a set of values was determined using a wide range of spatial scale values (between $\sigma = 1.0$ and 2.0 at 0.1 steps). The range of values giving the highest number of valid matches and those for which the corresponding output matched most closely the range of U and V values from the corresponding manual measurement was for values of spatial scale σ between 1.7 and 1.9 . Measurements were then taken at sub intervals providing the best matches as given in the Table 5.1. Subsequently these ranges were used to limit the search space for the correspondence method and the resultant values of U and V determined. The value of U and V closest to the ground truth measure were then taken as indicating the best value of the spatial scale σ for the given measurement. This process was repeated for all the image sets under examination. However, this process is quite time consuming and involved and for all the experiments carried out the variation in chosen scale giving the best response for the images was small and scales of 1.8 ± 0.05 were found to give the best fit for the full set. It was thus decided to fix the value of spatial scale used in the experiments to evaluate the effectiveness of the method proposed when compared to the earlier method used. This provides a more realistic assessment of the likely competitiveness of the method for use by bioscience

practitioners as they were more likely to resist processes that are technically complex in ways outside of their main area of interest.

| scale | 1.7 | | 1.75 | | 1.85 | |
|--------------|-------|-------|-------|-------|-------|-------|
| Search Space | x | y | x | y | x | y |
| Upper | -17 | -7 | -23 | -11 | -17 | -5 |
| Lower | -15 | -7 | -11 | -3 | -10 | -2 |
| | value | stdev | value | stdev | value | stdev |
| U | -11 | 4 | -14 | 3 | -12 | 2 |
| V | -9 | 3 | -6 | 2 | -4.8 | 0.6 |

Table 5.1 Typical results found in tuning the spatial scale parameter σ . The table shows the determined size of the search space indicated by the scale space optical flow measurement and the corresponding values obtained for U and V from the correspondence measurement. Image set used CG1 1 1. Manual value obtained U = -12, V = -5. Value of spatial scale leading to best match thus $\sigma = 1.85$. All measurements are in pixels per 100 seconds.

The results of the scale space optical flow measurement were then collected for all of the test images. The mean values obtained for the set of data together with their variation are given in Table 6.2. Comparison of these results with those obtained when using the region matching approach from previous method shows that the results are comparable as are, however, the levels of uncertainty obtained.

The scale space optical flow measurements give a better reliability than the tensor method reportedly used in RootFlowRT [6]. In their work less than

5% of the tensor values were reported to be valid. In the current work validity of the optical flow data was determined by comparison of the values across the region of interest. In this case segments of data 64 by 64 pixels were selected along the midline. The optical flow measurement was made on this data. After this all results were analysed and values outside of two (local) standard deviations from the local median of any 5 by 5 neighbourhood of each pixel were rejected as being not consistent with the luminance constraint. The search space for the correspondence match is then constrained to plus or minus one standard deviation for the set of optical flow measurements about the average measure for a given region. If the average, mode and median values are widely different the constraint will favour values closer to the median and the search space will be further limited.

5.4.2 Using the Scale Space measure to limit the Correspondence

Search Space

The values obtained from the scale space optical flow were next used to establish the initial search space for the region matching method outlined in Chapter 3. In order to do this the values obtained from the scale space optical flow analysis for the area of the image being assessed were first stored. The spread of data obtained for these values in the neighbourhood of a given point was assessed. This was done by first applying a median filter to the region. The neighbouring region of a given point was considered as the 25 neighbouring points to the point of interest (nearest neighbour, next

nearest neighbour etc. for the 5 by 5 region surrounding a point.) The deviation from the mean for these 25 resulting points was then calculated. This was then used to fix the region for the search of the region matching method. Consideration was added for the scale used in the measurement. So for example if a given pixel p_{ij} is reported by the scale space optical flow to have moved by u and v with a reliability of δu and δv the search space is fixed around $p_{i+u, j+v}$ in the second image with a span from $i + u + \delta u$ to $i + u - \delta u$ and $j + v + \delta v$ to $j + v - \delta v$. Median filtering rather than mean filtering is used because the influence of values which violate the flow continuity constraint is thereby less significant when a maximum of 25% of the values significantly violate this constraint.

It now becomes possible to compare the values obtained from this method with those obtained from the previous method (the one previously in use by biologists.)

5.5 Comparing Results

Figures 5.5 and 5.6 showed a plot of the motion vectors for the method previously in use. Figure 5.7 compares that with the result obtained using the method proposed in this thesis. Note that these vectors represent an estimate of the growth rate in the region of interest. The reason for comparing these two vector plots is to compare the spread of the values found. It is the size of this spread that leads to the errors in the commonly used method. In the method used in this thesis the spread is far smaller and the result far more reliable.



Figure 5.7 a comparison of the backwards forwards matching vectors for the method commonly in use with that proposed by this thesis. Note the picture on the left was previously shown in Figure 5.6 and shows many vectors are oriented in the wrong direction and some are much too large. Those for the proposed method are generally very close to the size and direction found from the ground truth measure.

This shows up clearly when comparing the mean values obtained for the growth rates from the two methods. The results in Table 5.2 are shown for both methods and the methods when using and not using backward forward matching. These are also compared to the ground truth values.

| Method | Horizontal growth $\mu\text{m/s}$ | Error $\mu\text{m/s}$ | Vertical growth $\mu\text{m/s}$ | Error $\mu\text{m/s}$ |
|--|-----------------------------------|-----------------------|---------------------------------|-----------------------|
| RootFlowRT without backward forward matching | -0.8 | 7 | 0.07 | 5 |
| RootFlowRT with forward backward | -0.1 | 0.3 | 0.03 | 0.1 |
| Thesis without forward backward | -0.17 | 0.06 | 0.03 | 0.05 |
| Thesis with forward backward | -0.125 | 0.0001 | 0.000 | 0.0001 |
| Manual | -0.11 | 0.01 | 0.00 | 0.01 |

Table 5.2 Comparing the results for horizontal and vertical growth rates in μm per second for the method proposed in this thesis with that obtained by RootFlowRT (for the example shown in Figure 5.2)

As can be seen from Table 5.2 the values obtained from the proposed method with or without block matching are more reliable than those obtained from the RootFlowRT and they are also more accurate. It might not at first seem that the method is more accurate as -0.1 ± 0.3 is close to -0.11 ± 0.01 . However the variance found is higher than the observed change over the whole root ($0.05 \mu\text{m}$ per second) and thus invalid in its return. Variance found in the new method is $0.0001 \mu\text{m}$ per second which makes it significantly more reliable.

In general plant biologists are interested in the growth rate parallel and perpendicular to the midline of the plant. In this work the midline has been added as a spline fit to a set of points chosen by the user clicking on the image of the plant root. The growth parallel to the midline can then be mapped by taking the unit vector describing the midline at a given point and calculating the cross product of this with the u and v vectors (those in the x and y direction in the image).

The improved accuracy can be clearly seen if a plot is made of the scatter in the results for a measurement along the midline. This is the measurement of growth rate of most interest to biologists. The scatter plot is for the region highlighted in red in Figure 5.2. On this graph (Figure 5.8) is also plotted the value calculated from the manual method.

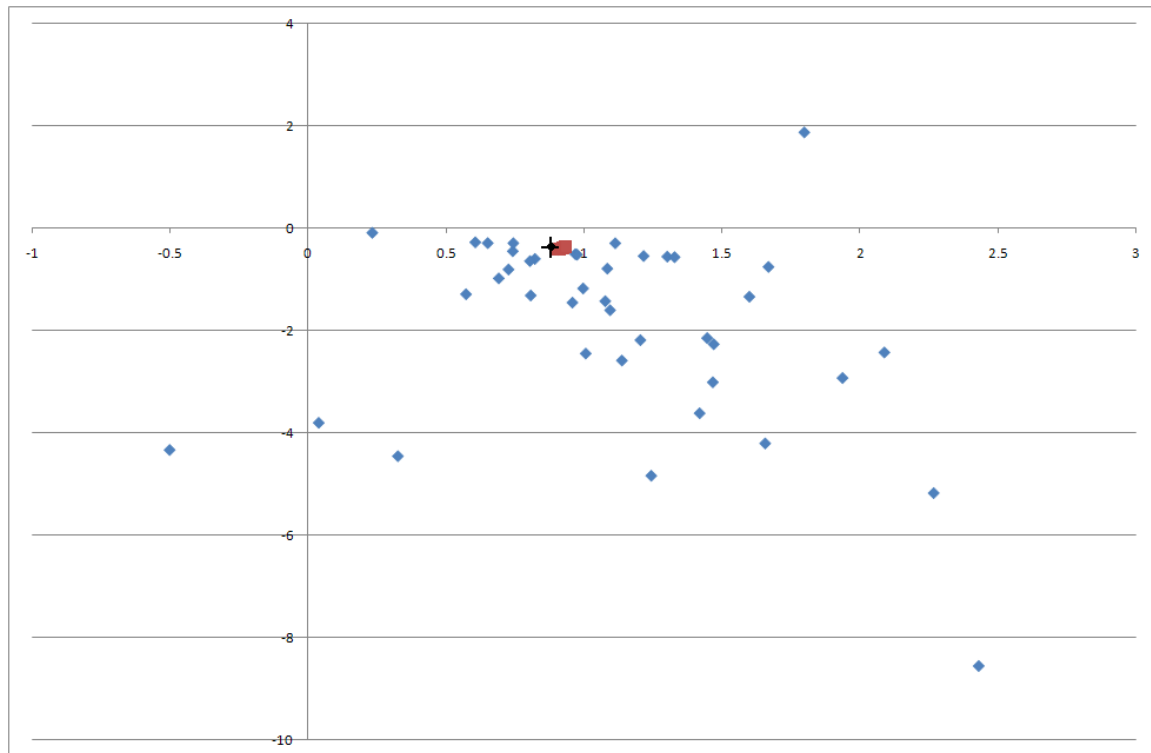


Figure 5.8 A scatter plot of the data obtained resolved as growth along the midline potted horizontally compared to growth perpendicular to the midline – plotted on the vertical axis. The scale of both axes is μm per second. The previous method results are plotted in light blue and show a wide scatter (from $-0.5 \mu\text{m}$ to $+2.5 \mu\text{m}$ per second in the parallel direction). Those for the method presented in this thesis are in pink and are all concentrated at the same point as the black cross which represents the estimate from the manual results (range from 0.90 to $0.95 \mu\text{m}$ per second in the parallel direction). The improvement of the current method for the perpendicular method is even more striking.

The results shown in Figure 5.8 and Table 5.2 show clear advantages of the method in this thesis over those of the previous method: greater reliability and greater accuracy. Obviously it was necessary to repeat this experiment for a wide range of images sequences from different plant samples with different surface characteristics. The method shows up as always better than the method currently in use and this is illustrated in the tables of results printed below.

To compare the results using and not using optical flow a set of 20 representative image sequences were analysed. These represented midline region elements for different plants with, in general, two stacks per plant type and at up to three points along a root within the stack. (These samples are identified in the images given in Figure 5.1 shown previously). The images were chosen for the initial tests were chosen as representative of the full range of image types commonly dealt with by the plant biologists. As can be seen from Figure 5.1 the images have many similarities but also significant differences. The reflectance near the tip tends to be high and the images contain areas of high intensity which might seem to limit the accuracy possible for the manual method. In general however, repeated attempts at manual measurements in the areas of interest returned values of +/- 1 pixel or better for all images and sets. As explained earlier the images were chosen because they either exhibited common characteristics for the majority of typical images both in growth rate and direction or they exhibited exceptionally high or low growth rates or they showed areas where the growth direction changed. In addition the second stacks of all images contained areas where side root growth had begun and it was interesting to see that this generally did not affect the resolution of the measurements made.

Another possible feature affecting the reliability of the measurement was changes in lighting throughout the image capture process. In general the image sequences were taken within a short number of minutes (typically less

than 3) so variations were small. Figure 5.9 below shows the first and ninth frames from the first stack for sample CGI1. In good reproduction there is a naked eye variation in average luminance levels but when measured equivalent regions have similar light distributions as shown by the histograms in Figure 5.10 which are from the mid root areas for the two images shown where the mean light level is seen to be slightly higher (mean gray level of 101 rather than 99 for image 1).

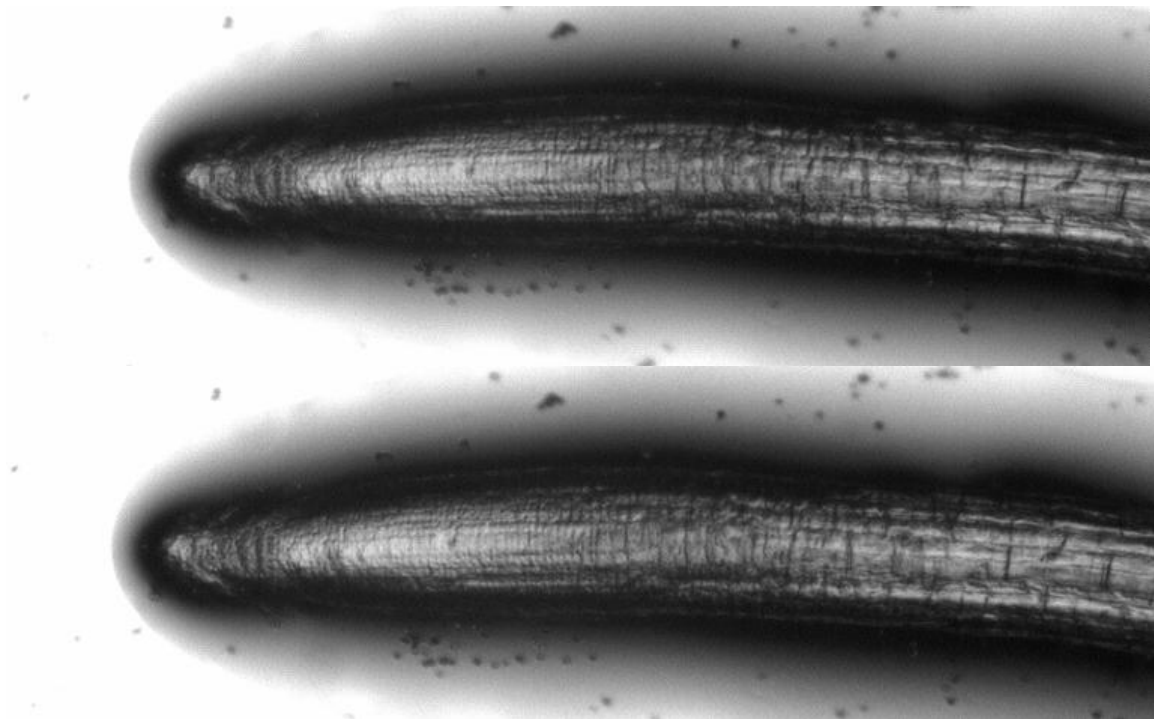


Figure 5.9 Image CGI1 Stack 1 Frames 1 and 9, showing small variation in light levels as observable by the naked eye.

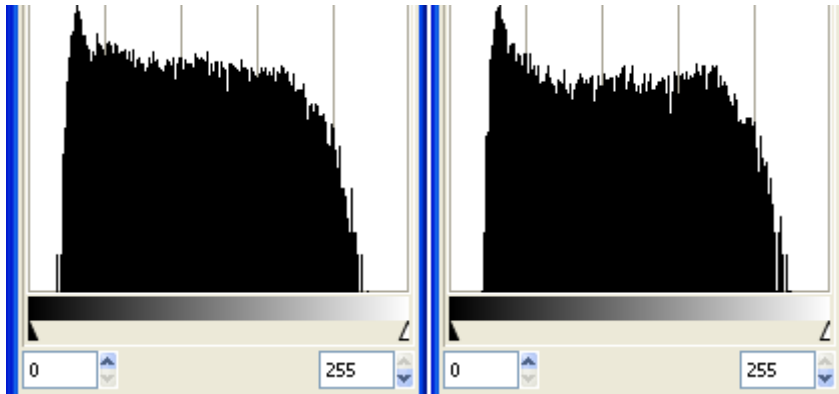


Figure 5.10 Histograms of the mid root areas for the image sets shown in Figure 5.9. Some variation is apparent with an increased number of bright pixels in the second image (Mean gray level 101 rather than 99 for the first image).

The samples were chosen to represent the range of image types encountered when root growth is being measured. For this reason some were chosen for lower variation of image luminance within the region. Others were chosen because the growth was large (more than one pixel change between images) compared to the majority (approximately 0.5 pixel change between successive images) and others where the growth was smaller than usual (as little as 0.3 pixels of motion between successive images). Finally images were chosen where the direction of growth was not close to horizontal in the image or where it changed noticeably in the image (see for example set AJOPA1 in Figure 5.1). The sets of values for the all 20 example measurements are listed in Table 5.2. The values shown in this table are the raw U and V vectors for the sample group. In Table 5.3 the values of midline parallel and perpendicular growth are given as well as the standard deviation in the growth rate for the various samples together with the manual measurement estimate for the nearest point to the sample point. The parallel and perpendicular growth is the estimated mean value along the

midline for the sample shown. Again it is stressed that it is the change in this measurement along the midline that is of most value to the final users and so the variation in these values is of vital importance. It is also stressed that in general the method proposed in this thesis is providing a more reliable answer than the value obtained by the manual method.

| | Optical Flow | | RootFlowRT | | Manual | | Final Result | |
|------------|--------------|--------------|------------|-------------|------------|------------|---------------|----------------|
| | U | V | U | V | U +/- 1 | V +/- 1 | U | V |
| AJH1 1 1 | -3 +/- 4 | -1 +/- 6 | -3 +/- 3 | 0 +/- 2 | -3 | 1 | -3.0 +/- 0.2 | 0.0 +/- 0.0 |
| AJH1 1 2 | -3.0 +/- 0.5 | 0.5 +/- 0.6 | -2 +/- 2 | 0 +/- 1 | -3 | 0 | -3.0 +/- 0.0 | 0.0 +/- 0.0 |
| AJH1 1 3 | -3.0 +/- 0.6 | 1 +/- 1 | -3 +/- 2 | 0.1 +/- 0.8 | -3 | -1 | -3.0 +/- 0.0 | 0.0 +/- 0.0 |
| AJH1 2 1 | -3 +/- 1 | 0 +/- 1 | -3 +/- 2 | 0 +/- 2 | -3 | 0 | -3.0 +/- 0.9 | 0.0 +/- 0.5 |
| AJH1 2 2 | -2 +/- 1 | 0 +/- 1 | -2 +/- 2 | 0 +/- 2 | -2 | 0 | -2 +/- 1 | 0.0 +/- 0.5 |
| AJH1 2 3 | -1 +/- 1 | 0 +/- 1 | -1 +/- 2 | 0 +/- 2 | -2 | 0 | -1 +/- 1 | 0.0 +/- 0.9 |
| CGI1 1 1 | -13 +/- 2 | -4 +/- 2 | -11 +/- 3 | -5 +/- 1 | -11 | -4 | -11.8 +/- 0.4 | -5.00 +/- 0.05 |
| CGI1 1 2 | -7 +/- 2 | -3 +/- 2 | -7 +/- 6 | -4 +/- 3 | -12 | -6 | -10 +/- 3 | -6 +/- 1 |
| CGI1 1 3 | -7 +/- 3 | -4 +/- 2 | -7 +/- 4 | -5 +/- 3 | -9 | -5 | -8 +/- 1 | -5.7 +/- 0.8 |
| CGI1 2 1 | -7 +/- 3 | -4 +/- 2 | -5 +/- 3 | -3 +/- 2 | -7 | -3 | -6 +/- 1 | -2.8 +/- 0.9 |
| CGI1 2 2 | -2 +/- 3 | -4 +/- 2 | -3 +/- 2 | -3 +/- 2 | -4 | -4 | -3 +/- 2 | -2.8 +/- 0.9 |
| CGI1 2 3 | -1 +/- 1 | -2 +/- 1 | -3 +/- 2 | -3 +/- 1 | -2 | -3 | -2 +/- 1 | -2.5 +/- 0.9 |
| AJOPA1 1 1 | -2 +/- 1 | -1 +/- 1 | -3 +/- 3 | 0 +/- 1 | -3 | 0 | -2.7 +/- 0.6 | -0.1 +/- 0.4 |
| AJOPA1 1 2 | -1 +/- 1 | -1 +/- 1 | -2 +/- 3 | 1 +/- 3 | -2 | 0 | -1.6 +/- 0.5 | 0.6 +/- 0.6 |
| AJOPA1 1 3 | -0.0 +/- 0.3 | 0.0 +/- 0.3 | 0 +/- 2 | 0 +/- 1 | -1 | 0 | -0.4 +/- 0.6 | 0.0 +/- 0.2 |
| UAJI1 1 1 | -7 +/- 1 | 1.0 +/- 0.9 | -3 +/- 4 | 0 +/- 3 | -5 | 1 | -5 +/- 3 | 1.0 +/- 0.9 |
| UAJI1 1 2 | -7 +/- 1 | 1.0 +/- 0.9 | -5 +/- 4 | 0 +/- 2 | -5 | 1 | -5 +/- 3 | 1.0 +/- 0.9 |
| UAJI1 1 3 | -6 +/- 1 | -1 +/- 1 | -2 +/- 3 | 0 +/- 3 | -4 | -1 | -3 +/- 2 | 0.0 +/- 0.0 |
| UAJI1 2 2 | -1.0 +/- 0.7 | 0.0 +/- 0.8 | -2 +/- 3 | 0 +/- 3 | -2 | 0 | -2.0 +/- 0.8 | 0.0 +/- 0.0 |
| UAJI1 2 3 | -2.0 +/- 0.3 | -0.8 +/- 0.5 | -2 +/- 2 | 0.0 +/- 0.8 | -2 | 0 | -2.0 +/- 1.0 | 0.0 +/- 0.0 |

Table 5.3 Comparison of Scale Space measured raw U and V vectors with raw U and V vectors for RootFlowRT and manual measurement. The values are average values for a given data set where the values are considered reliable. For definitions of what this means for a given measurement type see the main text

| Sample Name Stack No and Set no | RootFlowRT | | The Current Work | | Manual | |
|---------------------------------|--------------|---------------|------------------|----------------|--------------|---------------|
| | Parallel | Perpendicular | Parallel | Perpendicular | Parallel | Perpendicular |
| AJH1 1 1 | 3.0 +/- 1 | 0.3 +/- 0.7 | 3.5 +/- 0.4 | 1.0 +/- 0.1 | 3 +/- 1 | -1 +/- 1 |
| AJH1 1 2 | 2.5 +/- 1 | -0.1 +/- 0.4 | 2.999 +/- 0.001 | 0.05 +/- 0.05 | 3.0 +/- 0.5 | 0.1 +/- 0.5 |
| AJH1 1 3 | 3.0 +/- 1 | 0.1 +/- 0.5 | 4.96 +/- 0.01 | 0.61 +/- 0.09 | 5.0 +/- 0.5 | 0.8 +/- 0.5 |
| AJH1 2 1 | 3 +/- 2 | 0 +/- 2 | 2.95 +/- 0.01 | 1.13 +/- 0.03 | 3.2 +/- 0.5 | 0.2 +/- 0.5 |
| AJH1 2 2 | 2 +/- 2 | -1 +/- 2 | 1.4 +/- 0.3 | 0.7 +/- 0.2 | 1 +/- 1 | 1 +/- 1 |
| AJH1 2 3 | 1.4 +/- 0.8 | -0.1 +/- 0.5 | 1.26 +/- 0.01 | 0.63 +/- 0.02 | 0.9 +/- 0.5 | 0.4 +/- 0.5 |
| CGI1 1 1 | 11.7 +/- 0.6 | -5.2 +/- 0.2 | 11.8 +/- 0.3 | -5.03 +/- 0.05 | 12.0 +/- 0.5 | -5.0 +/- 0.5 |
| CGI1 1 2 | 10 +/- 3 | -5 +/- 3 | 10 +/- 2 | -6 +/- 2 | 10 +/- 1 | -6 +/- 1 |
| CGI1 1 3 | 8 +/- 2 | -4.6 +/- 0.7 | 9 +/- 1 | -4.7 +/- 0.4 | 9 +/- 1 | -5 +/- 1 |
| CGI1 2 1 | 6 +/- 2 | -3 +/- 2 | 5 +/- 1 | -2.9 +/- 0.4 | 5 +/- 1 | -3 +/- 1 |
| CGI1 2 2 | 4 +/- 2 | -2 +/- 2 | 4.4 +/- 0.7 | -2.0 +/- 0.3 | 5 +/- 1 | -2 +/- 1 |
| CGI1 2 3 | 4.4 +/- 0.8 | -1.0 +/- 0.2 | 3.7 +/- 0.4 | -1.1 +/- 0.2 | 4.0 +/- 0.5 | -1.0 +/- 0.5 |
| AJOPA1 1 1 | 2.7 +/- 0.6 | 0.9 +/- 0.6 | 2.5 +/- 0.3 | 1.0 +/- 0.2 | 2.0 +/- 0.5 | 1.0 +/- 0.5 |
| AJOPA1 1 2 | 2 +/- 1 | 0 +/- 1 | 1.3 +/- 0.3 | 0.9 +/- 0.4 | 1.0 +/- 0.5 | 1.0 +/- 0.5 |
| AJOPA1 1 3 | 1 +/- 1 | -0 +/- 1 | 0.6 +/- 0.4 | 0.04 +/- 0.06 | 1 +/- 1 | 0 +/- 1 |
| UAJI1 1 1 | 6 +/- 2 | -2 +/- 3 | 7 +/- 2 | 1 +/- 1 | 7 +/- 1 | 0 +/- 1 |
| UAJI1 1 2 | 6 +/- 3 | -1 +/- 1 | 7.4 +/- 0.4 | -1 +/- 1 | 7 +/- 1 | -1 +/- 1 |
| UAJI1 1 3 | 3 +/- 1 | -4 +/- 4 | 3 +/- 1 | -0.7 +/- 0.2 | 3 +/- 1 | 0 +/- 1 |
| UAJI1 2 2 | 3 +/- 2 | -2 +/- 3 | 2.0 +/- 0.3 | -0.30 +/- 0.05 | 2 +/- 1 | 0 +/- 1 |
| UAJI1 2 3 | 2.7 +/- 0.8 | -0.3 +/- 0.3 | 2.6 +/- 0.5 | -0.18 +/- 0.04 | 3.0 +/- 0.5 | 0 +/- 0.5 |

Table 5.4 Comparison of midline growth rates parallel and perpendicular to the midline for the sample set of images. These images were chosen at random. The first images of each stack are shown in Figure 6.8. The location of each set is indicated on the relevant stack image in that figure. Note that in all cases the current work gives a much better error than the RootFlowRT which is the method currently employed by biologists

| | RootFlowRT | Current research method |
|------------|------------|-------------------------|
| AJH1 1 1 | 36 | 56 |
| AJH1 1 2 | 40 | 58 |
| AJH1 1 3 | 50 | 31 |
| AJH1 2 1 | 29 | 49 |
| AJH1 2 2 | 43 | 63 |
| AJH1 2 3 | 48 | 64 |
| CGI1 1 1 | 50 | 52 |
| CGI1 1 2 | 20 | 26 |
| CGI1 1 3 | 33 | 45 |
| CGI1 2 1 | 32 | 54 |
| CGI1 2 2 | 54 | 44 |
| CGI1 2 3 | 68 | 65 |
| AJOPA1 1 1 | 49 | 78 |
| AJOPA1 1 2 | 47 | 77 |
| AJOPA1 1 3 | 55 | 84 |
| UAJI1 1 1 | 16 | 19 |
| UAJI1 1 2 | 27 | 28 |
| UAJI1 1 3 | 28 | 47 |
| UAJI1 2 2 | 47 | 75 |
| UAJI1 2 3 | 57 | 72 |

Table 5.5 Comparison of percentage of measurements which are “good” for the current method compared to the RootFlowRT. In both cases good is defined as the number of measurements for a given pixel where the growth rate is within one standard deviation of the value obtained in the 5 by 5 neighbourhood of the pixel.

| Sample Name Stack No and Set no | RootFlowRT % error rate | The Current Work % error rate |
|---------------------------------|-------------------------|-------------------------------|
| AJH1 | 63 | 18 |
| CGI1 1 1 | 64 | 10 |
| AJOPA1 1 1 | 59 | 18 |
| UAJI1 1 1 | 50 | 18 |

Table 5.6 Comparison of error rate as a percentage of the midline growth rate as detected by RootFlowRT compared to the current method

5.6 Discussion of the result comparisons

Note from Table 5.2 and 5.3 the error for the final measurement in this work is smaller than that from the manual measurement. In general this leads to a final value that is identical (within the error limits) for both the manual measurement and that used in this work. Where there is a difference it is the method used in this work that is giving the value closer to correct. For example where the growth over 9 frames is less than 1 pixel this is not detectable by the manual method but is by the method used in this work. In these examples the result from RootFlowRT may appear closer to the manual method but that is because the error from this method also makes it impossible to detect the change reliably. For example for the sample AJOPA1 1 1 in Table 5.2 the V value from the current method is -0.1 ± 0.4 pixels per 10 seconds whereas RootFlowRT gives -1 ± 1 and the manual method gives 0 ± 1 .

The number of pixels used to make the estimate is a significant factor in the measurement reliability. In the RootFlowRT method this is decided purely by the number of pixels which conform to the forward backward matching criteria. In the current work this has been extended to require that the measurement gives a result which is physically sensible – that is it conforms to the constraint that pixels move similarly to their nearest neighbours. In this case a neighbourhood of ± 2 pixels in the horizontal and vertical dimensions has been taken. This has been described in Chapter 4. Thus the comparison of Table 5.4 is somewhat unfair on the current method as the restriction is more stringent than that of RootFlowRT. However, in almost all cases the percentage of valid measurements is higher for the current method.

Finally the importance of measurement accuracy is stressed in Table 5.5. As has been pointed out a number of times the main objective of the biologists is to measure the change in growth rate along the midline. Table 5.5 presents the error in measurement as a percentage of the change in the parallel growth rate for the samples studied. In all cases the RootFlowRT shows an error in the measurement of at least 50% of the change being measured. Whereas for the current method the error is never more than 18% of the effect.

5.7 Growth on the Midline

The final point in the previous section is illustrated well by a visual comparison of the midline growth values throughout a midline for a given root. Figure 5.11 shows the growth vector magnitude along the midline at 1230 locations for sample CG1 (both stacks). In the figure the values without using the scale space refinement of the search space are given in black and those after limiting the search space using the scale space data are given in pink. The greater reliability and lower error limits of the post scale space data are clear.

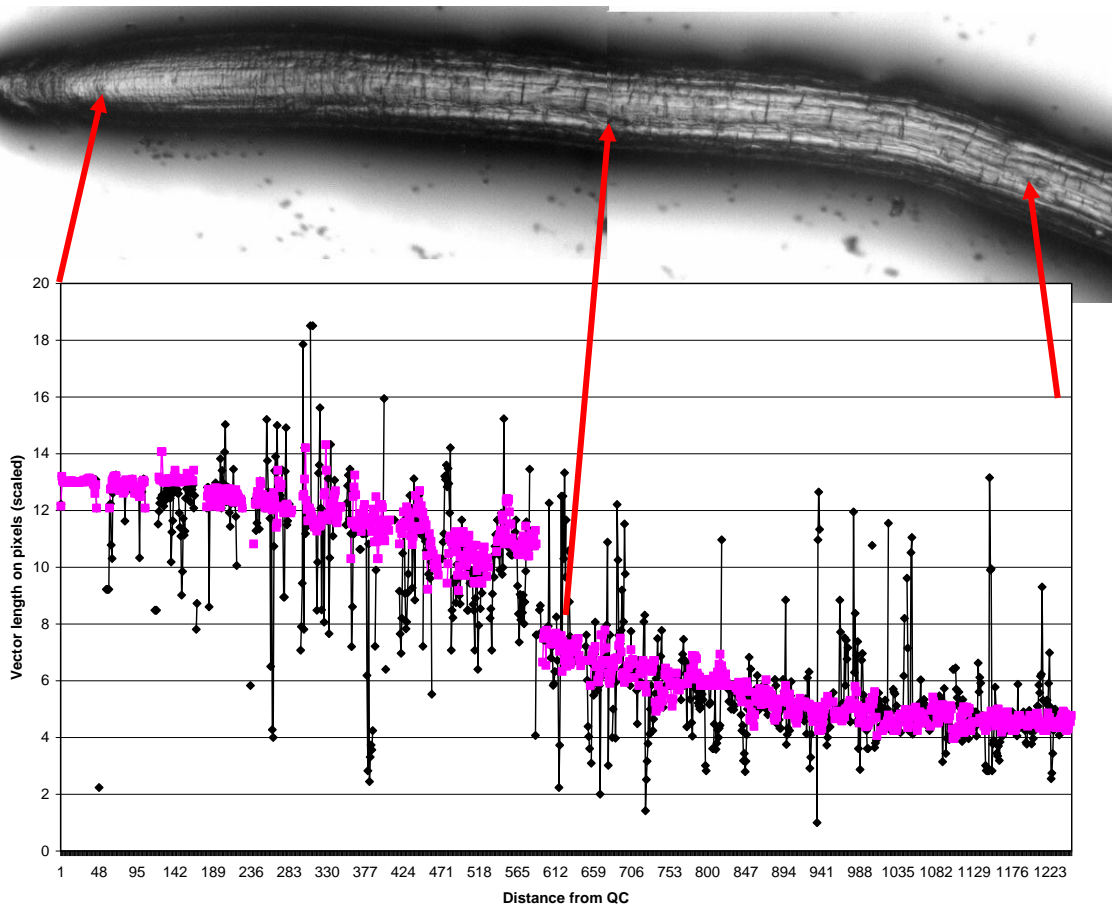


Figure 5.11 The growth rate along the midline for two successive stacks from the sample CG1 with arrows showing the approximate point the results correspond to. The values in black are result from not using the scale space values to limit the search space and those in pink from using the scale space values. This example is used because the rate of growth is higher than commonly found.

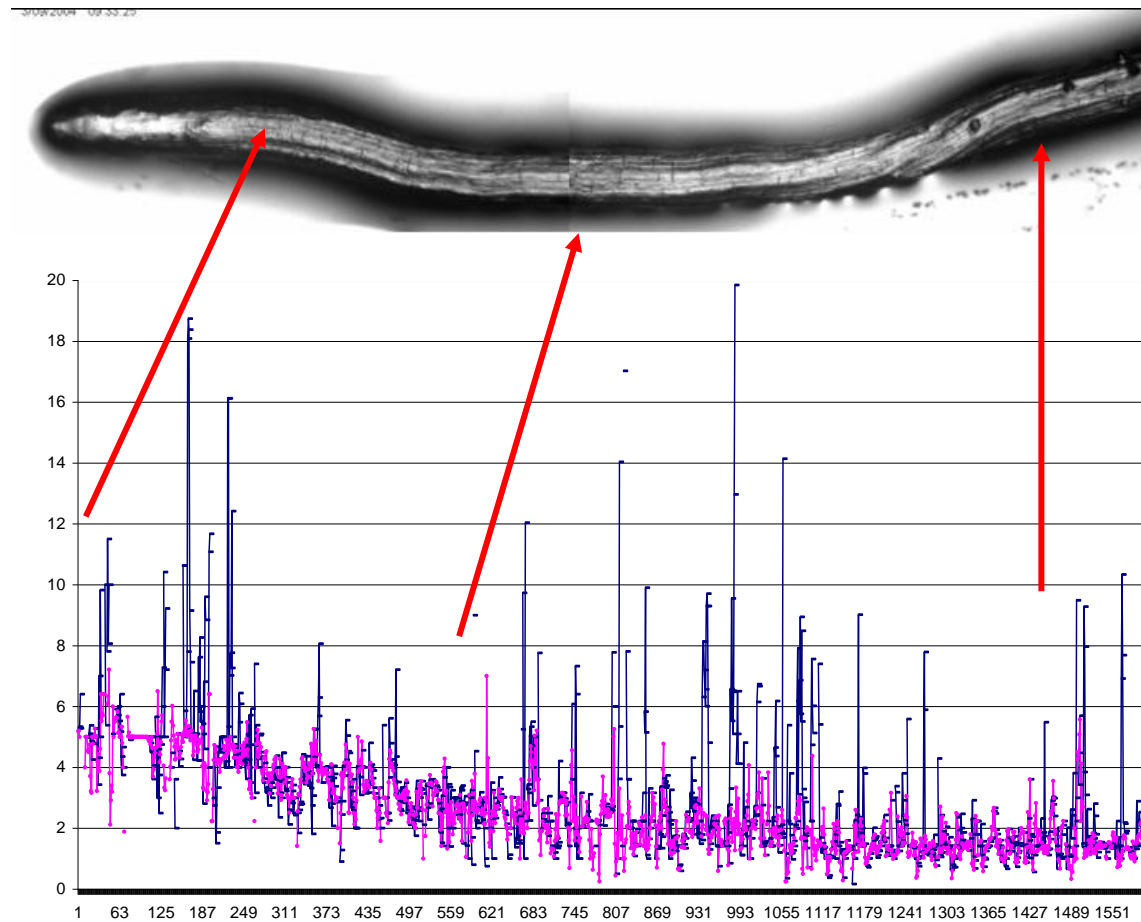


Figure 5.12 The growth rate along the midline for two successive stacks from the sample AJH1 with arrows showing the approximate point the results correspond to. The values in blue are result from not using the scale space values to limit the search space and those in pink from using the scale space values. This example is used because the rate of growth is in the range most commonly found. The data would normally be filtered to remove extreme data.

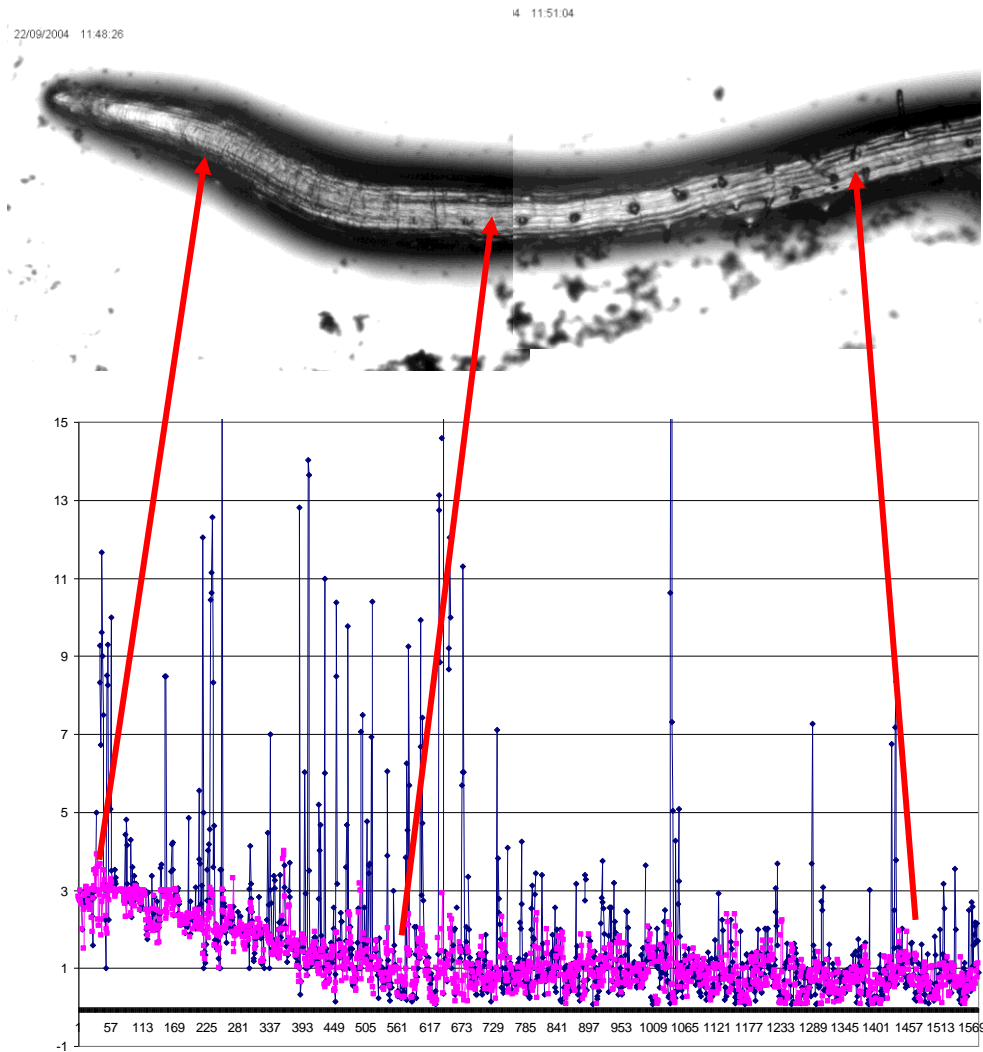


Figure 5.13 The magnitude of the growth rate along the midline for two successive stacks from the sample AJOPA1 with arrows showing the approximate point the results correspond to. The values in blue are result from not using the scale space values to limit the search space and those in pink from using the scale space values. This example is used because the rate of growth is smaller than usual. No attempt has been made to remove extreme data. While this would normally be done the figure does illustrate the large proportion of the values that would be unusable for a sample where such low growth rates are occurring if the information from the scale space optical flow is not included. It is also significant that the beginning of the region where the growth changes rapidly also corresponds to a point where the growth direction changes rapidly.

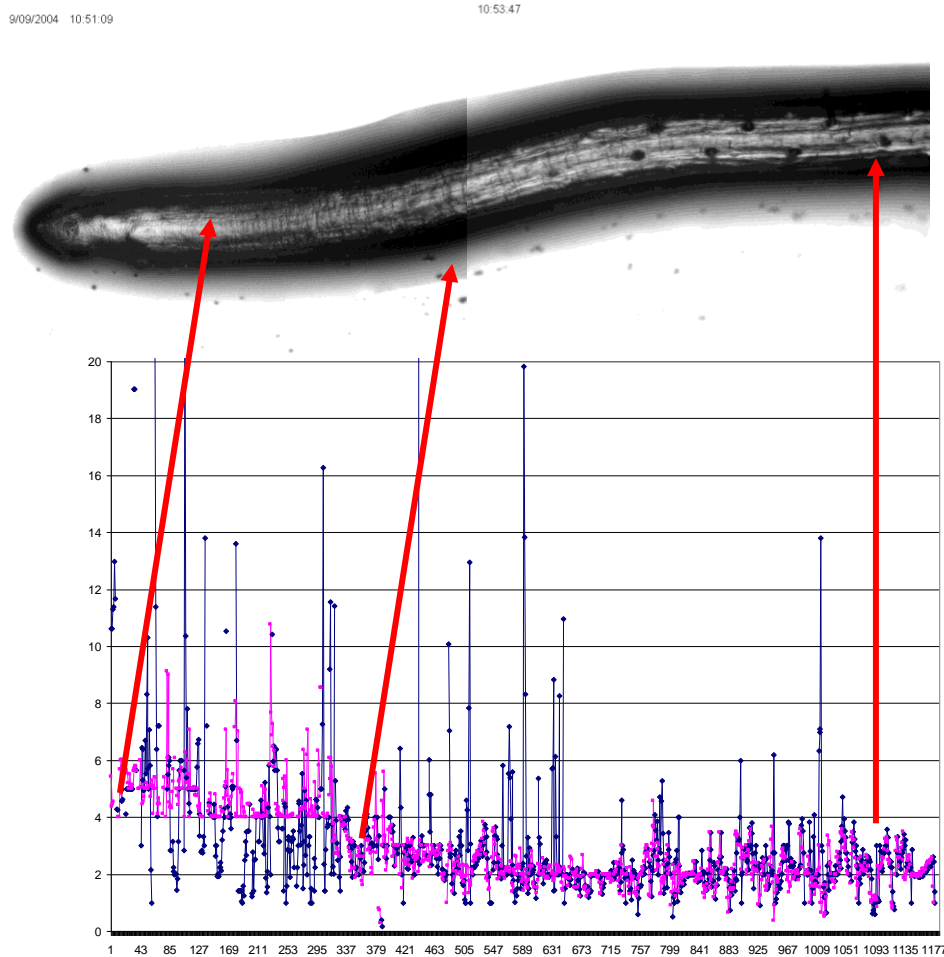


Figure 5.14 UAJ1 The magnitude of the growth rate along the midline for two successive stacks from the sample UAJ1 with arrows showing the approximate point the results correspond to. The values in blue are result from not using the scale space values to limit the search space and those in pink from using the scale space values. This example is used because the rate of growth is within the most common region the figure illustrate the large proportion of values that would be unusable for a sample such as this especially in the low contrast area at the left of the figure and through the most important region where change in the real growth rate is occurring rapidly (the middle region).

5.8 Value of the improvement in growth rate estimation

Inspection of the results shown in Tables 5.2 and 5.3 show that the method developed in the current work has a significantly higher level of reliability than that obtained for the previous method. This is shown to be particularly significant when measuring the growth rate along the midline for plant roots with very low growth rates. The area of greatest significance in many measurements is the transition region. Application of statistical filtering can significantly improve the results from the existing method but this involves rejecting outlying data. However for the slow growth rate plants the amount of data that would need to be rejected would lead to only sparse sets of data being accepted as reliable and limit the usefulness of the data in the transition regions.

For example a simple median filtering of the data (Figure 5.14) produces a much smoother response but the values for the previous method (in blue) still show significant variation at the end of the transition region. (Both sets of data also show clear evidence of misalignment when moving between stack 1 and stack 2 around sample 685.)

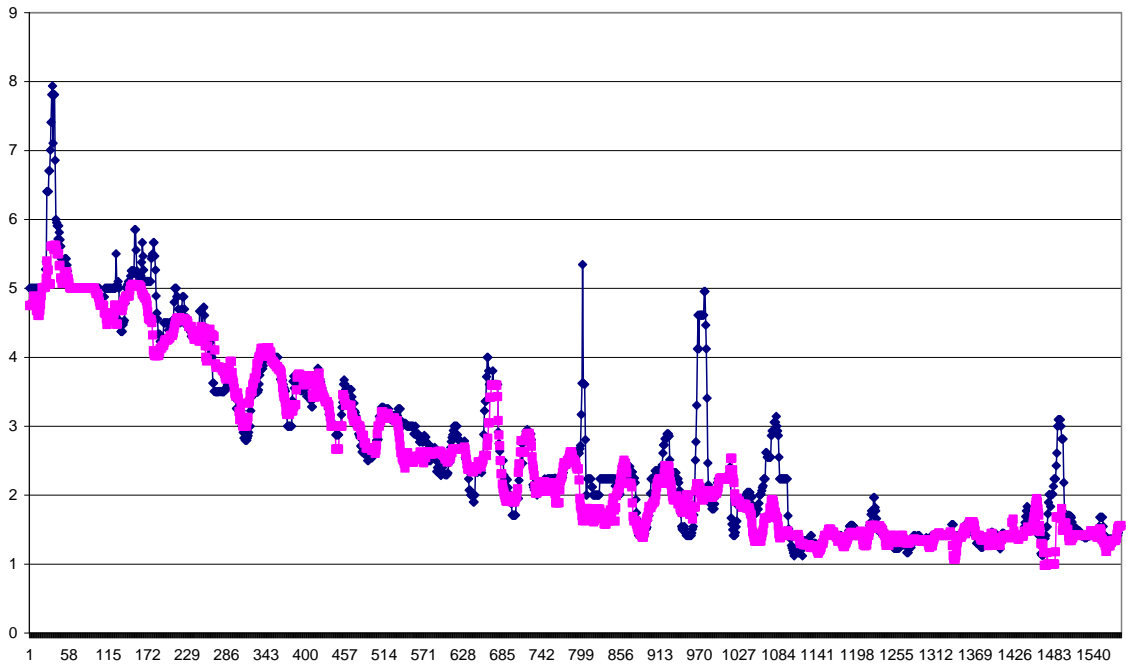

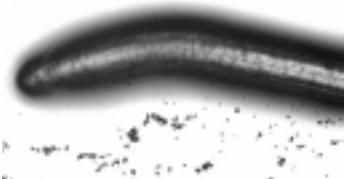






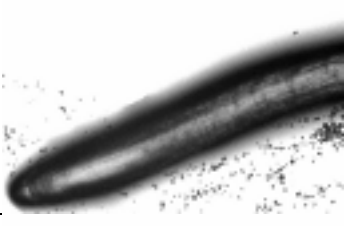











Figure 5.15 result of median filtering of the midline growth data for the sample AJH1 – a set showing lower than usual growth rates. The results from the previous method are shown in blue; those for the current method are shown in pink.



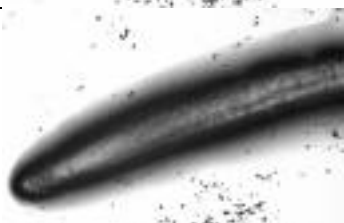



5.9 Extension Experiments

For further comparison of the effectiveness of the two methods (RootFlowRT and the current method) a further 37 experiments were carried out in which the value of the growth rate in the x direction was measured. The values are plotted in table 5.7. In this table is the image identifier given by the biologists [36]. An example from the image stack is also shown. The table lists the values of estimate of growth rate is given as accurately as the method allows. In all cases the current method gave a better error rate than the RootFlowRT method. In many cases the former method has a spread of measurements (noted as the Error in the table) greater than the value that is being measured. The images come in sets labelled by the plant identifier name and the sample number. The samples in a set are normally second sequences of the same image at slightly different times (approximately 2 minute intervals). The reliability of the former method is insufficient to allow this to be of much value.

| Plant | Sample | Image | Change in horizontal growth | | | |
|--------|--------|---|-----------------------------|-------|-----------------------|-------|
| | | | RootFlowRT value | Error | Current Value | Error |
| | | | pixels per 80 seconds | | pixels per 80 seconds | |
| uaraux | 1 |  | 0 | 3 | 0.2 | 0.1 |
| | 1a |  | 1 | 4 | 0.2 | 0.08 |
| | 2 |  | 0 | 3 | 0.3 | 0.7 |
| | 2a |  | 1 | 2 | 0.2 | 0.05 |
| | 3 |  | 0 | 2 | 0.4 | 0.1 |
| | 3a |  | 1 | 3 | 0.2 | 0.1 |

| Plant | Sample | Image | Change in horizontal growth | | | |
|-------|--------|---|-----------------------------|-----------------------|---------------|-------|
| | | | RootFlowRT value | Error | Current Value | Error |
| | | | pixels per 80 seconds | pixels per 80 seconds | 1.4 | 0.6 |
| | 3 |  | 2 | 1 | 1.8 | 0.7 |
| cf | 1 |  | 1 | 3 | 1.3 | 0.5 |
| | 2 |  | 2 | 1 | 1.9 | 0.4 |
| | 3 |  | 3 | 1 | 2.5 | 0.6 |
| uajh | 1 |  | 2 | 2 | 2.3 | 0.7 |
| | 2 |  | 2 | 3 | 2.4 | 0.3 |

| Plant | Sample | Image | Change in horizontal growth | | | |
|-------|--------|---|-----------------------------|-----------------------|---------------|-------|
| | | | RootFlowRT value | Error | Current Value | Error |
| | | | pixels per 80 seconds | pixels per 80 seconds | 1.8 | 0.5 |
| | 2 |  | 2 | 2 | 1.8 | 0.8 |
| | 3 |  | 2 | 2 | 1.9 | 0.8 |
| aji | 1 |  | 2 | 2 | 2.1 | 0.2 |
| | 2 |  | 2 | 1 | 2.2 | 0.5 |
| | 3 |  | 2 | 1 | 2.1 | 0.7 |
| ajk | 1 |  | 1 | 3 | 0.8 | 0.1 |

| Plant | Sample | Image | Change in horizontal growth | | | |
|-------|--------|---|-----------------------------|-----------------------|---------------|-------|
| | | | RootFlowRT value | Error | Current Value | Error |
| | | | pixels per 80 seconds | pixels per 80 seconds | 0.9 | 0.8 |
| cg | 1 |  | 3 | 3 | 2.9 | 0.7 |
| | 2 |  | 2 | 2 | 2.2 | 0.7 |
| | 3 |  | 2 | 2 | 2.2 | 0.7 |
| | 4 |  | 2 | 1 | 2.3 | 0.7 |
| ci | 1 |  | 3 | 4 | 3.2 | 0.5 |
| | 2 |  | 3 | 4 | 3.4 | 0.6 |







| Plant | Sample | Image | Change in horizontal growth | | | |
|-------|--------|---|-----------------------------|-----------------------|---------------|-------|
| | | | RootFlowRT value | Error | Current Value | Error |
| | | | pixels per 80 seconds | pixels per 80 seconds | 3.1 | 0.6 |
| uaji | 1 |  | 3 | 1 | 3.7 | 0.5 |
| | 2 |  | 4 | 2 | 3.5 | 0.8 |
| | 3 |  | 4 | 2 | 3.8 | 0.8 |
| uan | 1 |  | 1 | 1 | 0.7 | 0.5 |
| | 2 |  | 1 | 2 | 0.9 | 0.4 |
| | 3 |  | 1 | 2 | 0.8 | 0.5 |

Table 5.7 Comparing the results from RootFlowRT and the current method for a wider range of targets. In all cases the current work gives a higher resolution due to improved result reliability

More recently the Plant Biology group at the University have not been able to use RootFlowRT on the specimens they have been study so they asked that the images be measured using the current software. A typical image from that group is shown in Figure 5.16



Figure 5.16 Image for which the RootFlowRT software fails.

An experiment was carried out on the image set for which the image in Figure 5.16 is the first of a sequence and a set of other similar sequences. In no example set was it possible to obtain a value for the growth rate using the RootFlowRT software. However values of growth rate comparable with manual evaluation were achieved

using the current method. The major reason for the failure of RootFlowRT would seem to be the extremely low contrast in many areas of the image. This could be enhanced by use of histogram equalisation but this would also improve the performance of the current method and the reliability of the results for the current method would still be greater.

5.10 Summary

In order to compare the proposed technique to the previously adopted method it was first necessary to develop ground truth measures for the growth rate for a representative sample of images. For this reason a set of example images were chosen that exhibited the major characteristics of the plant root images and the spread in those images. The images selected were shown in Figure 5.1. They represent the range of growth rates found in the full image sets provided by the School of Plant Biology. The growth rates vary from ~ 2 pixels per image (0.2 pixels per second) down to 0.25 pixels per image. (Values reported in the growth rate tables are for a total sequence of 9 images so are values range from ~ 12 down to ~ 1 pixel per 8 images). The images were first analysed manually, though a piece of software was devised to make this more efficient where measurements could be made by clicking on zoomed areas of images that were being compared. This process was found to be reliable to better than ± 1 pixel in a set (measuring between the first and 9th images of a set).

Measurements were then made using the previous method (RootFlowRT) commonly in use by biologists. Systematic analysis showed that the previously noticed bias of these results to underestimate the growth was untrue as the problem was merely a low reliability of the results. Only by removing a significant proportion of the data (making measurements based on less than ten percent of measurements for large areas of images) were the results reliably close to the ground truth measure.

The previous work had attempted to use a tensor based method founded on the work of Horn and Schunck [20]. However the method was flawed in the way the differential operator was designed and applied and they only obtained a 5% reliability for their results. In the current work a scale space differential method was used based on the work of ter Har Romeney [29] and this proved to give a much higher level of reliability (see Table 6.2) normally as good as the results of the correspondence method used in the previous work. Varying the spatial scale was shown to improve these results but in order to make the method more accessible to practitioners (generally plant biologists not computer scientists) it was decided to fix the value of spatial scale used to one that works reasonably well for the full range of images.

It was thus possible to use the results of the scale space based optical flow measurement to determine a suitable search space for the correspondence measurement. This was done by using the mean value for a given pixel obtained by the scale space measure as the origin for the search space and fixing the limits of the search space as plus or minus twice the standard deviation on the measurements in the region of the pixel being measured. In this way the reliability of the measurements on the midline were consistently improved (see Table 6.3).

Clearly in all the examples the biggest advantage of the proposed method over that currently in common use is the improved level of noise in the measurements. For the samples where the growth rate is large (e.g. CGI1 near the tip) the variance in the results is much smaller (see figure 6.4 for example).

Chapter 6 Conclusions and Suggestions for Further Work

In chapter 1 it was claimed that the needs of population growth have led to great urgency in the development of plants which are faster growing and can survive in harsher conditions, with less susceptibility to disease, and in smaller areas with greater competition. This has led plant biologists to search for new ways to improve plant growth. However this also introduces the need to accurately measure the results of their experiments. Until recently the main approach to measuring the effectiveness of these experiments has been to use traditional bright field microscopes to inspect the exterior of the plants. Recent experiments involving confocal microscopes and dyeing of feed types has been described in chapter 2. These methods give the opportunity to look down to the cell level at the effectiveness of the biological experiments. However, as explained in chapter 2 these methods are very expensive and require far greater skill to set up so the traditional methods remain extremely useful. However, as explained at various points the current techniques in use by biologists and in particular RootFlowRT are extremely error prone and thus reduce the reliability of the results. This problem has been noted by the developer of RootFlowRT in private communication. The work of this thesis has determined the reason for the errors in the previous methods and produced a method that has a much higher reliability and accuracy than the previous method. The results of this work are now being used by the School of Plant Biology at the University of Nottingham in their recent studies.

To develop the current method two main testing processes were undertaken. The method is based on combining the findings from a block matching correspondence method with those of a Scale Space Optical Flow approach. Both approaches were seen to add value to the total process however initially the methods were tested separately and their results compared. This has been reported in chapter 4. For this purpose a set of test images was created by transforming an original image from one of the data sets by known amounts. These results showed that:

- For integer displacements in any direction the correspondence method was extremely accurate with virtually no errors in the final filtered results
- A-priori knowledge of the velocity of motion reduced the time taken for these matches and was useful in eliminating errors
- For non integer pixel motions the Scale Space approach gave more reliable results when the scaling applied was tuned to the problem
 - However the resolution of this method is limited by the scale used
- Obtaining the correct results from the Scale Space Optical Flow was time consuming and needed expert tuning
 - It was thus decided to use a combination of the two approaches. The scale space method was applied with a general value of scale to obtain a first estimation of motion velocity across the images of interest
 - This a-priori velocity information allowed high reliability from the correspondence methods

The value of the current work has been highlighted by looking at a set of test cases as reported in Chapter 5. A subsequent set of experiments on 37 real image sequences confirmed these results. New data provided by the Biology School of recent images using higher resolution cameras proved impossible to measure using the RootFlowRT technique but were successfully measured using the current technique.

6.1 Issues with RootFlowRT

These experiments to confirm the value of the proposed method also identified the bigger problems of the RootFlowRT approach. As was reported in chapter 2 the RootFlowRT approach makes use of two methods:

- A tensor method based on an extension of the Horn and Schunk approach
- A correspondence method dependant on forward backward block matching to evaluate the match

The problems from the tensor approach were evident in the results provided by the developers of RootFlowRT. They reported [jiang thesis reference] that only 5% of the results of their tensor method were reliable. However they offered no explanation of this. One direct problem became evident by analysing their code in order to determine where their issues were occurring. A significant fact appeared to be their use of a Sobel operator to obtain their first differential. This has two problems. First of all it is not an accurate measure of differential of an image. Secondly it introduces aliasing effects which work against the accuracy of the process. Subsequent work – notably that of Florack et al [24] have improved on this and the implementation of this using a Gaussian Scale Space approach removes those errors.

A second problem was evident once detailed analysis of the intermediate results of the RootFlowRT correspondence method were analysed. As was shown in Figure 5.6 even when the forward backward matching was indicating valid correspondence the actual matches accepted (and thus their contribution to the determined growth rate measure) contained many non physical matches that violate the concept that neighbour pixels move together. In the tests as much as 20% of the accepted results using the RootFlowRT approach are up to or greater than 100% in error both in magnitude and direction

6.2 Comparison of Results

The initial results on the 20 sample image areas were confirmed by measurements on 200 sample images provided by the School of Plant Biology. The method developed in this thesis out performed the RootFlowRT in all areas.

- Accuracy
 - Average error in measurement of parallel and perpendicular growth rate
 - +/- 0.002 μm per second for the current method
 - +/- 0.5 μm per second for the RootFlowRT approach
 - Average percentage of pixels providing useful results
 - RootFlowRT Tensor method 5%
 - Scale Space approach 50%
 - RootFlowRT correspondence 45%
 - Current method 54%
 - Validity of final results (percentage of measurements in the correct direction and size)

- RootFlowRT 70%
- Current Method 95%
- Maximum spread of invalid results
 - RootFlowRT +/-200% in size and 100% in direction
 - Current method +/- 10% in size or direction

The final two points are the most significant for the value of the results in making measurements of the rate of growth of plant roots. With only 70% of the results being valid the influence of the invalid results is great. With the spread of error in the results that are wrong for RootFlowRT the final number can be less reliable (in terms μm per second) than the change in growth on the whole root. As this is the major measure of interest to the plant biologists the advantage of the current work is thus evident. For the newer higher resolution lower contrast images however comparison is not possible as these images were not able to be processed by the RootFlowRT software. The current technique worked and so has been shown once more to be of greater value.

6.3 Future work

The value of the current work in eliminating the errors in the previous method has been acknowledged by the plant biologists. However the current software implementation is only a prototype and changes are needed to improve the value for the plant biologists. Major steps that could be undertaken include:

- Adding auto detection of the midline and quiescent point
- Automating the process of detection of growth parallel and perpendicular to the midline
- Adding statistical data to the output to enable evaluation by experimenters

- Adding a conversion to the output data from pixels per second to μm per second and referencing the input to the quiescent point

Auto mid line detection should be reasonably straight forward. At the moment the method depends on the user clicking on the image or adding the pixel locations by hand. This is error prone and auto detection would also aid in the second point - automating the midline growth measurement. Currently this process is achieved by the user indicating by clicking on the image where the end and start points for the midline are and the system maps a set of 60 by 60 blocks to this for the calculation purposes. Automating the midline capture would aid the mapping of more shape dependant areas for measurement, rather than simple square blocks. The final point is a simple one as the data for the images (number of pixels per μm) is known to the user and could easily be entered as a parameter (at the moment these conversions were made in Excel when the data was being analysed).

In addition to these simply practical developments it would be good to experiment with a direct matching of the Gaussian Scale Space approach to the adaptive block matching method. The Gaussian low pass filter can be used directly as a scaling device to reduce the images for the block matching method. Alternative scale approaches such as using suitable wavelet functions could also be adopted.

In conclusion the aim of finding a reliable and accurate way of measuring the growth of plant roots has been achieved. The results indicate a significant improvement in accuracy and reliability over previous methods.

References

- [1] World Food Programme. <http://www.wfp.org/global-food-crisis-indepth?gclid=CIDkzt3n3KYCFc0e4Qodp1KS1g> accessed Jan 2011
- [2] Weis T. 2010 "The Accelerating Biophysical Contradictions of Industrial Capitalist Agriculture" *Journal of Agrarian Change* Volume 10, Issue 3, pages 315–341, July 2010
- [3] FAO (Food and Agriculture Organization of the United Nations), 2008. *The State of Food Insecurity in the World, 2008*. Rome: FAO (<ftp://ftp.fao.org/docrep/fao/011/i0291e/i0291e00.pdf>) accessed March 2011
- [4] Svistoonoff S, Creff A, Reymond M, Sigoillot-Claude C, Ricaud L, Blanchet A, Nussaume L and Desnos T, 2007 "Root tip contact with low-phosphate media reprograms plant root architecture" *Nature Genetics*, Vol 39, pp. 792 - 796
- [5] Chavarría-Krauser A, Nagel K, Palme K, Schurr U, Walter A, Scharr H 2008 "Spatio-temporal quantification of differential growth processes in root growth zones based on a novel combination of image sequence processing and refined concepts describing curvature production" *New Phytologist* Volume 177, Issue 3, pp 811–821, February 2008
- [6] van der Weele C, Jiang H, Palaniappan K, Ivanov V, and Baskin T, 2003 "A New Algorithm for Computational Image Analysis of Deformable Motion at High Spatial and Temporal Resolution Applied to Root Growth. Roughly Uniform Elongation in the Meristem and Also, after an Abrupt Acceleration, in the Elongation Zone" *Plant Physiology* 132:1138-1148
- [7] Ma Z, Baskin T, Brown K, and Lynch J 2003 "Regulation of Root Elongation under Phosphorus Stress Involves Changes in Ethylene Responsiveness." *Plant Physiol*, March 2003, Vol. 131, pp. 1381-1390
- [8] Roudier F, Fernandez A, Fujita M, Himmelspach R, Borner G, Schindelman G, Song S, Baskin T, Dupree P, Wasteneys G and Benfey P, 2005 "COBRA, an Arabidopsis Extracellular Glycosyl-Phosphatidyl Inositol-Anchored Protein, Specifically Controls Highly Anisotropic Expansion through Its Involvement in Cellulose Microfibril Orientation" *The Plant Cell* Vol 17 pp 1749-1763
- [9] Paredez A, Somerville C and Ehrhardt D 2006 "Visualization of Cellulose Synthase Demonstrates Functional Association with Microtubules" *Science* 9 June 2006: Vol. 312 no. 5779 pp. 1491-1495
- [10] Baskin T, 2000 "On the constancy of cell division rate in the root meristem" *Plant Molecular Biology* Volume 43, Numbers 5-6, 545-554

- [11] Ueda T, Yamaguchi M, Uchimiya H and Akihiko Nakano A 2001 "Ara6, a plant-unique novel type Rab GTPase, functions in the endocytic pathway of *Arabidopsis thaliana*" *The EMBO Journal* (2001) 20, 4730 – 4741
- [12] Zeidler D, Zähringer U, Gerber I, Dubery I, Hartung T, Bors W, Hutzler P, and Durner J, 2004 "Innate immunity in *Arabidopsis thaliana*: Lipopolysaccharides activate nitric oxide synthase (NOS) and induce defense genes" *Proceedings of the National Academy of Sciences of the USA* 101, pp. 15811–15816
- [13] Wu A, Ding L and Zhu J 1996 "SOS1, a Genetic Locus Essential for Salt Tolerance and Potassium Acquisition" *The Plant Cell*, Vol. 8, pp 617-627
- [14] Jiang Z and Staude W 1989. "An Interferometric Method for Plant Growth Measurements" *Journal of Experimental Botany* Volume 40, Issue 10 pp. 1169-1173
- [15] Meurer, G., 1968. "Rapid inhibition of gherkin hypocotyls in blue light." *Ada botanica neerlandica*, Vol 17, pp 9-14
- [16] Penney D, Penney P and Marshall D, 1974 "High resolution measurement of plant growth." *Canadian Journal of Botany*, Vol 52, pp 959-69.
- [17] Dixon L, Leverone J 1995 "Light requirements of *Thalassia testudinum* in Tampa Bay Florida" *Surface Water Improvement and Management Program Southwest Florida Water Management District 7601 U.S. Highway 301 North Tampa, Florida 33637*
- [18] Barron J and Liptay A, 1994 "Optical Flow to measure minute increments in plant growth" *Bioimaging* Volume 2, Issue 1, pp 57–61
- [19] Palaniappan K., Jiang H, Baskin T, 2004 "Non-Rigid Motion Estimation Using the Robust Tensor Method" 2004 Conference on Computer Vision and Pattern Recognition Workshop (CVPRW'04) Volume 1
- [20] Horn B and Schunck B, 1981 "Determining optical flow" *Artificial Intelligence* Volume 17, pp. 185–203.
- [21] Gruner A, Hoverter N, Smith T, and Knight C, 2010 "Genome Size Is a Strong Predictor of Root Meristem Growth Rate" *Journal of Botany* Volume 2010, Article ID pp 390414 - 390418
- [22] Lucas B, and Kanade T 1981 "An iterative image registration technique with an application in stereo vision" *Proc. DARPA IU Workshop*. Pp 121-130
- [23] Simoncelli E, Adelson E and Hoeger D, 1991 "Probability distributions and optical flow *IEEE Proc. Of CVPR Maui* pp 310-315

- [24] Florack L, Niessen W, Nielsen M 1998 "The intrinsic structure of optic flow incorporating measurements of duality." *International Journal of Computer Vision* 27(3), pp 263–286
- [25] Niessen W, Duncan J, ter Haar Romeny B, Viergever M 1995 "Spatiotemporal analysis of left ventricular motion." *Medical Imaging 1995, San Diego*, pp. 192–203. SPIE (1995)
- [26] Niessen W, Duncan J, Nielsen M, ter Haar Romeny B, Viergever M 1997 "A multiscale approach to image sequence analysis." *Computer Vision and Image Understanding* 65(2), pp 259–268
- [27] Suinesiaputra A, Florack L, Westenberg J, ter Haar Romeny B, Reiber J, Lelieveldt B. 2003 "Optic flow computation from cardiac MR tagging using a multiscale differential method a comparative study with velocity encoded MRI." In: Ellis, R, Peters T, (eds.) *MICCAI 2003. LNCS*, vol. 2878, pp. 483–490. Springer, Heidelberg
- [28] van Assen H, Florack L, Suinesiaputra A, ter Haar Romeny B, Westenberg, J 2007 "Purely evidence based multi-scale cardiac tracking using optic flow." *MICCAI 2007 workshop on Computational Biomechanics for Medicine II*, pp. 84–93
- [29] ter Har Romeny B 2002 "Front End Vision and Multiscale Image Analysis" Kluwer Academic Publishers
- [30] Becciu A, van Assen H, Florack L, Kozerke S, Roode V and ter Haar Romeny B, 2009 "A Multi-scale Feature Based Optic Flow Method for 3D Cardiac Motion Estimation." X.-C. Tai et al. (Eds.): *SSVM 2009, LNCS 5567*, pp. 588–599, Springer-Verlag Berlin Heidelberg
- [31] Florack L, van Assen H 2007 "Dense multiscale motion extraction from cardiac cine MR tagging using HARP technology." *Mathematical Methods in Biomedical Image Analysis. Workshop of the ICCV (2007)*
- [32] Barron J 2004 "Experience with 3D optical flow on gated mri cardiac datasets." *Proceedings of the 1st Canadian Conference on Computer and Robot Vision*, pp. 370–377
- [33] Pan L, Prince J, Lima J, Arts N, 2005 "Fast tracking of cardiac motion using 3DHARP." *IEEE transactions on Biomedical Engineering* 52(8), pp 1425–1435
- [34] Sampath S, Prince J 2007 "Automatic 3D tracking of cardiac material markers using slice-following and harmonic-phase MRI." *Magnetic Resonance Imaging* 25, pp 197–208.

- [35] Swarup R, Kramer E, Perry P, Knox K, Ottoline Leyser H, Haseloff J, Beemster G, Bhalerao R and Bennett M 2005 "Root gravitropism requires lateral root cap and epidermal cells for transport and response to a mobile auxin signal" *Nature Cell Biology* 7, 1057 - 1065
- [36] Perry P. 2005 Private communication.
- [37] Pawley JB (editor) (2006). *Handbook of Biological Confocal Microscopy* (3rd ed.). Berlin: Springer. ISBN 038725921X
- [38] Roberts T, McKenna S, Wuyts N, Valentine T and Bengough A 2007 "Performance of Low-Level Motion Estimation Methods for Confocal Microscopy of Plant Cells in vivo" WMVC '07 Proceedings of the IEEE Workshop on Motion and Video Computing
- [39] Sethuraman V, Taylor S, Pridmore T, French A and Wells D 2009. "Segmentation and Tracking of Confocal Images of Arabidopsis thaliana Root Cells using Automatically-Initialized Network Snakes" 3rd International Conference on Bioinformatics and Biomedical Engineering ICBBE 2009 pp 1-4.
- [40] David Nistér, Oleg Naroditsky, and James Bergen 2006 "Visual Odometry for Ground Vehicle Applications" *Journal of Field Robotics* Volume 23, Issue 1 3-20 16 September 2005
- [41] Heikkila M., Pietika M. 2006 "A Texture-Based Method for Modeling the Background and Detecting Moving Objects" *IEEE TRANSACTIONS ON PATTERN ANALYSIS AND MACHINE INTELLIGENCE*, VOL. 28, NO. 4 pp 657 - 662
- [42] Ojala T, Pietikainen M, and Harwood D, "A Comparative Study of Texture Measures with Classification Based on Feature Distributions," *Pattern Recognition*, vol. 29, no. 1, pp. 51-59, 1996.
- [43] Ojala T, Pietika M, and Ma T, "Multiresolution Gray-Scale and Rotation Invariant Texture Classification with Local Binary Patterns," *2002 IEEE Trans. Pattern Analysis and Machine Intelligence*, vol. 24, no. 7, pp. 971-987
- [44] Prati A, Mikic I, Trivedi M, and Cucchiara R, 2003 "Detecting Moving Shadows: Algorithms and Evaluation," *IEEE Trans. Pattern Analysis and Machine Intelligence*, vol. 25, no. 7, pp. 918-923
- [45] Wren C, Azarbayejani A, Darrell T, and Pentland A, 1997 "Pfinder: Real-Time Tracking of the Human Body," *IEEE Trans. Pattern Analysis and Machine Intelligence*, vol. 19, no. 7, pp. 780-785

- [46] Friedman N and Russell S, 1997 "Image Segmentation in Video Sequences: A Probabilistic Approach" Proc. Conf. Uncertainty in Artificial Intelligence, pp. 175-181
- [47] Stauffer C and Grimson W, 1999 "Adaptive Background Mixture Models for Real-Time Tracking," Proc. IEEE CS Conf. Computer Vision and Pattern Recognition, vol. 2, pp. 246-252
- [48] Kaew Tra Kul Pong P and Bowden R, 2001 "An Improved Adaptive Background Mixture Model for Real-Time Tracking with Shadow Detection," Proc. European Workshop Advanced Video Based Surveillance Systems
- [49] Zivkovic Z, 2004 "Improved Adaptive Gaussian Mixture Model for Background Subtraction," Proc. Int'l Conf. Pattern Recognition, vol. 2, pp. 28-31
- [50] Zang Q and Klette R, 2004 "Robust Background Subtraction and Maintenance" Proc. Int'l Conf. Pattern Recognition, vol. 2, pp. 90-93
- [51] T. Matsuyama, T. Ohya, and H. Habe, "Background Subtraction for Non-Stationary Scenes," Proc. Asian Conf. Computer Vision, pp. 622-667, 2000
- [52] Venkatesh Babu R., Pe´rez P and Bouthemy P 2007 "Robust tracking with motion estimation and local Kernel-based colour modelling" Image and Vision Computing 25 pp 1205-1216
- [53] Hager G and Belhumeur P, 1998 "Efficient region tracking with parametric models of geometry and illumination", IEEE Transactions on Pattern Analysis and Machine Intelligence Volume 20 Number 10 pp. 1025-1039.
- [55] Isard M and Blake A, 1996 "Contour tracking by stochastic propagation of conditional density" European Conference on Computer Vision, pp. 343-356.
- [56] Fieguth P and Terzopoulos D, 1997 "Color based tracking of heads and other mobile objects at video frame rates", IEEE Conference on Computer Vision Pattern Recognition, pp. 21-27.
- [57] Comaniciu D, Ramesh V and Meer P, 2003 "Kernel-based object tracking", IEEE Transactions on Pattern Analysis and Machine Intelligence Volume 25 Number 5, pp. 564-577.
- [58] Yang J and Waibel A, 1996 "A real-time face tracker", WACV, pp. 142-147.
- [59] Wren C, Azarbayejani A, Darrell T and Pentland A, 1997 "Pfinder: real time tracking of the human body", IEEE Transactions on Pattern Analysis and Machine Intelligence Volume 19 Number 7, pp. 780-785.

- [60] Bradski G, 1998 "Computer vision face tracking as a component of a perceptual user interface" Workshop on Application of Computer Vision, Princeton, NJ, pp. 214–219.
- [61] Weng S, Kuo C and Tu S, 2006 "Video object tracking using adaptive Kalman filter" J. Vis. Commun. Image R. Volume 17 pp. 1190–1208
- [62] Bergen J, Anandan P, Hanna K and Rajesh Hingorani 1992 "Hierarchical model-based motion estimation" Computer Vision — ECCV'92 Lecture Notes in Computer Science, 1992, Volume 588/1992, pp. 237-252
- [63] Brox T, Bruhn A, Papenberg N and Weickert J, 2004 "High Accuracy Optical Flow Estimation Based on a Theory for Warping", Computer Vision - ECCV Lecture Notes in Computer Science, Volume 3024, pp 25-36
- [64] Bruhn A, Weickert J and Schnörr C 2005 "Lucas/Kanade Meets Horn/Schunck: Combining Local and Global Optic Flow Methods" International Journal of Computer Vision Volume 61 Number 3, pp. 211-231
- [65] DeCarlo D and Metaxas D, 1996 "The integration of optical flow and deformable models with applications to human face shape and motion estimation" 1996 IEEE Computer Society Conference on Computer Vision and Pattern Recognition Proceedings CVPR '96, pp 231 - 238
- [66] Bigun J, Granlund G and Wiklund J 1991 "Multidimensional orientation estimation with applications to texture analysis and optical flow" IEEE Transactions on Pattern Analysis and Machine Intelligence, Volume: 13 Issue:8 pp 775 – 790
- [67] Ghanbari M, 1990 "The cross-search algorithm for motion estimation [image coding]" IEEE Transactions on Communications, Volume 38 Issue 7 pp. 950 – 953
- [68] Po L and Ma W 1996 "A novel four-step search algorithm for fast block motion estimation" IEEE Transactions on Circuits and Systems for Video Technology, Volume: 6 Issue:3 pp. 313 - 317
- [69] Zhu S and Ma K, 2000 "A new diamond search algorithm for fast block-matching motion estimation" IEEE Transactions on Image Processing, Volume: 9 Issue: 2 pp. 287 – 290
- [70] Li R, Zeng B and Liou M 1994 "A new three-step search algorithm for block motion estimation" IEEE Transactions on Circuits and Systems for Video Technology, Volume: 4 Issue:4 pp. 438 – 442

- [71] Chan M, Yu Y and Constantinides A 1990 "Variable size block matching motion compensation with applications to video coding" IEE Proceedings Communications, Speech and Vision, Volume: 137 Issue:4 pp. 205 – 212
- [72] Gao X, Duanmu C and Zou C, 2000 "A multilevel successive elimination algorithm for block matching motion estimation" IEEE Transactions on Image Processing, Volume: 9 Issue:3 pp. 501 – 504
- [73] Chen Y, Hung Y and Fuh C 2001 "Fast block matching algorithm based on the winner-update strategy" IEEE Transactions on Image Processing, Volume 10 Issue 8 pp. 1212 – 1222
- [74] Puri A, Hang H and Schilling D 1987 "An efficient block-matching algorithm for motion-compensated coding" ICASSP '87 IEEE International Conference on Acoustics, Speech, and Signal Processing pp. 1063 – 1066
- [75] Singh A 2003 "Featureless techniques for estimating camera motion (scale and rotation) in videos" NUS MSc Thesis
- [76] Spain B, Smith MG, "Functions of mathematical physics", Van Nostrand Reinhold Company, London, 1970. Chapter 11 deals with Hermite polynomials.

Appendix A Practical issues in the implementation

A number of practical issues were faced when undertaking the development of the algorithm. The methods were tested on a set of test images as described in Chapter 4 and later on a set of standard images (shown in Appendix B). This allowed the testing of the effect of varying a number of the parameters of significance to the way in which both the block matching correspondence method and the scale space optical flow method work. The details of some of these experiments are presented here. The initial work was done using Mathematica though the final work was developed in C++

A.1 Applying the Median Filter

The median filter is implemented here for the purpose of minimizing measurement errors and removing noise in order to produce more reliable vectors. In experiments on the test images and the standard image sets two different sizes of Median Filter were applied to vectors produced by the image analysis, which were 3*3 and 5*5. This was to determine what difference the size of the filter made to the effectiveness of the measurements. With the test images the correct result was known so the value of the filter could be better established. The danger in using too small a filter is that regions of faulty results just reinforce themselves while too big a filter can mask actual gradual changes. The filter is used to enforce the idea that neighbouring pixels will move together. This fails of course at object boundaries but in the actual experimental data measurements are only made within the growth area of the image and so this rule should be applicable throughout. However, the actual growth rate does change gradually with the distance along the root so a too large filter would introduce errors. The larger the filter also the longer the computation time. When the results of the

motion analysis produce neighbouring points that are moving in significantly different directions the median filter will generally remove spurious points. The figures below illustrate ways in which the filter aids the correct interpretation of the data.

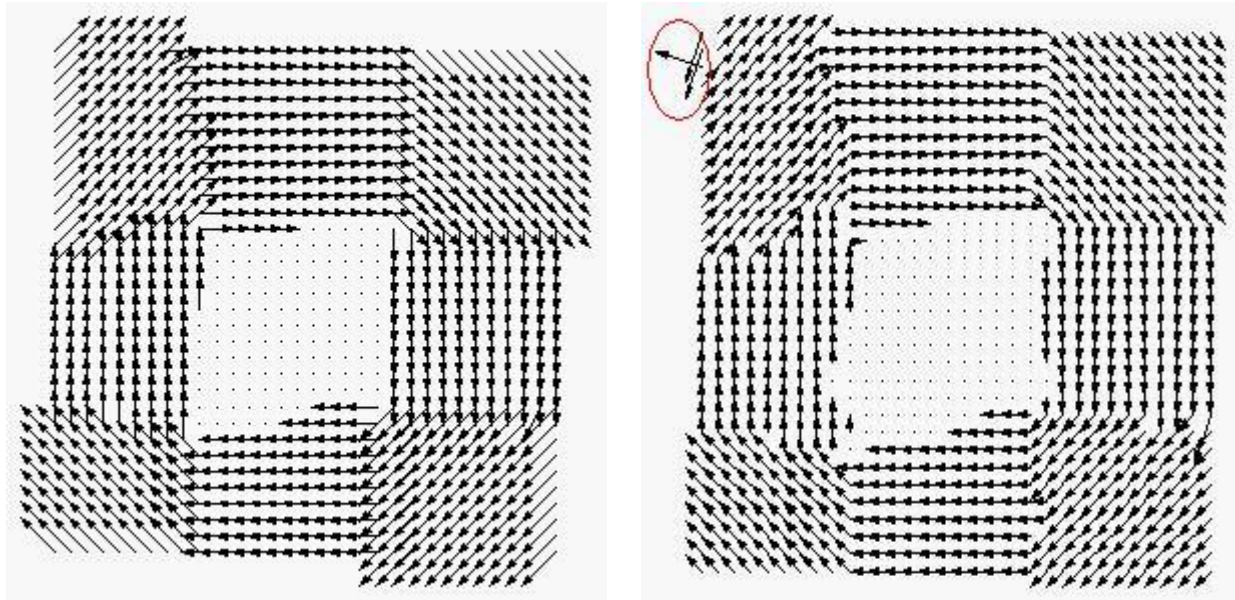


Figure A.1 5 Degree Rotation Image Sequence Motion Estimation Vector Field both images observed at BS=3, SS=1; Left Image with applied 5*5 Median Filter and Right Image without Median Filter

The vectors circled at upper-left corner in the right image of Figure A1 were calculated to have motion vectors in the opposite direction to their neighbours, these are examples of errors that will very often happen at the border pixels since in these areas there are fewer reference positions to match. This can be corrected by applying a median filter. The vector plot on the left of Figure A.1 is the resultant vector field after applying a 5*5 median filter, which corrects the error pixels and shows all pixels moving in the expected direction. Also note a block of pixels in the top right of the right hand plot of Figure A.1 shows a large number of vectors that were too large. This has also been removed by the filtering.

The following figures show the effect of median filtering on sequences with larger rotations Figure A.2 for 15° rotations and Figure A.3 for 30° rotations

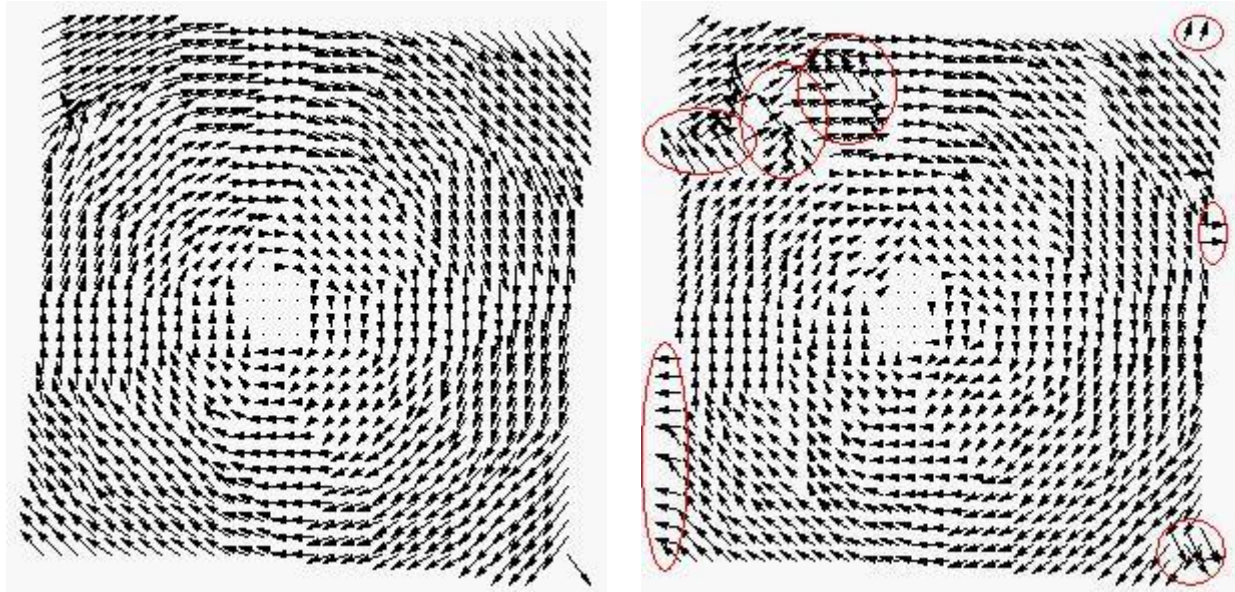


Figure A.2 15 Degree Rotation Image Sequence Motion Estimation Vector Field both images observed at BS=8, SS=2; Left Image with applied 5*5 Median Filter and Right Image without Median Filter

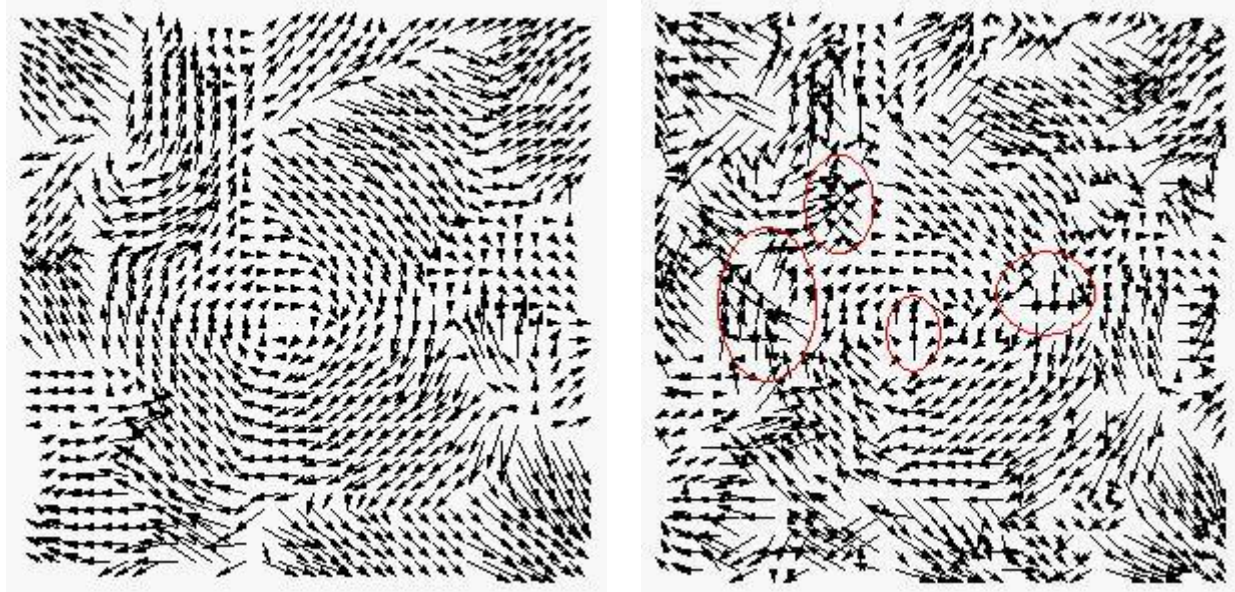


Figure A.3 30 Degree Rotation Image Sequence Motion Estimation Vector Field both images observed at BS=2, SS=2; Left Image with applied 5*5 Median Filter and Right Image without Median Filter

As mentioned earlier, the median filter will help more for larger motion image sequence to remove noise and minimize errors. For example in Figure A.2 the 15 Degree rotation image sequence, the vector field has more erroneous results than 5 Degree rotation filter image sequence. As can be seen in Figure A.3 with no median filter applied to the 30 Degree rotation image sequence, a rotating vector field hardly shows.

The median filter was also used to improve the motion field when using the Scale Space Optical Flow method as the following examples illustrate:

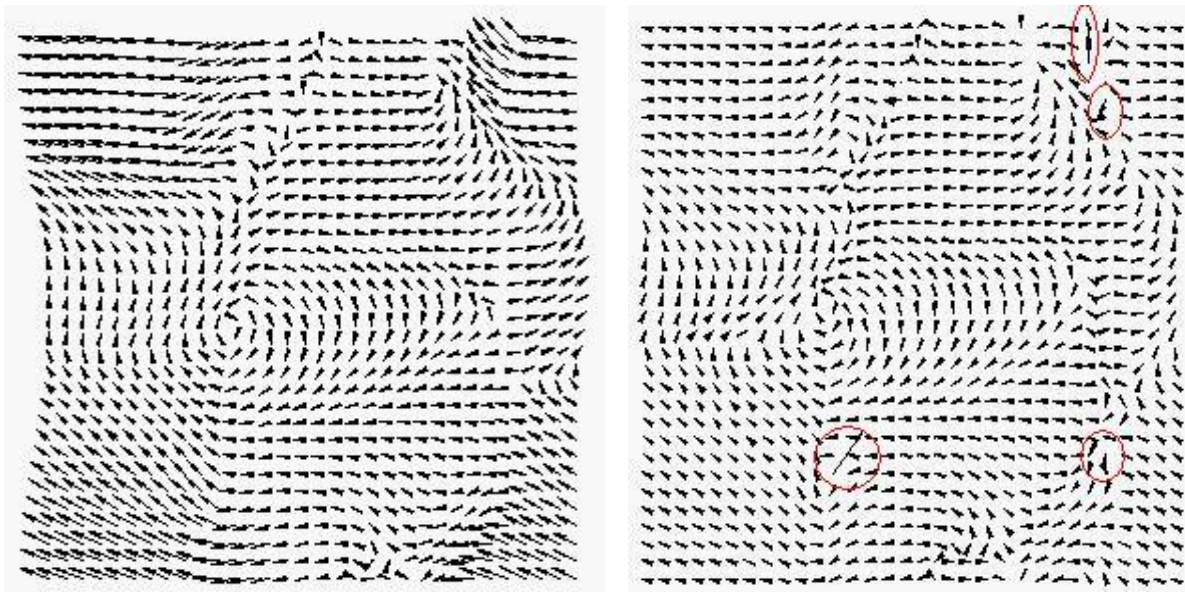


Figure A.4 5 Degree Rotation Image Sequence Optical Flow Vector Field both images observed at $\sigma=10, \tau=1$; Left Image with applied 5*5 Median Filter and Right Image without Median Filter

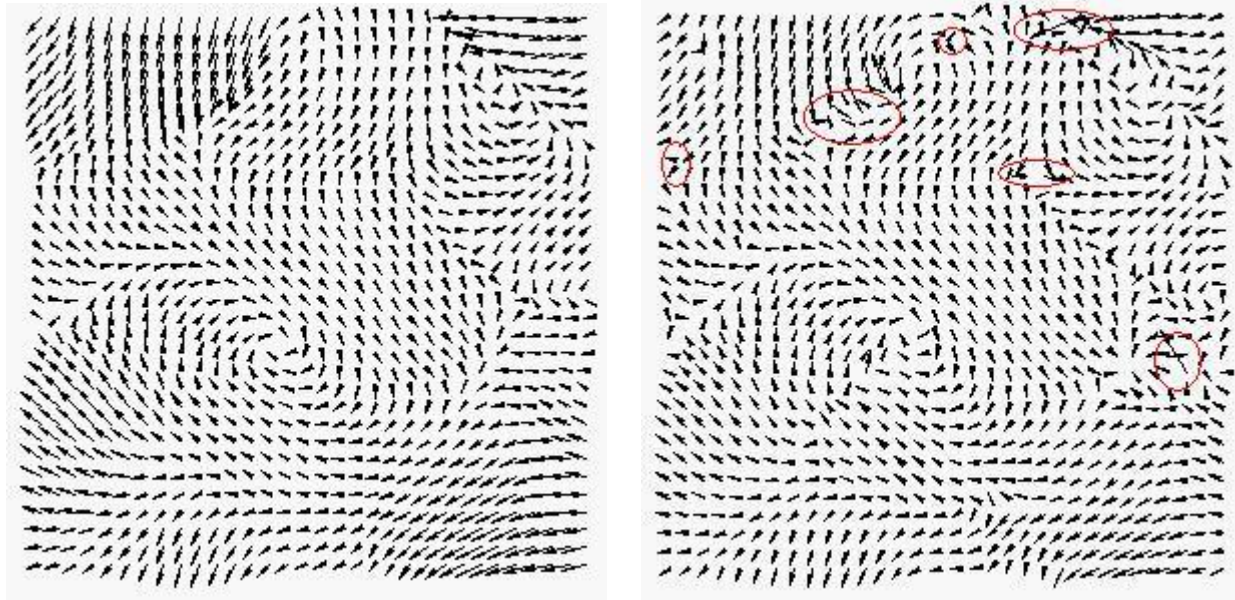


Figure A.5 15 Degree Rotation Image Sequence Optical Flow Vector Field both images observed at $\sigma=6$, $\tau=1$; Left Image with applied 5*5 Median Filter and Right Image without Median Filter

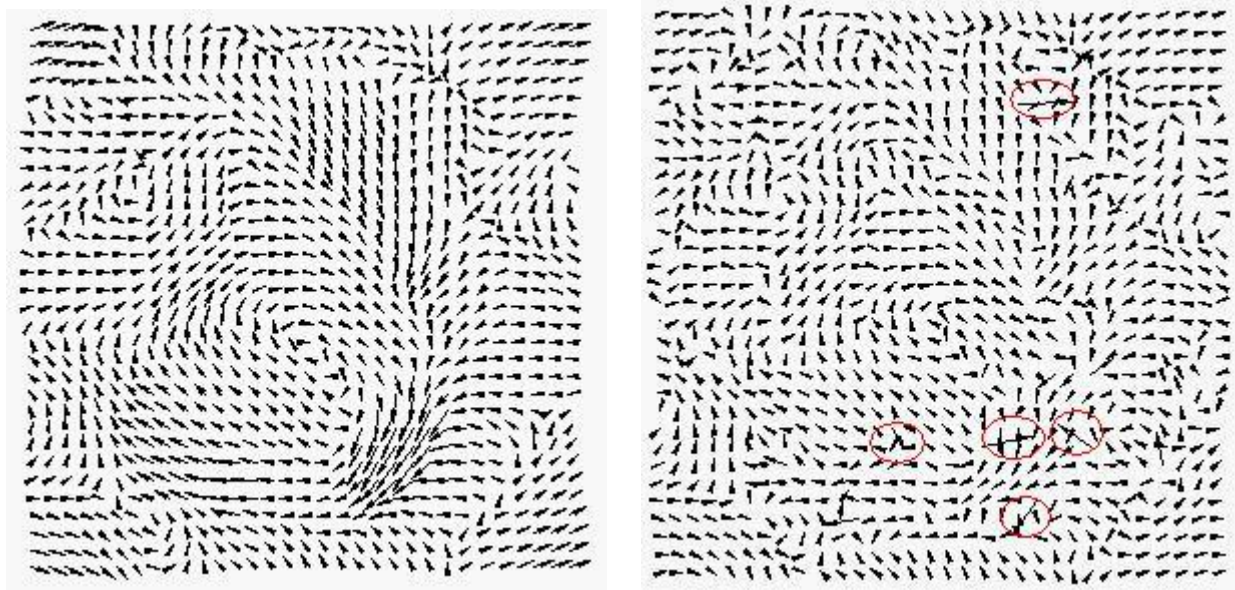


Figure A.6 30 Degree Rotation Image Sequence Optical Flow Vector Field both images observed at $\sigma=3$, $\tau=1$; Left Image with applied 5*5 Median Filter and Right Image observed at without Median Filter

With increased motion when no median filter is used, vector fields return results with more errors and especially as seen in Figure A.6 for a 30 Degree Rotation Image

Sequence which barely shows the rotation in the right image and the flow is very different for each neighbour pixel. After use of the median filter, (Figure A.6 the left image) the unexpected results are greatly reduced and it clearly shows the direction that pixels have been rotated forming a smooth flow for all pixels. (These examples were produced using Mathematica. In this case the need to produce values for edge pixels was addressed by mirroring of the image pixels at the edges. The result has produced unreliable results at the edge for the size of the Gaussian mask used. Such problems were removed in the actual experiments by the inclusion of surrounding pixels in the calculation for a given region rather than mirroring.)

A.2 Effect of changing Block-Size (BS) on the Motion Estimation

From the assumptions that pixels move with their neighbours, the smaller block size will reduce the calculation time and increase the speed. Conversely larger block size will cause longer processing time but give more reliable results. From the experiment observed for larger motion for example from 5 Degree to 15 Degree, a larger size of block will return better results than a small size of block. However, if the motion gets extremely large for example 30 Degrees then a smaller block size will be more appropriate. The following figures provide examples (SS is Search Space):

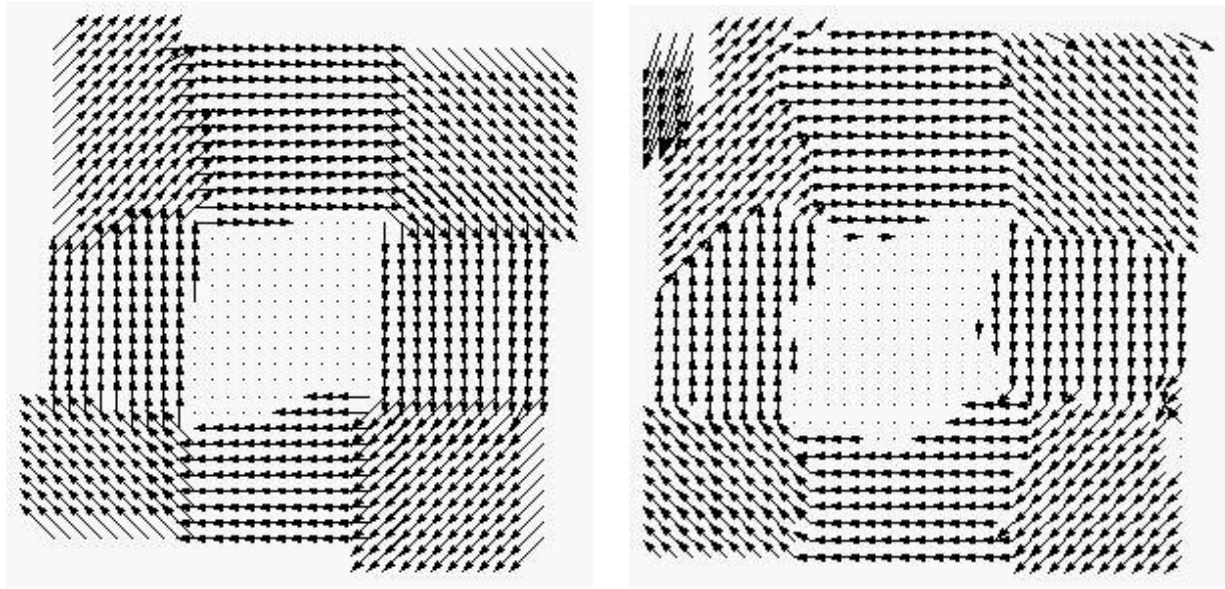


Figure A.7 5 Degree Rotation Image Sequence Motion Estimation Vector Field Left Image observed at BS=3, SS=1 and Right Image observed at BS=1, SS=1

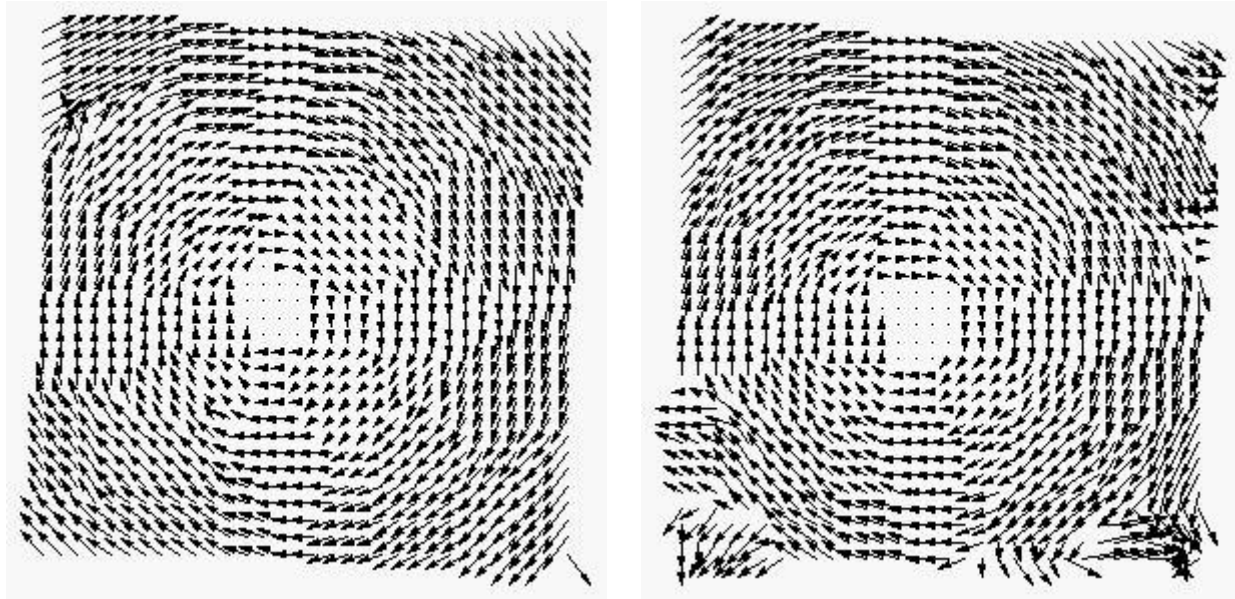


Figure A.8 15 Degree Rotation Image Sequence Motion Estimation Vector Field Left Image observed at BS=8, SS=2 and Right Image observed at BS=2, SS=2

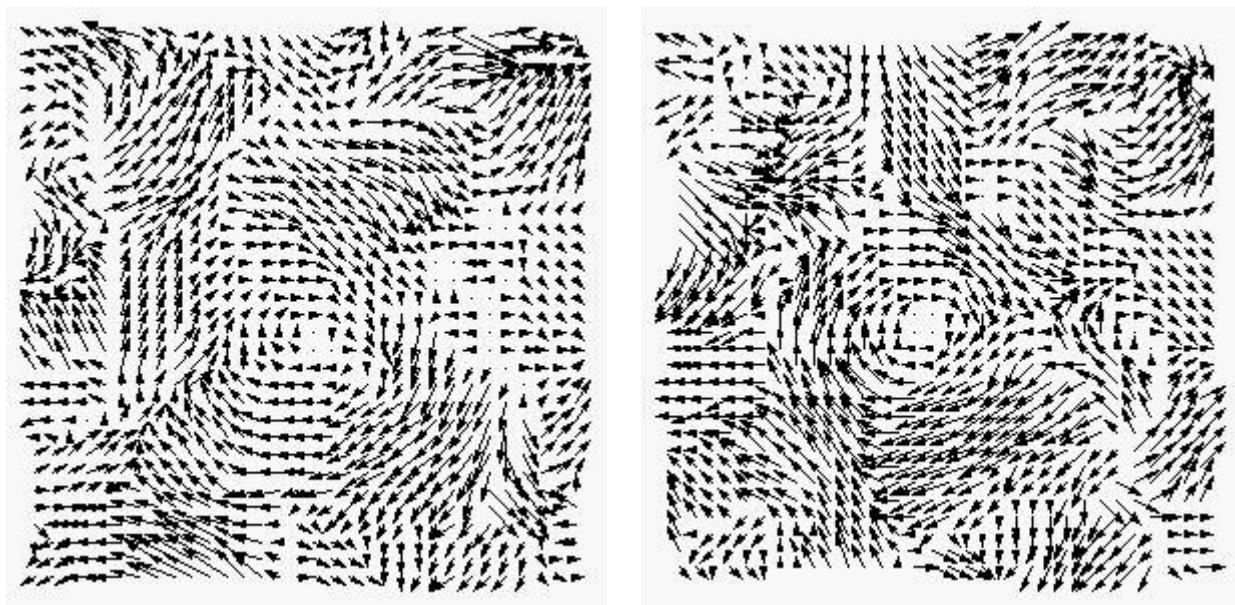


Figure A.9 30 Degree Rotation Image Sequence Motion Estimation Vector Field Left Image observed at BS=2, SS=2 and Right Image observed at BS=1, SS=2

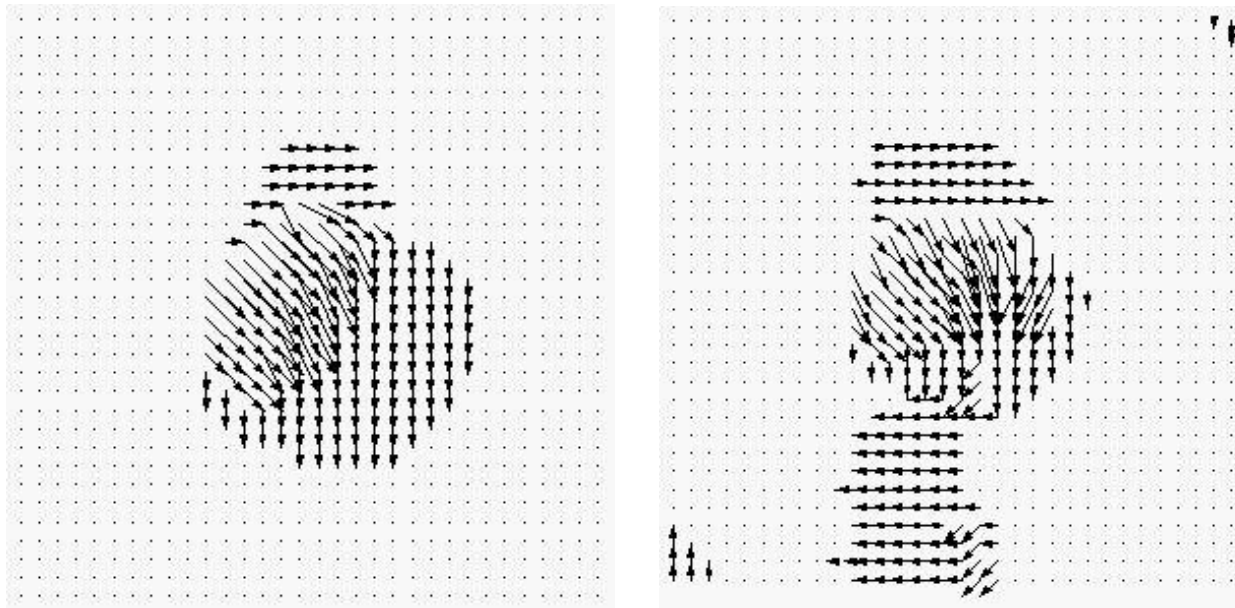


Figure A.10 Suzie Image Sequence (see appendix B) Motion Estimation Vector Field Left Image observed at BS=8, SS=2 and Right Image observed at BS=1, SS=2

Figure A.10 is analysing the Suzie Image Sequence (shown in Appendix B), to detect the movement of Suzie closing her left eye. The left-hand field plot with larger block size shows the expected results and the right-hand field with smaller block size shows more complex results, some of which are wrong demonstrating that errors have been detected.

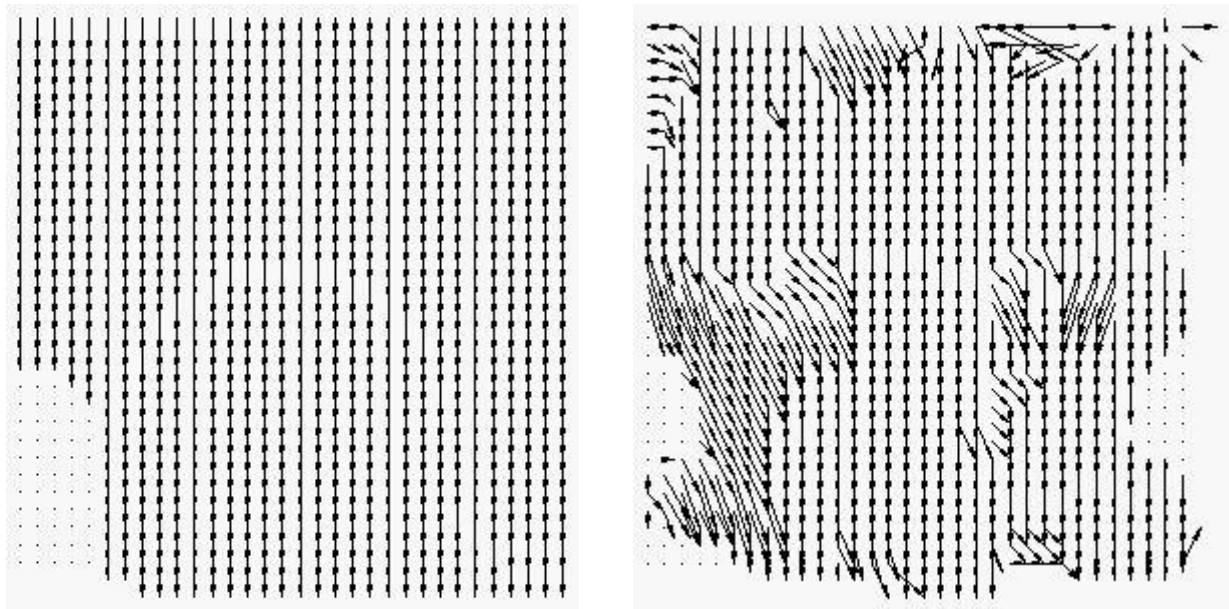


Figure A.11 Claire Image Sequence (see Appendix B) Motion Estimation Vector Field Left Image observed at BS=6, SS=2 and Right Image observed at BS=1, SS=2

In Figure A.11 the Claire Image Sequence in which the detection of the movement is made as Claire nods her head, the vector field should have all the vectors moving down, the left image in the figure observed at BS=6 and shows the expected results but with smaller block size such as the right image in the figure with BS=1 most of the pixels are going down but other pixels are going in different directions.

A.3 Motion Estimation Vector Field with respect to different size of Search-Space (SS)

The Search Space is determined by a pre-estimate of the motion field, with larger Search Space, more locations are looked at for matching. It might be assumed that allowing a greater search space would necessarily lead to a more accurate answer as there is then less dependence on the a-priori estimation of the motion. However this assumption breaks down in the real images as the motion is usually not by integer pixel amounts and many areas of the image have similar features. Also the larger the search space the more time will be consumed. If the size of search space is too small the system will return errors in vector field where the motion is larger than /beyond the pre-estimated area. The size of the initial search space would be set to match the estimated maximum velocity in the images.

The following examples illustrate the effect of changing search space:

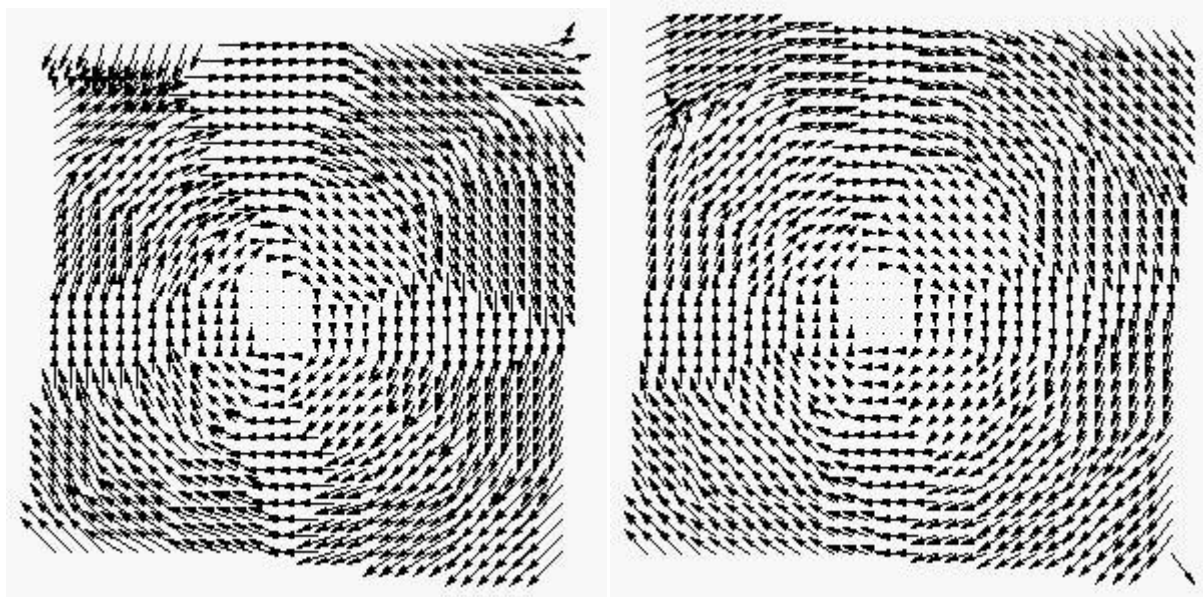


Figure A12 15 Degree Rotation Image Sequence Motion Estimation Vector Field Left Image observed at BS=8, SS=2 and Right Image observed at BS=8, SS=1

In Figure A.12 the 15 Degree Rotation Image Sequence Motion Estimation Vector Field is shown. Both outputs are determined at the same block size but with different search space, the left image is observed at $SS=2$ which shows more accurate motion estimation results than the right image at $SS=1$. For lower rotational speeds a smaller search space would be useful. Also the location of the search space is important. If the a-priori estimation of the speed of motion is good then a small search space suitably positioned would be better. For the test images the velocity is known exactly. In the RootFlowRT system the velocity is assumed unknown which results in large errors as shown in Chapter 5.

Another good example to illustrate the advantage of using an appropriate search space to return better results is shown below:

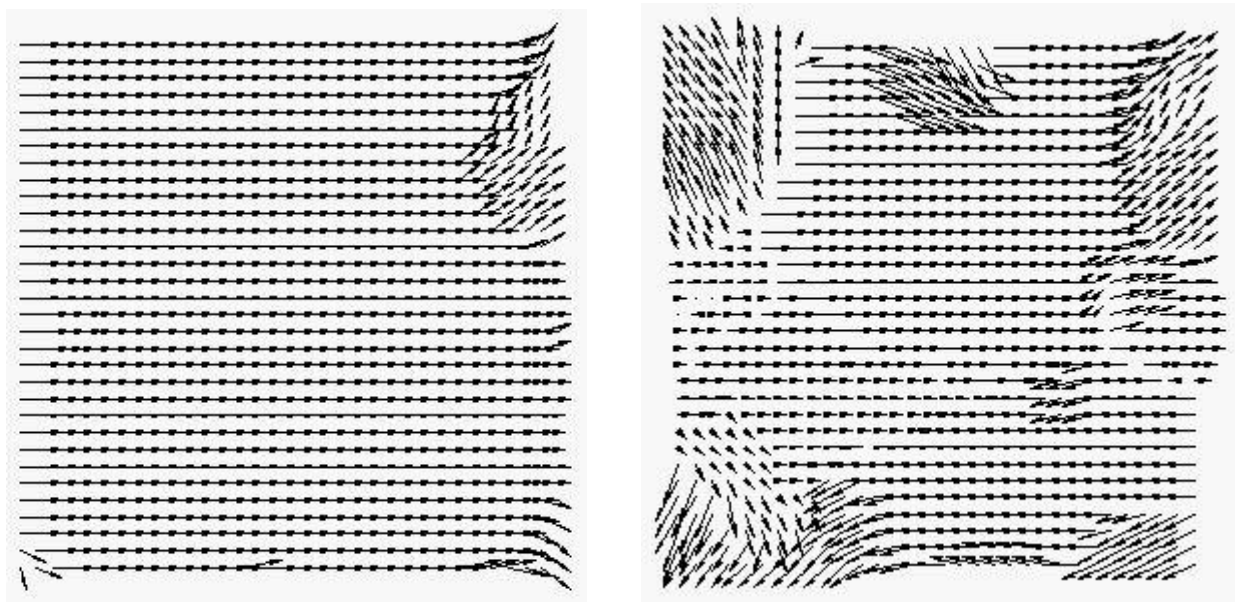


Figure A13 Bus Image Sequence (see appendix B) Motion Estimation Vector Field Left Image observed at $BS=3$, $SS=3$ and Right Image observed at $BS=3$, $SS=2$

Figure A13 shows the Bus Image Sequence Motion Estimation Vector Field. Both outputs are obtained at $BS=3$ but with different search space values. In the test

sequence a bus is passing, by the movement of the background, since the bus is going to the left, all the background objects should go to the right. By comparison of the two different outputs, the larger size of search space can be seen to give the better result when the actual velocity is unknown and the object is distinct from its background

A.4 Effect of varying σ on the Scale Space Optical Flow Vector Field

The calculation of the Optical flow field involves a convolution with a Gaussian Derivative mask. The extent of the mask is determined by the value of σ , the spatial scale. This convolution is equivalent to first applying a Gaussian to the image then applying a differential operator. The Gaussian is a low pass filter which means that the convolution with the image produces an image containing fewer high frequencies. The nature of the Gaussian means that in the spatial domain high frequency image trends are reduced smoothly.

With a larger value of σ , a larger Gaussian Kernel will be applied. It is difficult to select an appropriate spatial scale σ , but for larger movements in the image sequence, smaller σ values are likely to be selected. The following example illustrates how the results are affected by different choice of values of σ :

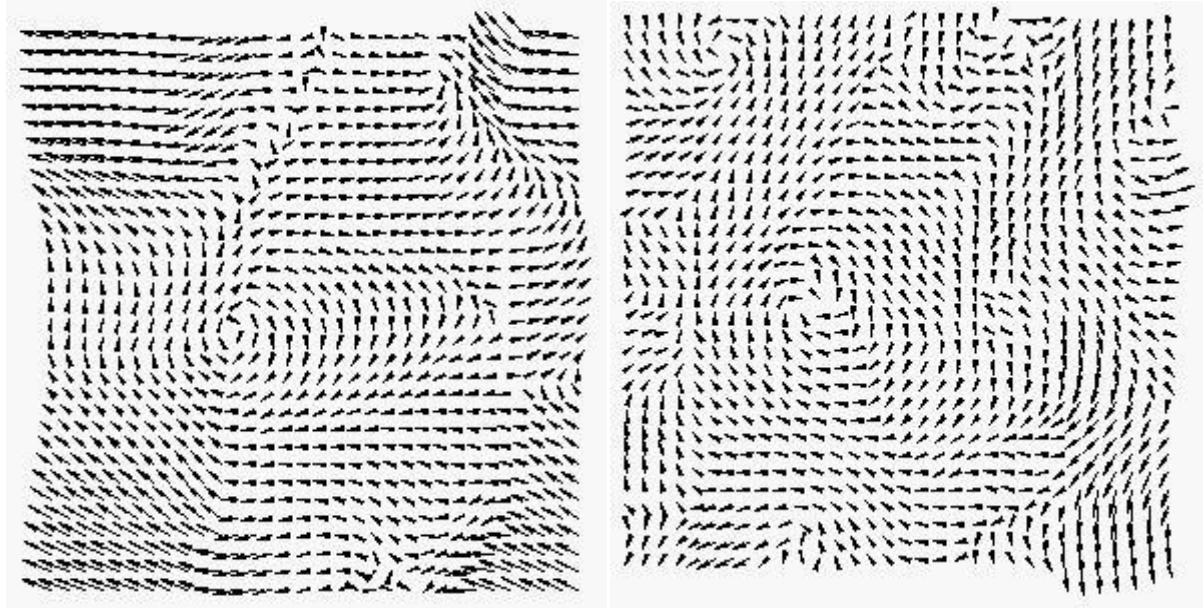


Figure A.14 5 Degree Rotation Image Sequence Optical Flow Vector Field Left Image observed at $\sigma=10$, $\tau=1$ and Right Image observed at $\sigma=2$, $\tau=1$

In Figure A14, the 15 Degree Rotation Image Sequence Optical Flow Vector Field is shown. Both outputs are obtained at $\tau=1$ (a temporal scale of 1 so the images used are consecutive images in a sequence) but with different σ value. With the larger σ a smoother vector field results. With the larger motion the σ value should be reduced accordingly, as high velocity of motion results in high frequency effects. Below are further examples:

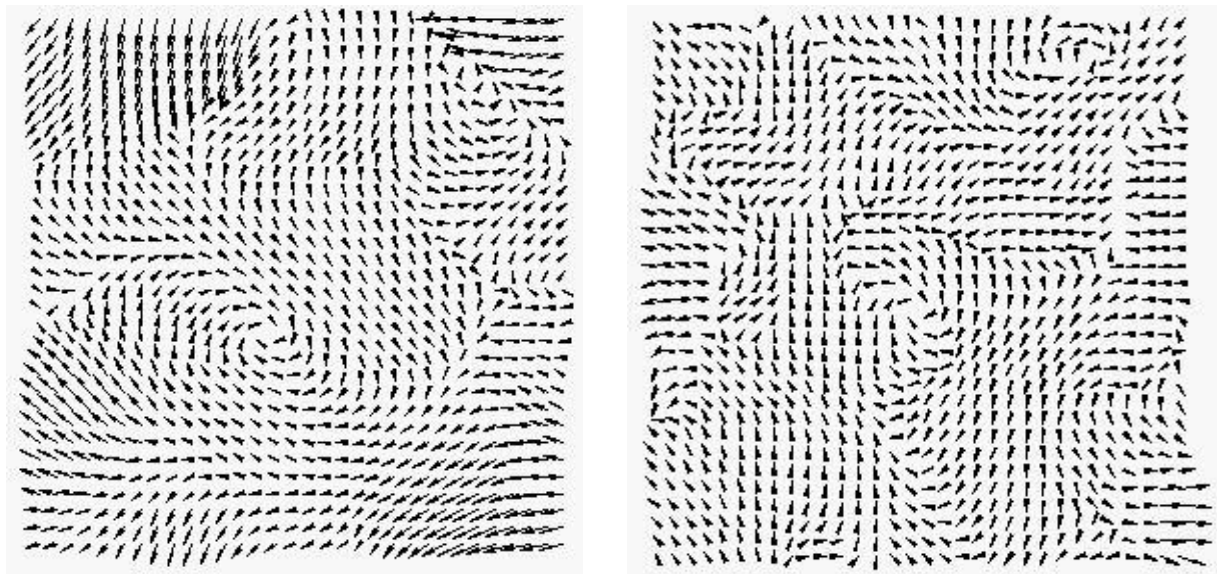


Figure A.15 15 Degree Rotation Image Sequence Optical Flow Vector Field Left Image observed at $\sigma=6$, $\tau=1$ and Right Image observed at $\sigma=2$, $\tau=1$

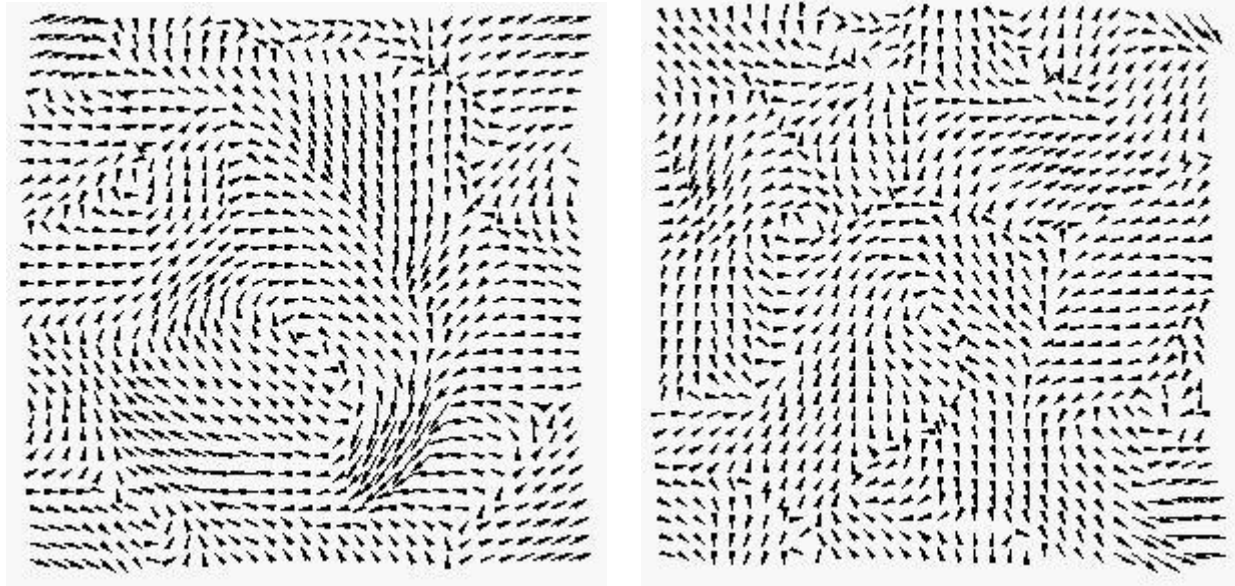


Figure A.16 30 Degree Rotation Image Sequence Optical Flow Vector Field Left Image observed at $\sigma=3$, $\tau=1$ and Right Image observed at $\sigma=2$, $\tau=1$

The best observation of 5 degree rotation image sequence is for $\sigma=10$ but $\sigma=6$ for the 15 degree rotation and $\sigma=3$ for 30 degrees. In practice with the real image sequences a σ of 1.8 was used (see chapter 4)

A.5 Effect of varying the value of τ on Optical Flow Vector

The temporal scale of the Scale Space approach is τ . Optical Flow is calculated between consecutive images in an image sequence. The value of τ is the time step between the consecutive images used. With $\tau=1$ for example, the calculation of the vector field for an image involves calculation between an image and its next neighbours in the sequence. The range of the possible values for τ depends on how many images there are in the sequence; to have a valid value τ must not require using more than the number of images in the sequence. This adds an extra tuning a feature for optical flow motion estimation. With this advantage optical flow is able to calculate the flow in the sequence between any number of input images. However this has the

obvious result of the execution time increasing with the number of images in the sequence – the speed of execution will be extremely slow.

A.6 No Discontinuities in Vector Field

As stated above the Optical Flow system uses convolution in the spatial domain. Evaluation of the convolution on the boundaries requires some form of extension of the image. The method used when measuring the test images was wrapping. In this method the upper-left pixel in the images is assumed as adjacent to the lower-right pixel, pixels at the left border are adjacent to those on the right border and so on. This will affect the result for vector fields, for example, if the motions for the lower-right corner area are flowing out, the motion for the top-left corner area must be flowing in. This is illustrated below:

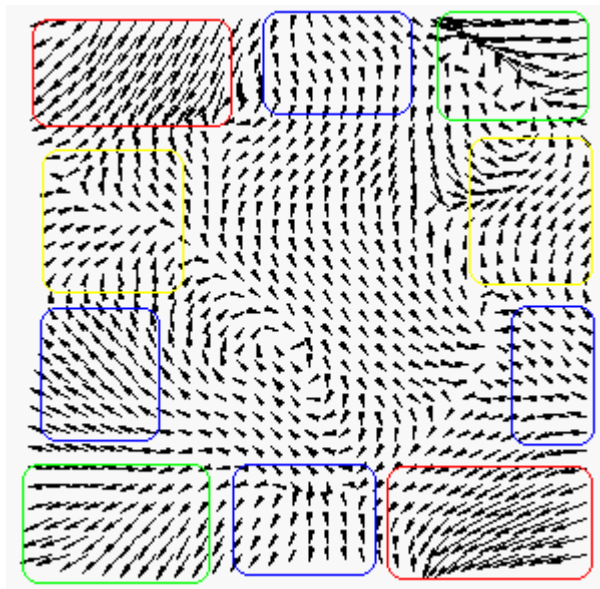


Figure A.17 30 Degree Rotation Image Sequence Motion Estimation Vector Field observed at $\sigma=8$, $\tau=1$

The extent of the border effect will depend on the value of σ . The larger the value of σ the larger the convolution mask and so the larger the area over which this effect is observed.

Appendix B Standard Test Image Sequences

A number of image sequences are commonly used in testing motion estimation applications. These images have known characteristics with obvious and known motions that are more complex than those found in the plant images but they were still useful in testing the parameters used in the proposed method. Some of these have been referred to in Appendix A as they demonstrate how the tuning of the parameters can affect the reliability and accuracy of the results. In this section the image are represented as are the results of some manipulation on these images using the methods later employed on the plant growth images. The image sequences are known as:

- Suzie – a woman answer the phone using clear motions
- Clair – a female news reporter reads the news and in so doing her features change
- Bus image – a bus passes some background scenery which is also moving. This is the most complex sequence and one in which the camera is moving rather than stationary.

The results shown in the following figures are illustrative of what happens as the values are changed for the two main parameters available for the methods used in the analysis. Thus values of Block Size (BS) and Search Space (SS) have been varied for the correspondence method and the spatial scale σ and temporal scale τ have been varied for the Scale Space Optical Flow method. In these experiments the position of the search space for the correspondence method has been centred on the pixel under analysis. In practice in the experiments it was necessary to take into account the velocity determined by the Optical Flow method to determine where the search space should be centred.

In the illustrations here the limits of the image used have been determined by selecting the image from inside a larger image but the method of dealing with edge pixels have not used the opportunity to read from a larger image.

The results of the extensive set of experiments of which these figures only illustrate a small proportion were used to help determine what factors were important in designing the final software. They were, however, not directly applicable as the nature of the images were not the same as that of the experimental image. They are thus presented here for illustration only.

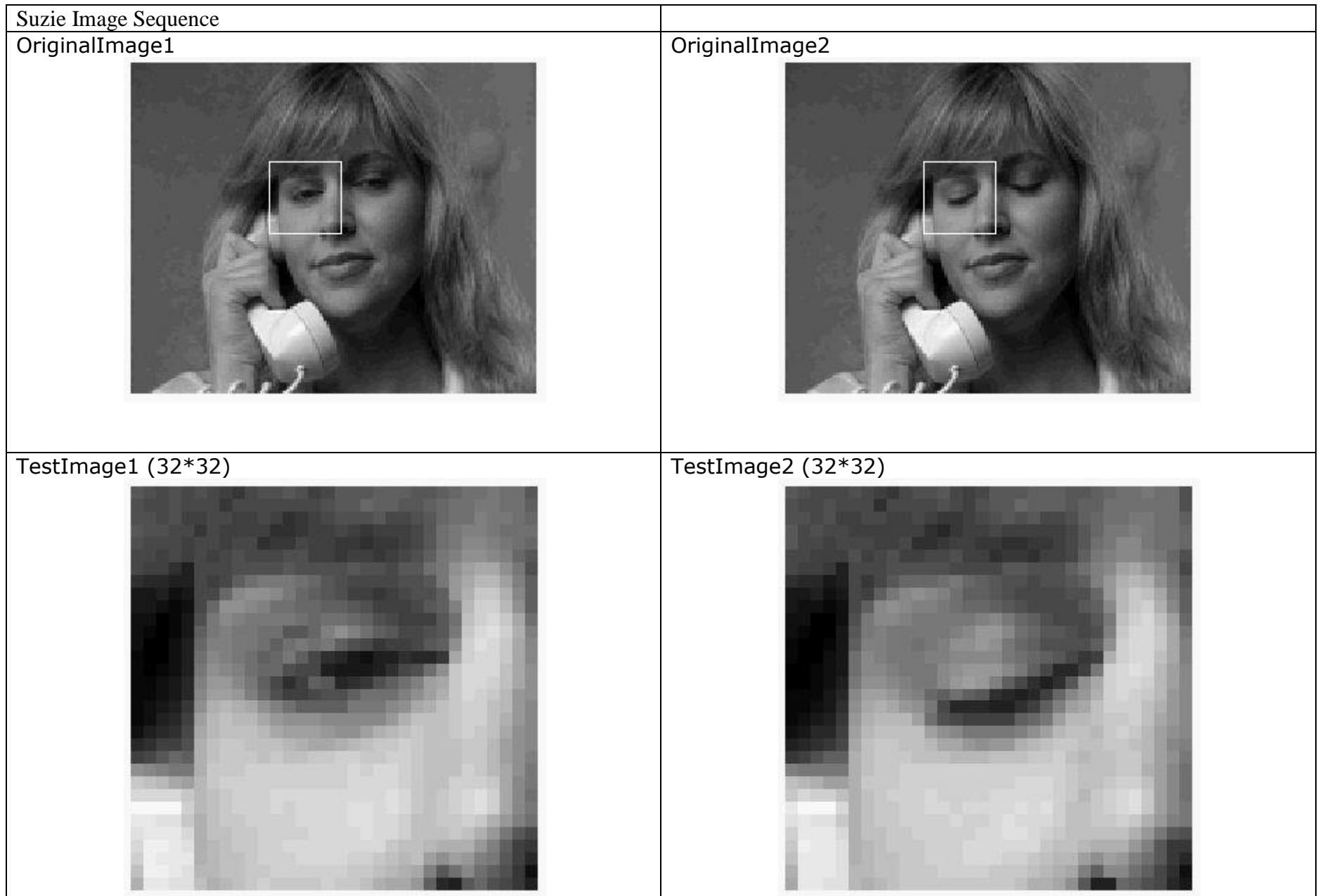


Figure B.1 Two images from the Suzie sequence with the section of the image highlighted that was used in the analysis shown in following

Biological plant root growth detection from spatial and temporal resolution image sequence

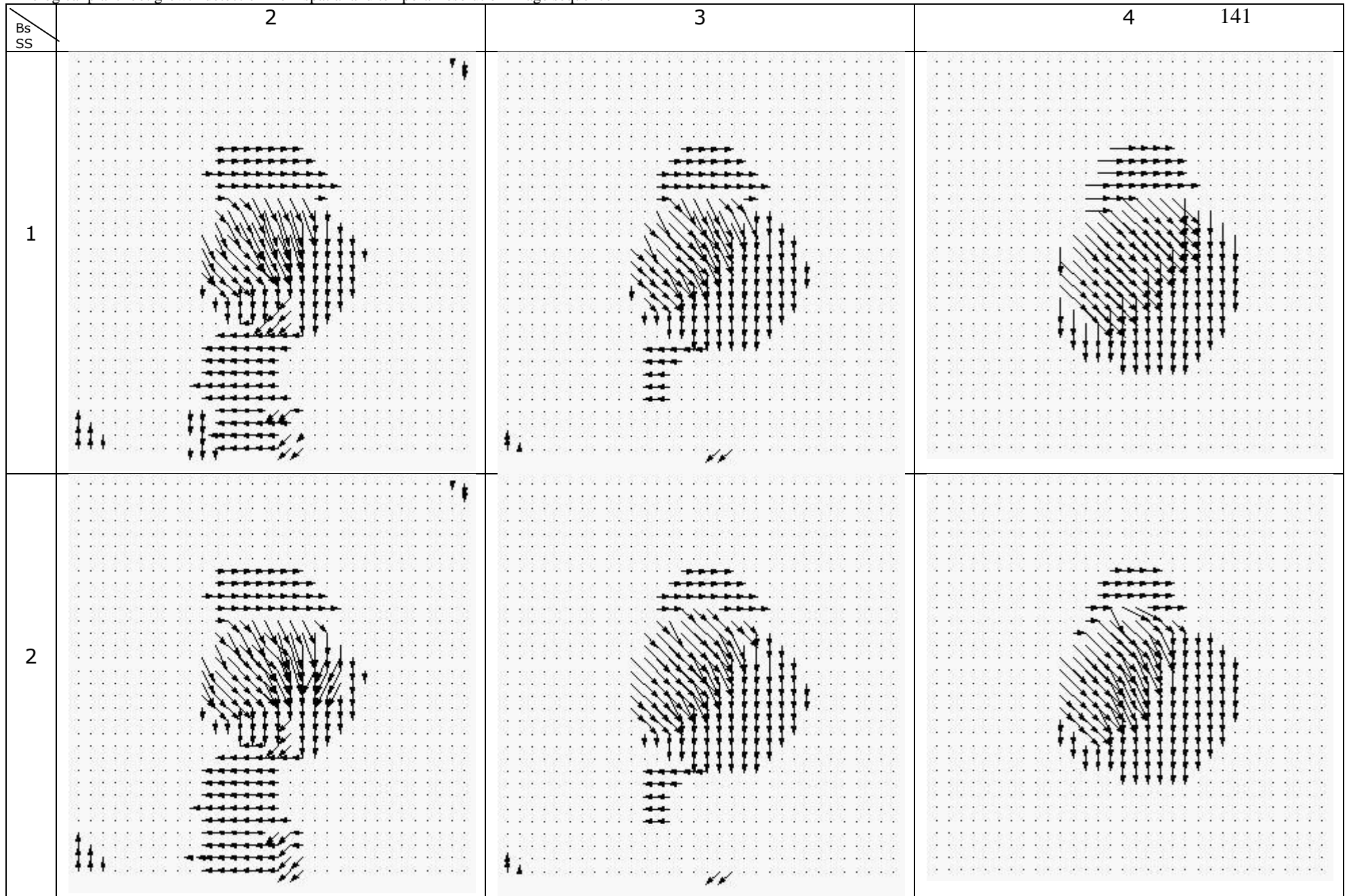


Figure B.2 Motion Estimation Vector Field for Suzie Image Sequence with 5*5 Median Filter and vary value for BS(Block Size), SS(Search Space):

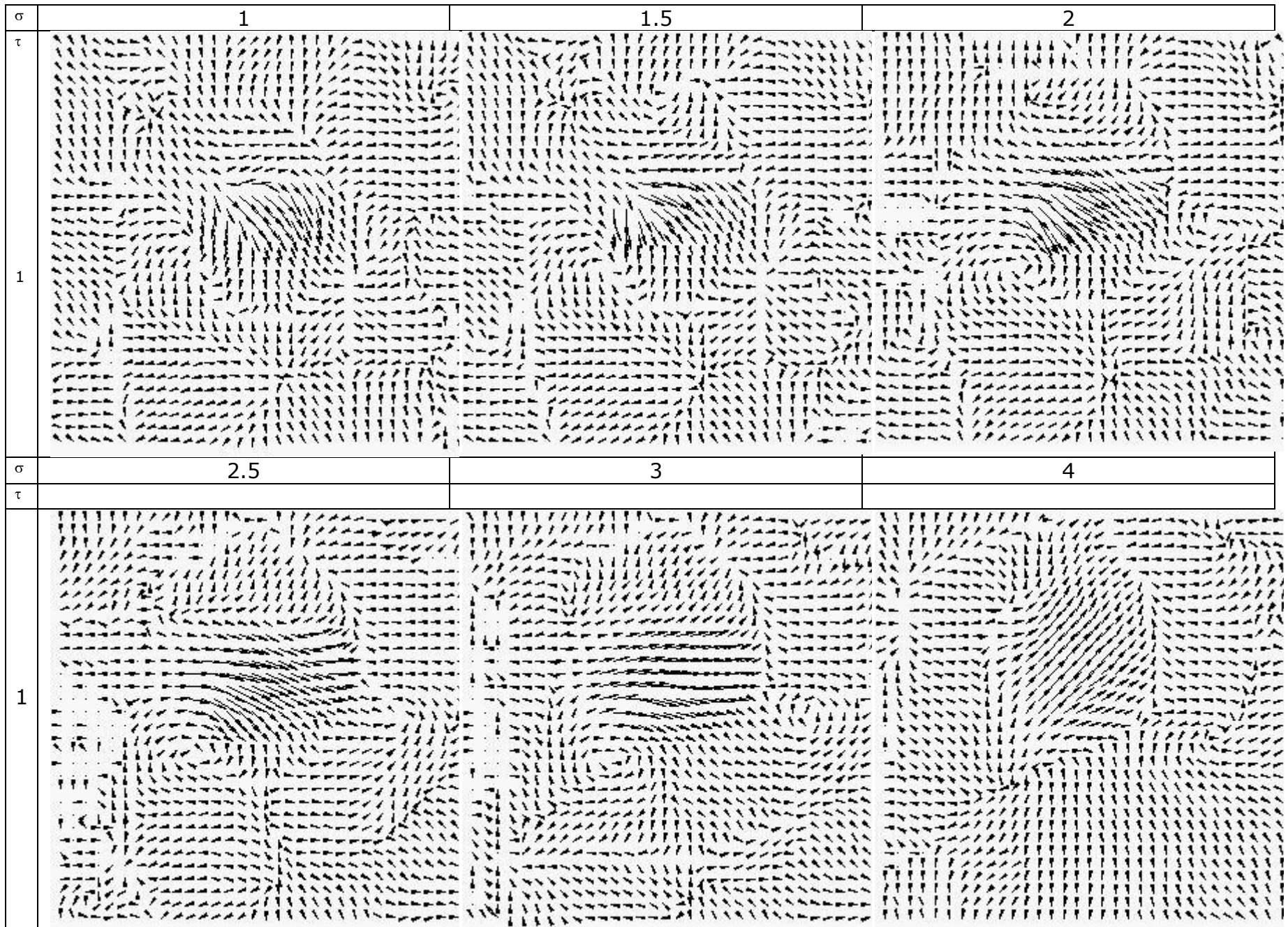


Figure B.3. Optical Flow Vector Field for the Suzie Image Sequence with 5*5 Median Filter; $\tau=1$ and vary value for σ

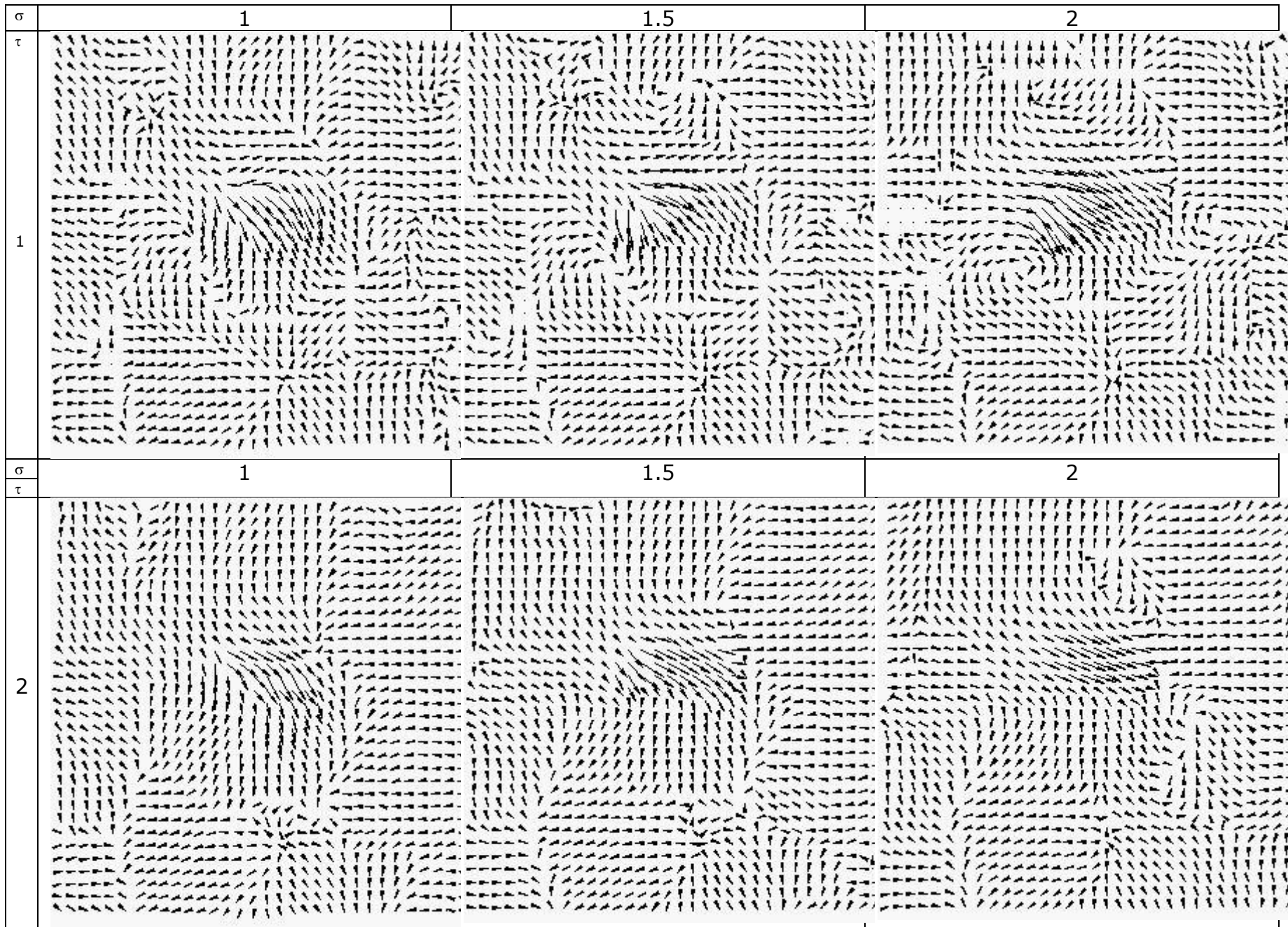


Figure B.4. Optical Flow Vector Field for the Suzie Image Sequence with 5*5 Median Filter and vary value for σ and τ :

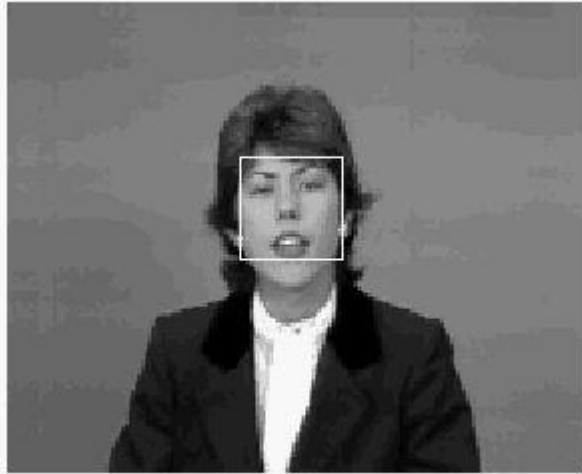
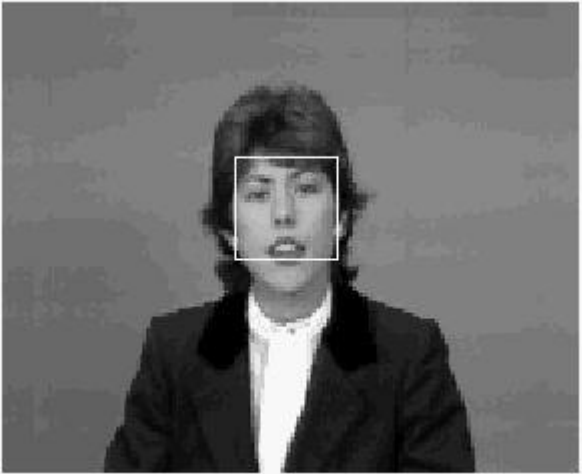


| | |
|--|--|
| Claire Image Sequence | |
| OriginalImage1  | OriginalImage2  |
| TestImage1 (32*32)  | TestImage2 (32*32)  |

Figure B.5 Two images from the Claire sequence with the section of the image highlighted that was used in the analysis shown in following

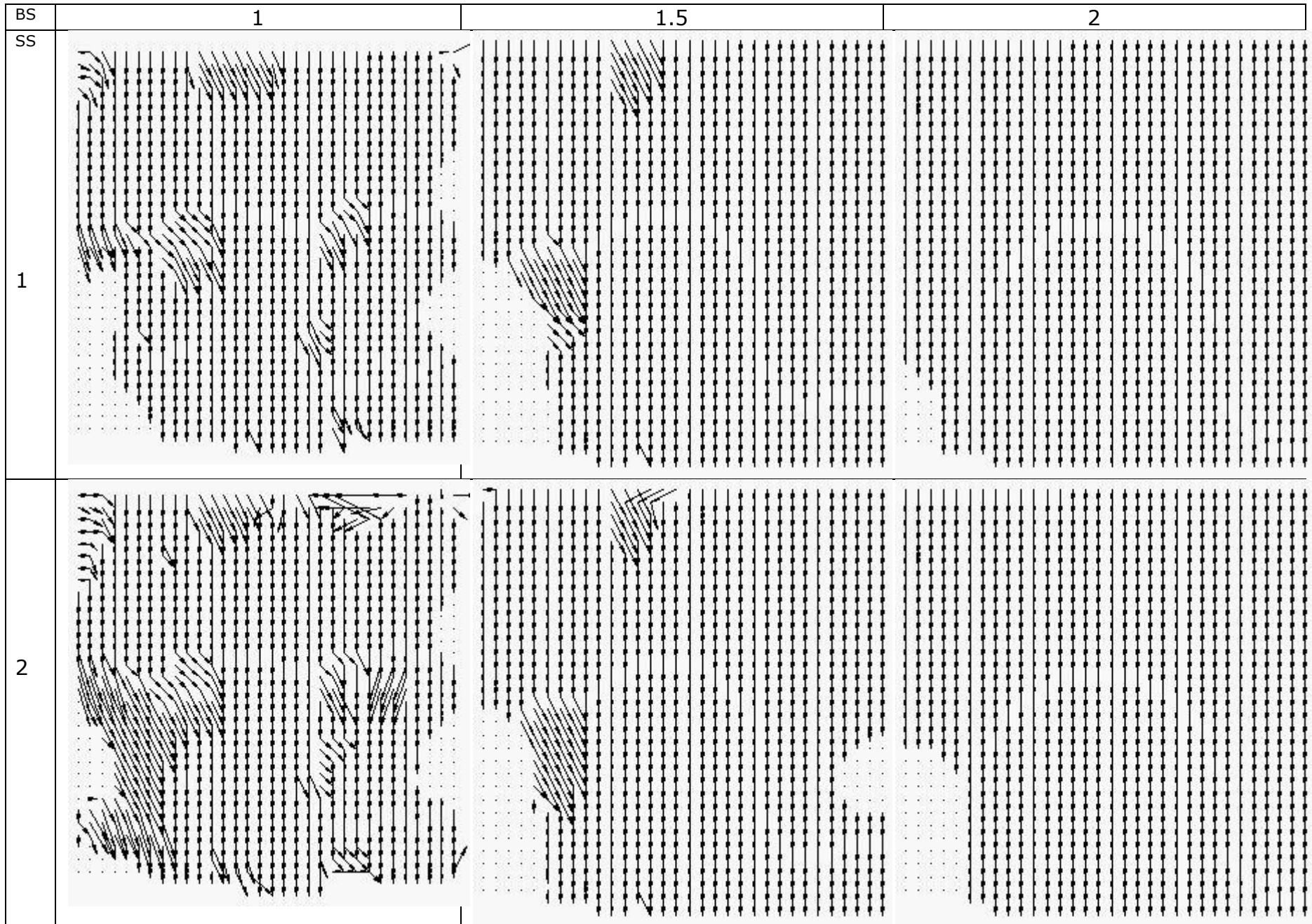


Figure B.6 Motion Estimation Vector Field for Claire Image Sequence with 5*5 Median Filter and vary value for BS(Block Size), SS(Search Space):

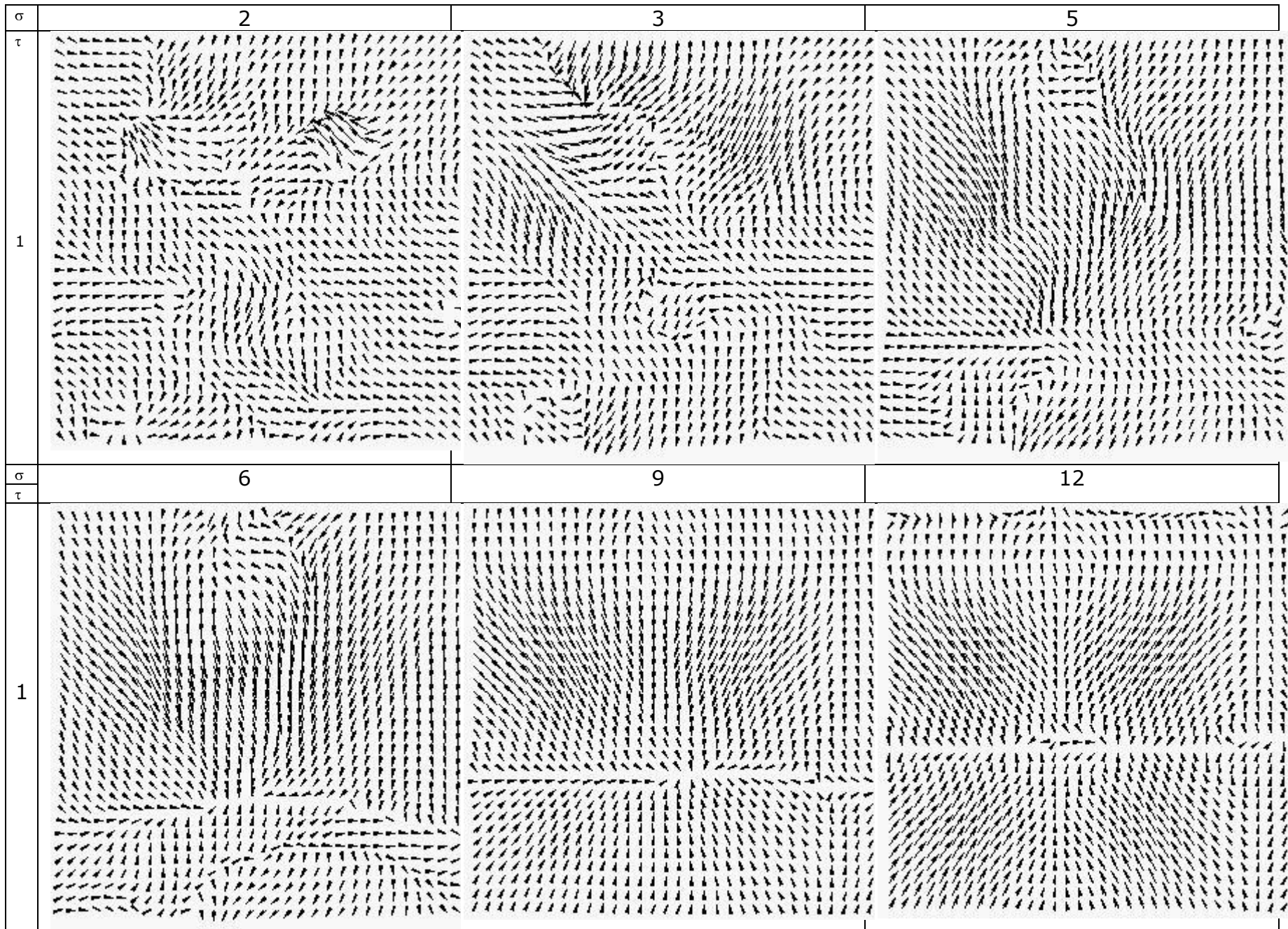


Figure B.7. Optical Flow Vector Field for Claire Image Sequence with 5*5 Median Filter; $\tau=1$ and vary value for σ :



Figure B.8 Two images from the Bus sequence with the section of the image highlighted that was used in the analysis shown in following

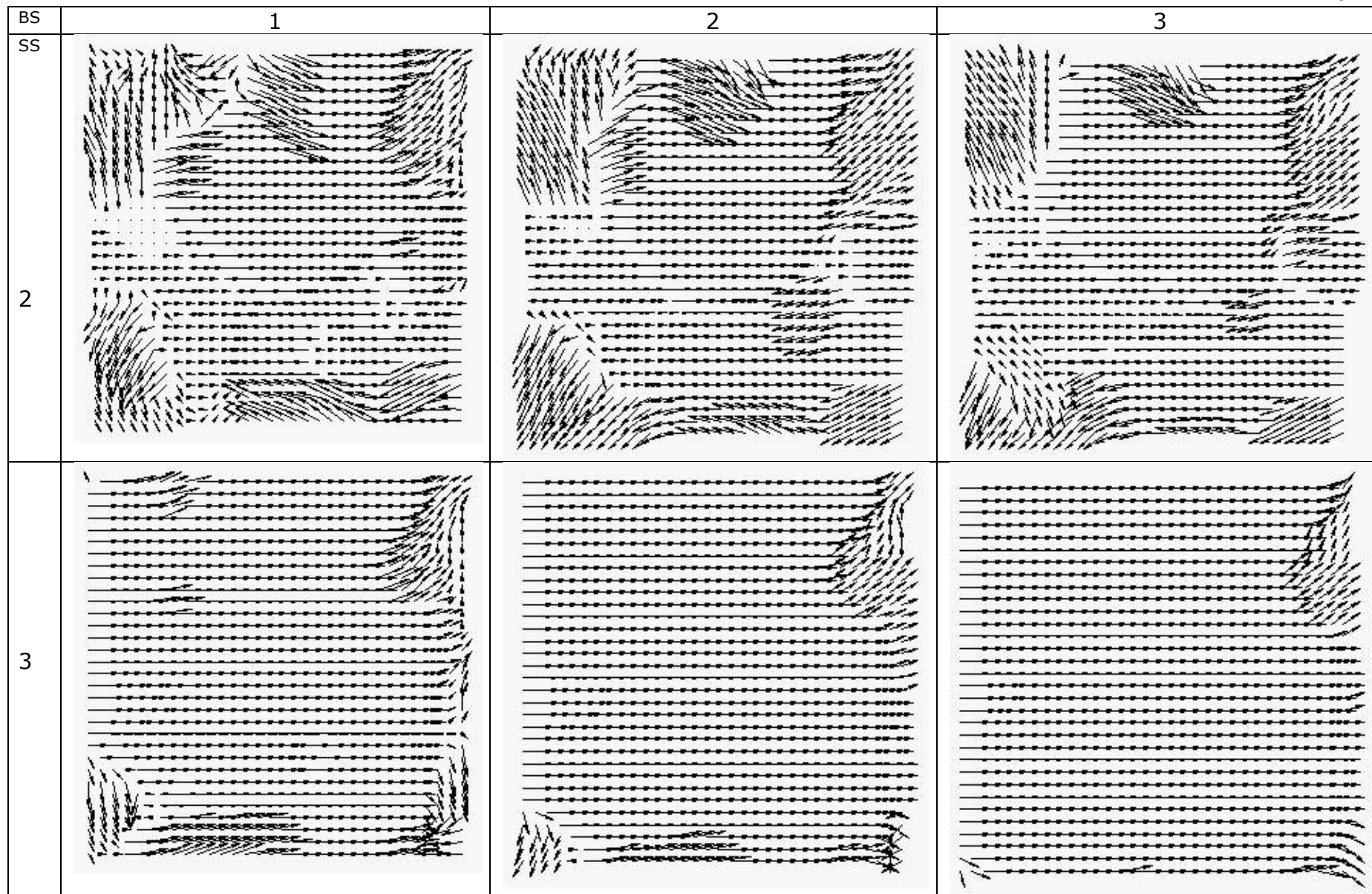


Figure B.9 Motion Estimation Vector Field for Bus Image Sequence with 5*5 Median Filter and vary value for BS(Block Size), SS(Search Space):

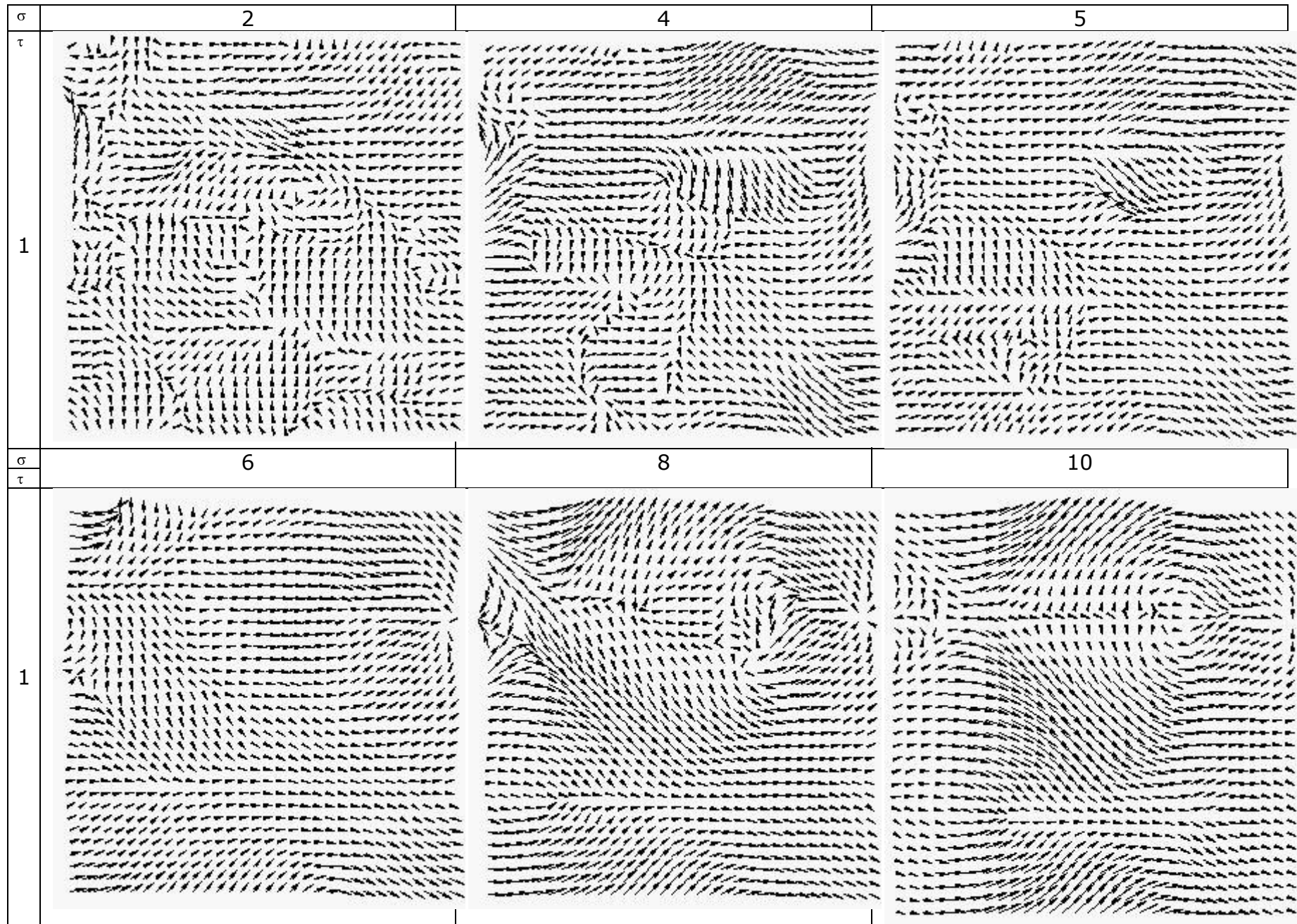


Figure B.10 Optical Flow Vector Field for Bus Image Sequence with 5*5 Median Filter; $\tau=1$ and vary value for σ